ASSESSMENT OF CYCLIC BEHAVIOR OF FRAME CORNER CONNECTIONS FABRICATED FROM STEEL COLD-FORMED SECTIONS

By

YASSER NASR IBRAHIM MOSTAFA

A Thesis Submitted to the
Faculty of Engineering at Cairo University
in Partial Fulfillment of the
Requirements for the Degree of
MASTER OF SCIENCE
in
STRUCTURAL ENGINEERING

FACULTY OF ENGINEERING, CAIRO UNIVERSITY
GIZA, EGYPT
2022

ASSESSMENT OF CYCLIC BEHAVIOR OF FRAME CORNER CONNECTIONS FABRICATED FROM STEEL COLD-FORMED SECTIONS

By

YASSER NASR IBRAHIM MOSTAFA

A Thesis Submitted to the
Faculty of Engineering at Cairo University
in Partial Fulfillment of the
Requirements for the Degree of
MASTER OF SCIENCE
in
STRUCTURAL ENGINEERING

Under the Supervision of

Prof. Dr. Sherif A. Mourad

………………………………..

Professor of Steel Structures and Bridges
Structural Engineering Department
Faculty of Engineering, Cairo University

Prof. Dr. Maged T. Hanna

………………………………..

Professor of Steel Structures
Housing and Building National Research Center, HBRC

Dr. Hazem H. Elanwar

……………………………………

Assistant Professor
Structural Engineering Department
Faculty of Engineering, Cairo University

FACULTY OF ENGINEERING, CAIRO UNIVERSITY
GIZA, EGYPT
2022

ASSESSMENT OF CYCLIC BEHAVIOR OF FRAME CORNER CONNECTIONS FABRICATED FROM STEEL COLD-FORMED SECTIONS

By
YASSER NASR IBRAHIM MOSTAFA

A Thesis Submitted to the
Faculty of Engineering at Cairo University
in Partial Fulfillment of the
Requirements for the Degree of
MASTER OF SCIENCE
in
STRUCTURAL ENGINEERING

Approved by the
Examining Committee

____

Prof. Dr. Sherif A. Mourad, Thesis Main Advisor
- Professor of Steel Structures and Bridges, Cairo University

____

Prof. Dr. Maged T. Hanna, External Advisor
- Professor of Steel Structures, HBRC

____

Prof. Dr. Mohammed Hassanien Serror, Internal Examiner
- Professor of Steel Structures, Faculty of Engineering, Cairo University

____

Prof. Dr. Mostafa Fahmi Hassanein, External Examiner
- Professor, Structural Engineering department, Tanta University

FACULTY OF ENGINEERING, CAIRO UNIVERSITY
GIZA, EGYPT
2022

Engineer's Name: Yasser Nasr Ibrahim Mostafa
Date of Birth: 29/10/1994
Nationality: Egyptian
E-mail: Yasser.nasr@bue.edu.eg
Phone: 01020504909
Address: 7th District, Nasr City, Cairo
Registration Date: 01/03/2019
Awarding Date: …./…./2022
Degree: Master of Science
Department: Structural Engineering

Supervisors:

Prof. Dr. Sherif A. Mourad
Dr. Hazem H. Elanwar
Prof. Dr. Maged T. Hanna

Examiners:

Prof. Dr. Sherif A. Mourad (Thesis main advisor)
Prof. Maged T. Hanna (External Advisor)
- Professor, Structural Engineering department, HBRC

Prof. Dr. Mohammed Hassanien Serror (Internal examiner)
Prof. Dr. Mostafa Fahmi Hassanein (External examiner)
- Professor, Structural Engineering department, Tanta University

Title of Thesis:

ASSESSMENT OF CYCLIC BEHAVIOR OF FRAME CORNER CONNECTIONS FABRICATED FROM STEEL COLD-FORMED SECTIONS

Key Words:
Cold-formed sections; Corner connection; Cyclic loading; Finite element modelling; Self-drilling screws

Summary:

This research investigates the performance of rigid connections of cold-formed steel under quasi-static cyclic loading and aims to provide a framework for modelling and analysis of screw as well as bolted-fastened connections subjected to cyclic loading. The rigid connections studied in this research were categorized into two types: screw fastened connections and bolted connections. A total of 3 specimens were tested under cyclic loading, two of which were screw-fastened using 6 mm self-drilling screws, and one specimen using ordinary bolts of 12 mm diameter and grade 4.6. Numerical models were developed using finite element software and validated against the test specimens. Cold-formed sections were modeled using shell elements while self-drilling screws were modeled using a user-element subroutine (UEL) developed using Fortran code and linked to finite element software, however, bolts were modelled using solid elements.

Disclaimer

I hereby declare that this thesis is my own original work and that no part of it has been submitted for a degree qualification at any other university or institute.

I further declare that I have appropriately acknowledged all sources used and have cited them in the references section.

Name: Yasser Nasr Ibrahim　　　　Date: ../../2022

Signature:

Acknowledgments

I would like to express the deepest gratitude to my respected supervisor, **Prof. Dr. Sherif Mourad**, who gave me the honor to be one of his students. I thank him for his continuous advice and encouragement, guidance, extreme caring, and great effort to provide me with an excellent atmosphere for doing this research.

I would also like to thank my advisor, **Prof. Dr. Maged Tawfik,** for his continuous help and support in the experimental program throughout this research. With his support and precious recommendations, many obstacles in the laboratory have been overcome and many problems have been solved. Also, his recommendations and guidance in the numerical modeling process made this research possible.

I would also like to thank my advisor, **Dr. Hazem Al-Anwar**, for his precious support, guidance, and valuable comments on my work throughout this research, especially the parts related to literature review, and analysis of results.

Also, I wish to express my sincere gratitude for **EMCON** for their huge support in fabrication and erection of test specimens, and for **HBRC** where the whole experimental program was carried out. Moreover, I would like to thank my colleague and friend **Eng. Ahmed Massoud** for his great support and efforts in fabrication, erection, transportation, and testing of specimens. I would also like to thank my colleague and friend **Eng. Mohamed Hosny** for his support at every stage in the research.

Finally, I must express my gratitude to my parents for providing me with support and continuous encouragement throughout my years of study and through the process of researching and writing this thesis.

Yasser Nasr Ibrahim

Table of Contents

List of Tables

List of Figures

Abstract

This research investigates the performance of cold-formed steel connections subjected to quasi-static cyclic loading. In addition, it provides a procedure for modelling and analysis of screw as well as bolted-fastened connections subjected to cyclic loading. The rigid connections studied in this research were categorized into two types: screw fastened connections and bolted connections. In order to investigate the connection behavior, three specimens were tested under cyclic loading, two of which were screw-fastened using 6 mm self-drilling screws, and one specimen using ordinary bolts of 12 mm diameter and grade 4.6. Numerical models were developed using ABAQUS as the finite element software and validated against the test specimens. Cold-formed sections were modeled using shell elements while self-drilling screws were modeled using a user-element subroutine (UEL) developed using Fortran code and linked to finite element software, while bolts were modelled using solid elements. Moreover, this research illustrates the difference between using the adopted methods of modelling the self-drilling screws and bolts versus the use of point-based fasteners and/or attachment lines which is commonly used for monotonically loaded models. Finally, a parametric study was developed in which the effect of changing the gusset plate thickness, bolts/screws arrangement, and stiffeners' locations was investigated.

The study showed that screw-fastened connections are capable of dissipating energy through ductile deformation under cyclic loading. Moreover, adding an additional stiffening plate connecting the column's flanges with the beam's flanges improved the moment capacity and energy dissipation capacity of the connection.

Chapter 1 : Introduction

1.1. Introduction

Steel construction practice depends mainly on conventional moment-resisting frames, concentrically braced frames, and eccentrically braced frames as steel lateral load (wind and earthquakes) resisting systems in addition to the alternative approaches of using energy dissipative systems. These lateral load resisting systems have proved to be reliable through previous research and large-scale testing. Moreover, their behavior is carefully observed and recorded when implemented in real structures and subjected to past earthquake events leading to more research in improving the design of these systems.

Recently, Cold-Formed Steel (CFS) structures have been less familiar yet of growing importance, which consist of steel sheets or plates formed by bending brake or press brake operations or in roll-forming machines. CFS has drawn attention in the field of seismic design. Structures subjected to seismic actions usually requires using lateral load resisting systems of adequate strength and ductility, therefore, innovative systems using cold-formed steel (CFS) sections have emerged. Whereby, high structural and environment performance have been sustained. One of the most popular cold-formed lateral load resisting systems is the CFS shear wall panels. They proved to be effective for low- and mid-rise buildings offering a very good alternative to conventional systems while using lightweight framing elements that reduce the seismic mass, which consequently reduces the seismic forces [1].

Cold-formed steel sections have been used for construction of entire mid-rise buildings as shown in Figure 1-1, nonetheless, hot-rolled moment resisting frames and braced frames are still the most popular steel systems resisting lateral loads since local instability failure can affect the ductility of CFS. Hot-rolled steel sections are used as lateral load resisting systems for higher buildings along with cold-formed steel that carries the static gravity loads [1].

The North American Standard for Seismic Design of Cold-formed Steel Structural Systems AISI S400-20 [2] approves the use of CFS-light frame shear walls with different sheathing materials and bracing for low- to mid-rise buildings. Currently, there is no standard code of practice in Egypt for using cold-formed steel as lateral load resisting system, moreover, Eurocode 8 does not provide clear guidance for using CFS as lateral load resisting system, therefore, AISI S400 stands as the leading reference for designing these types of systems. On the other hand, several researches have been adopted for improving the current design specifications for steel CFS and investigating moment resisting frames and beam-to-column moment connections to include in the AISI S400. Meanwhile, the AISI S400-20 includes a single moment resisting frame configuration for resisting lateral loads Figure (1-2).

In order to have better understanding for the behavior of cold-formed steel moment resisting frames, further research must be undertaken. Research on CFS beam-to-column moment connections against both monotonic and cyclic loading shall provide more insights to the behavior of such connections when subjected to seismic actions.

Figure 1-1: Full scale mid-rise cold-formed steel building [1]

Figure 1-2: AISI seismic resistant moment resisting frame [2]

1.2. Research Objectives

This research aims to investigate the behavior of beam-to-column moment connections against cyclic loading. The study includes using screw-fastened moment connections and bolted moment connections. The research also aims to provide tools and framework for finite element modelling and analysis of screw-fastened and bolted connections where ABAQUS software is used. Consequently, this investigation is carried out using experimental tests where specimens are tested against cyclic loads and experimentally verified numerical analysis of CFS beam-to-column moment connections using the experimental tests' output for verifying the numerical models.

The research depends mostly on American standards whether for testing or the analysis of results. The AISC cyclic loading protocol is adopted as well as the ASCE and AISI for the analysis of the output data either from the experimental tests or the numerical analysis.

1.3. Problem Statement

This research aims to investigate the performance of cold formed steel connections under cyclic loading where bolts and/or self-drilling screws are used as beam-to-column moment connections, and to develop a computationally efficient framework for these connections.

1.4. Thesis Outline

This research is presented in six chapters presented as follows:

Chapter 1 provides an introduction to seismic design in cold-formed steel construction industry, research objectives and research statement.

Chapter 2 provides a comprehensive literature review divided into four main parts: seismic design, cold-formed steel sections, CFS bolted connections and CFS screw-fastened connections

Chapter 3 discusses the experimental program carried out during the research as physical cyclic testing of specimens took place.

Chapter 4 presents the finite element modelling of screw-fastened and bolted connections.

Chapter 5 discusses the parametric study using the experimentally verified models.

Chapter 6 presents a summary of results, conclusion and future recommendations.

Chapter 2 : Literature Review

2.1. Introduction

This research focuses on the efficiency of cold-formed steel (CFS) sections in seismic zones as well as the efficiency of using self-drilling screwed connection subjected to low-cyclic fatigue as in the case of earthquakes. Therefore, this chapter discusses previous research that studied the energy dissipation capacity of CFS sections with different geometries with focus on the connections used in the cases mentioned. Previous research includes experimental studies in addition to finite element modelling and analysis of cold formed sections. Consequently, this chapter will discuss the different finite element techniques used for modelling the cold formed section in addition to the experimental data performed.

This chapter is divided into four sections that starts with the seismic assessment of structural elements and systems in different codes, then other research points are discussed as mentioned below:

- Seismic assessment of structures,
- Cyclic behavior of cold-formed sections (CFS),
- Cyclic behavior of CFS bolted connections, and
- Cyclic behavior of CFS screw-fastened connections

2.2. Seismic Assessment of Structures

Introducing non-prequalified steel connections into the designs requires procedures and acceptance criteria for these connections to be used as per the different codes and standards. The ASCE/SEI 41-17 [3] stipulates some requirements for the acceptance of steel connections used to resist seismic actions. ASCE 41-17 [3] states that component acceptance criteria depends on whether the component is classified first as primary or secondary, then, each action should be classified as deformation controlled (ductile) or force controlled (nonductile).

Components classified as primary are those which can accommodate deformations and resist forces so that the structure can achieve the required performance level. Other components that are not required to resist seismic forces but can accommodate deformations in the structure are classified as secondary components. Classifying components as whether they are force controlled or displacement controlled depends on the component force versus the deformation curves shown in Figure (2-1)

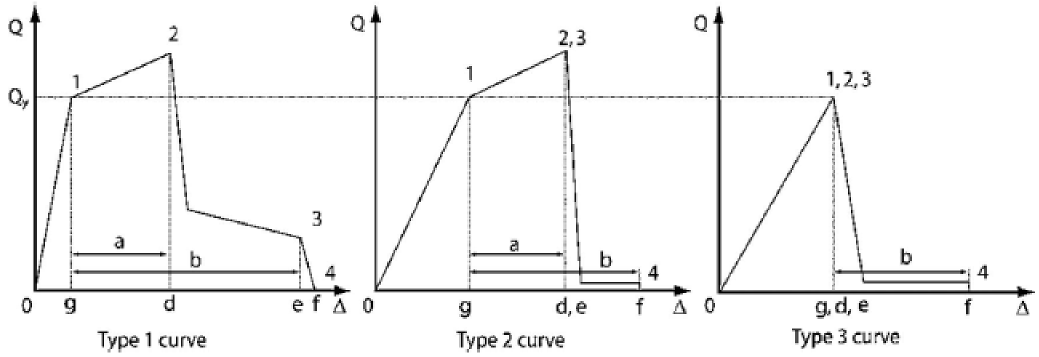

Figure 2-1: Component Force vs. Deformation Curves [3]

Type 1 curve shown in Figure (2-1) is a representative of ductile, deformation-controlled component where the plastic region starts beyond point 1, the loss of seismic force resisting capacity starts at point 3, and the gravity load resisting capacity is lost at point 4. If the plastic range d ≥ 2g for primary components exhibiting this performance, then these components shall be classified as deformation-controlled, otherwise, components are classified as force-controlled.

Similarly, for Type 2 curve, where the loss of seismic force resisting capacity starts at point 3, and the gravity load resisting capacity is lost at point 4, the only difference is the shape of the load-deformation curve of the component. In a similar manner, if the plastic range e ≥ 2g for primary components exhibiting this performance, then these components shall be classified as deformation-controlled, otherwise, components are classified as force-controlled.

Unlike Type 1 and Type 2 curves, Type 3 curve is a representative of nonductile/brittle behavior where the elastic region starts at point 0 till point 1, loss of seismic force resisting capacity starts at point 3, and the gravity load resisting capacity is lost at point 4 with no significant plastic deformation. Primary components are classified as force-controlled if they exhibit such behavior.

ASCE/SEI 41-17 [3] permits using experimental tests to identify the required seismic load-deformation relationships, which can be used later in developing a numerical or analytical models and determine the behavior of the structure subjected to different earthquakes. ASCE/SEI 41-17 also states that at least three experimental tests should be carried out while the boundary conditions, loads and construction details replicate the building conditions. Moreover, the experimental program must include cyclic loading protocols in order to assess the behavior of the components at different displacement levels.

Finally, ASCE/SEI 41-17 [3] stipulates for developing the acceptance criteria and structural modeling parameters based on experimental data, an envelope of the cyclic load-deformation curves is drawn at the peaks of the cycles forming a smooth backbone curve shown in Figure (2-3). Monotonic testing can be used to supplement the experimental program and the backbone curve form the monotonic tests can also be used for nonlinear modeling and analysis for these components. If multiple tests are to be performed for the same subassembly, an average backbone curve is used as shown in Figure (2-4).

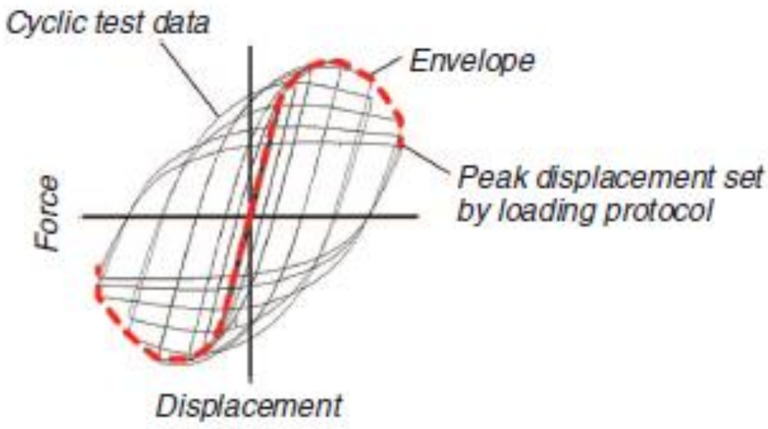

Figure 2- 2: Cyclic test envelope [3]

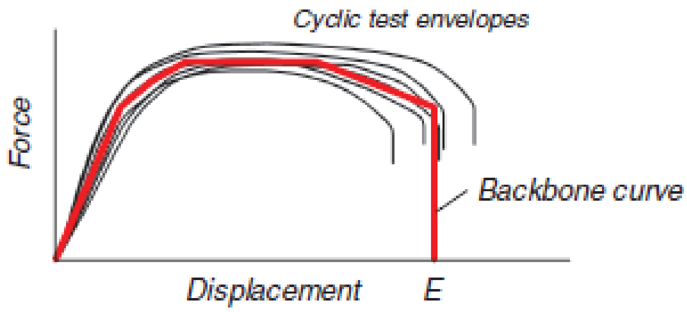

Figure 2- 3: Backbone curve construction using cyclic test envelopes [3]

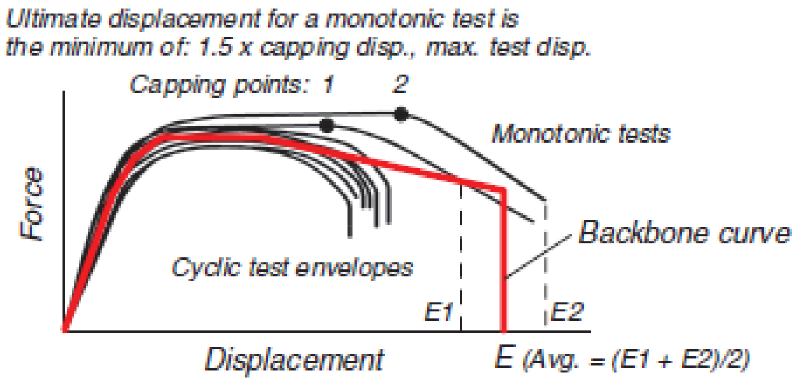

Figure 2- 4: Backbone curve construction using cyclic test envelopes supplemented with monotonic tests [3]

FEMA-356 [4] provides two idealization models for calculating the nominal yield strength and ultimate rotation of moment connections. First, the envelope of the cyclic moment-rotation is obtained, then, the point at which the secant slope intersects the envelope curve is considered to be at 60% of the nominal yield strength. Moreover, the area under the idealized bilinear curve should be equal to the area under the actual envelope curve up to the target displacement (θ_t). The FEMA-356 [4] idealized models are suitable for cold-formed steel connection since it is able to capture both the ascending and descending post-yield responses as illustrated in Figure (2-5). The energy dissipated during the cyclic displacement can be calculated from the area under the original envelope curve or the area under the idealized bilinear curve.

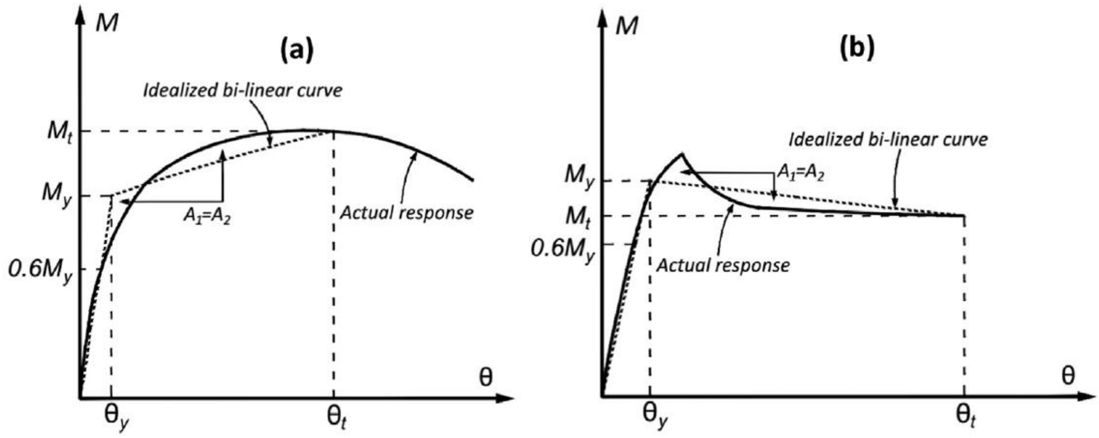

Figure 2- 5: FEMA idealization model (a) Post-yield ascending response (b) Post-yield descending response [4]

Another aspect of energy dissipation capability of moment connections is the damping coefficient. Ye et al. [5] used the following equation for calculating the equivalent viscous damping coefficient, C_e:

$$\boldsymbol{C_e = \frac{1}{2\pi}\frac{S_{ABC}+S_{CDA}}{S_{OBE}+S_{ODF}}} \qquad \textit{\textbf{Eq. 2-1}}$$

As illustrated in Figure (2-6), points B and D represent the maximum positive and maximum negative moment capacities of a hysteresis loop respectively, where the value $S_{\Delta ABC} + S_{\Delta CDA}$ is the energy dissipated during one complete cycle at the expected rotation as illustrated in Figure (2-6), while $S_{\Delta OBE} + S_{\Delta ODF}$ represents the total strain energy at the expected rotation assuming the connection behaves elastically. Unlike the area under the envelope curve method for obtaining the energy dissipated, the plumpness of the hysteresis loops can be obtained using this approach of calculating the equivalent viscous damping coefficient which will be very useful in this research later. Ye et al. [5] calculated the viscous damping coefficients for the peak moment loops and for the loops that reaches the target rotation at 20% drop in the peak moment capacity.

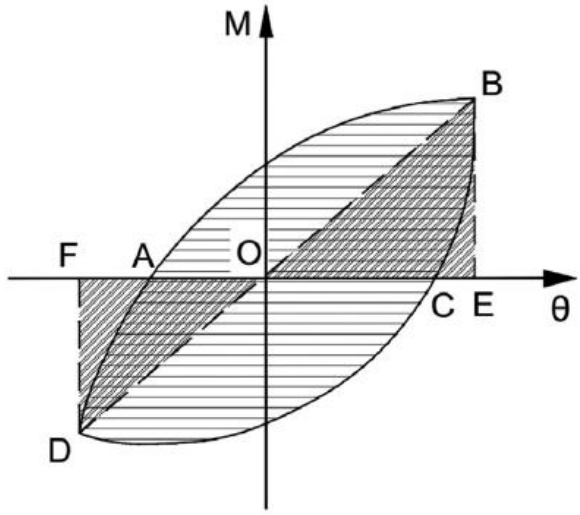

Figure 2-6: Definition of Equivalent Viscous Damping [5]

Seismic design guidelines in most international code provisions, such as Eurocode 8 and AISC 341-16, classify moment resisting frames resisting seismic loads into three main categories, Ordinary Moment Resisting Frames (OMF), Intermediate Moment Resisting Frames (IMF) and Special Moment Resisting Frames (SMF). This classification depends on the ductility capacity of these frame types. AISC 371-16 [6] stipulates that the IMF must accommodate 2% (0.02 rad) to 4% (0.04 rad) inter-story drift with less than 20% degradation in strength, which means that at the specified inter-story drift, the moment capacity should be at least 80% the maximum moment capacity recorded during the test. SMF must accommodate over 4% (0.04 rad) inter-story drift with less than 20% degradation in strength and OMF are those which can accommodate less than 2% (0.02 rad) inter-story drift with 20% degradation in strength.

AISC 341-16 [6] provides guidelines for qualifying cyclic tests of beam-to-column moment connections required to resist seismic actions. First, AISC 341-16 [6] stipulates that cyclic testing of steel beam-to-column moment connections must follow a certain protocol where the story drift angle, θ, is imposed on the specimen as indicated below:

- six cycles at θ=0.00375 rad
- six cycles at θ=0.005 rad
- six cycles at θ=0.0075 rad
- four cycles at θ=0.01 rad
- two cycles at θ=0.015 rad
- two cycles at θ=0.02 rad
- two cycles at θ=0.03 rad
- two cycles at θ=0.04 rad

- continue loading at increments of θ equal to 0.01 rad, with two cycles of loading at each step, where θ is illustrated in Figure (2-7) for cantilever beams.

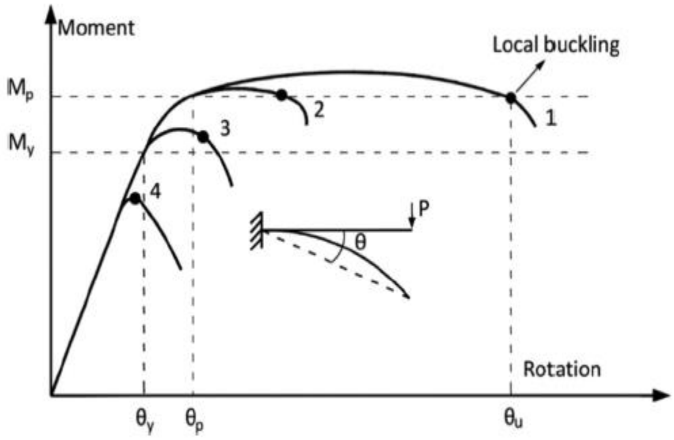

Figure 2-7: Cross-section classification definition in EC3 (class 1, 2, 3 and 4) and beam rotation [5]

AISC 341-16 [6] also states that samples of the plates used for the steel section should be taken and tested in tension with a loading rate matches, as closely as possible, the main specimen's loading rate. The yield strength that obtained from the tension test should follow the definition in ASTM A370, and using the offset method at 0.002 in/in strain.

2.3. Cyclic Behavior of Cold-Formed Steel Sections

Padilla-Llano et *al.* [7] conducted an experimental investigation on the cyclic flexural behavior of cold formed steel sections. The cyclic loading protocol adopted in this research was FEMA461 and the tests were conducted on simply supported single C-channel CFS using 4-point bending. It was found that the cold-formed sections are capable of dissipating energy even after local buckling of the flange/web occurs. This is attributed to the stresses redistribution at regions around the damaged half-wave(s). A huge strength degradation was observed after surpassing the peak moment capacity; however, it was also found that residual moment capacity of 0.2 My, on average, remained while large deformations were taking place (θ/θ_y>2).

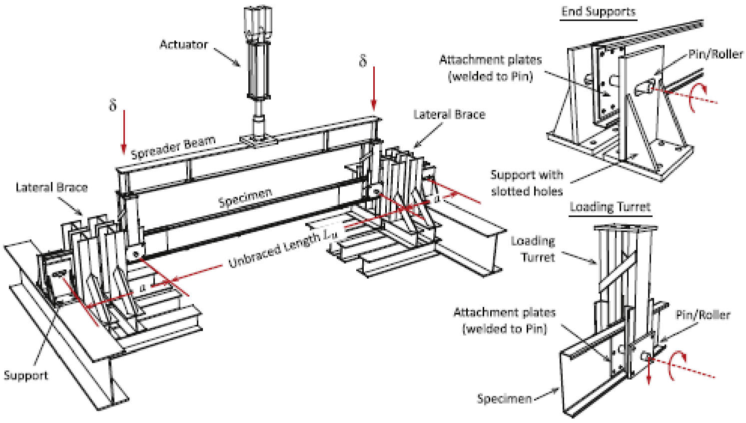

Figure 2- 8: Experimental setup for beams tested in bending [7]

Local buckling, distortional buckling and lateral torsional buckling modes affected the cyclic stiffness degradation, cyclic strength degradation, and pinching of the hysteric response differently. The two sources of energy dissipation were the cold-bending and inelastic strains that formed at the buckled parts of the members, in addition to that, number of buckled parts and the buckling mode controlled the amount of energy dissipated during loading. It was found that members experiencing lateral torsional buckling resulted in the lowest energy dissipation compared to those with local and distortional buckling. Moreover, members with two flexural hinged formed showed less capability of energy dissipation than those with single flexural hinge. Finally, it was found that the most significant factor that affects the energy dissipation capability of CFS is the slenderness ratio. The more the slenderness ratio of the section the less capable the section is in terms of energy dissipation. Also, the section elastic modulus, S, affects the capability of the section to dissipate energy.

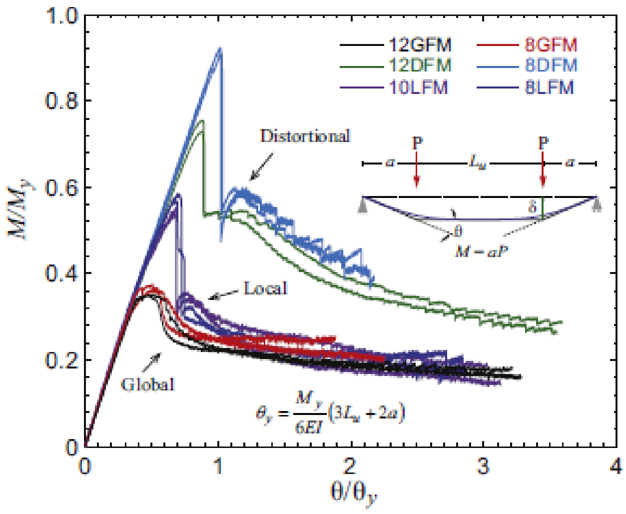

Figure 2- 9: Moment-rotation relationships for beams tested [7]

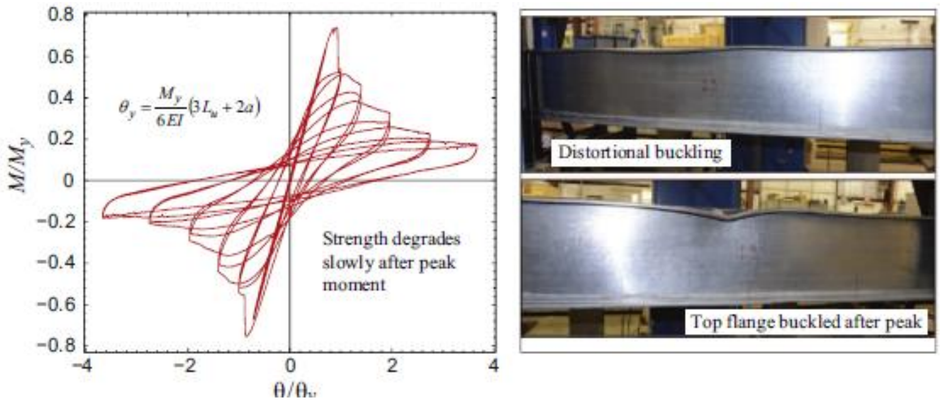

Figure 2- 10: Hysteresis loops for beams failed in distortional buckling [7]

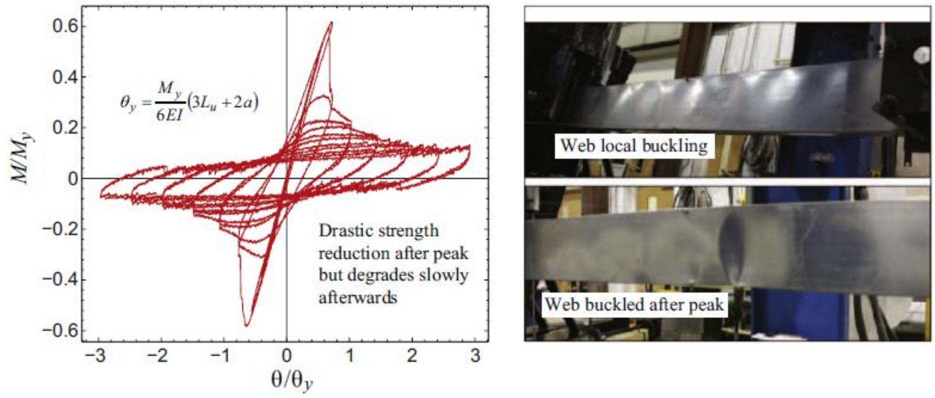

Figure 2- 11: Hysteresis loops for beams failed due to web local buckling [7]

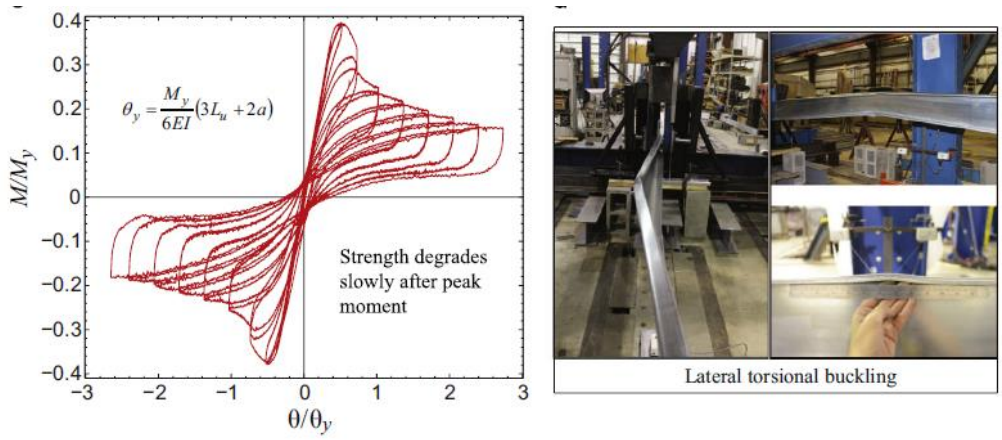

Figure 2- 12: Hysteresis loops for beams failed due to lateral torsional buckling [7]

Haidarali et *al.* [8] conducted a research on simply supported CFS Z-sections under 4-point load bending. The research was conducted using FE analysis experimentally validated against previous researches. Haidarali et al. [8] divided the tests into two series, the first was Z-sections prone to combined distortional/local buckling failure modes and the other was Z-sections prone to local buckling only. Moreover, the research included modelling the entire test setup once, and then a more simplified modeling approach of the tests was adopted and it was found that the latter was preferable since both approaches gave acceptable results given that the simplified approach was computationally less expensive. Material and geometric nonlinearities were accounted for while modelling the Z-sections. Four stress-strain curves definitions were used, and it was found that no significant effect was encountered for the different strain hardening values provided by the four models, however, the gradual yielding of the material had larger impact on the behavior of the sections and it was found that the compound Ramberg Osgood model was the best choice for material modeling. Geometric nonlinearities were modeled with the aid of CUFSM software developed by Shafer (2006). The local and distortional buckling modes were obtained using elastic buckling analysis conducted using CUFSM in order to obtain the initial geometric imperfections to be used in ABAQUS. Haidarali et *al.* [8] then used the cumulative distribution functions for the maximum geometric imperfections proposed by Shafer and Pekoz [9] and it was found that imperfections for local buckling d1=0.34t and imperfections for distortional buckling d2=0.94t gave very good agreement with the experimental tests, therefore, these values can be used as initial magnitudes for geometric imperfections.

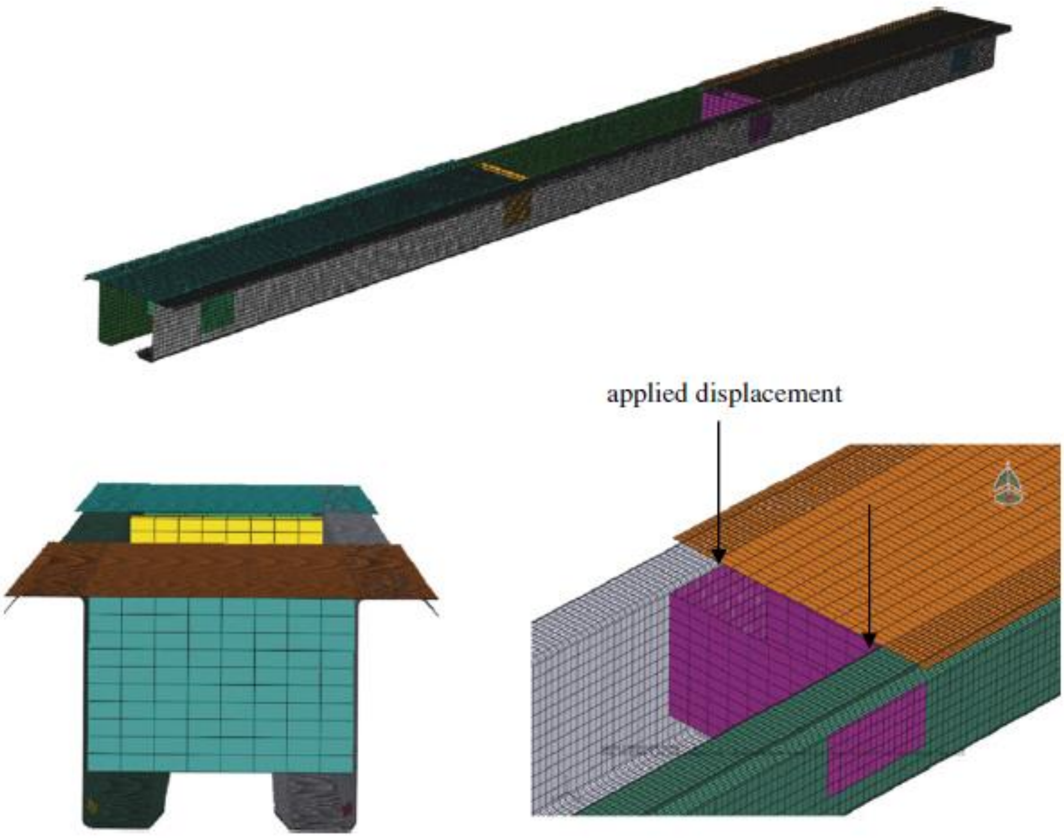

Figure 2- 13: Double-member FE model arrangement [8]

Mojtabae et *al.* [10], investigated the seismic performance of cold-formed steel using static monotonic pushover analysis and cyclic loading. The research included testing a half-scale moment frame with two box-shaped columns and two channels back-to-back beams (strong column-weak beam approach). FEM was also used and validated against the experimental results. The validated finite element model was then used for assessing the effect of changing different parameters on the ductility, energy dissipation capacity and moment capacity of the frame. It was found that local buckling of the column's web at the connection was the dominant failure mode, however, the frame performed well in terms of ductility and energy dissipation. It was also found that increasing the column axial loads resulted in a huge reduction in ductility, lateral load and energy dissipation capacities and the slenderness ratio had a significant effect on the ductility and energy dissipation capacities. It was also found that the frame could meet the AISC 341-16 [6] seismic requirements for special moment resisting frame in terms of inter-story drift which reach 4% at 20% reduction in moment capacity.

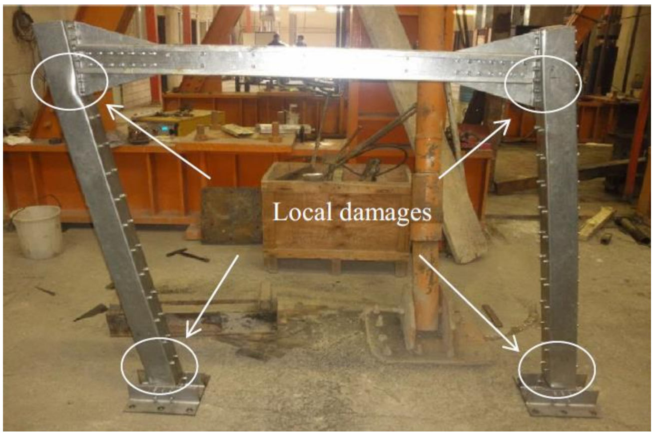

Figure 2- 14: Permanent deformations and local damages observed at the ultimate displacement [10]

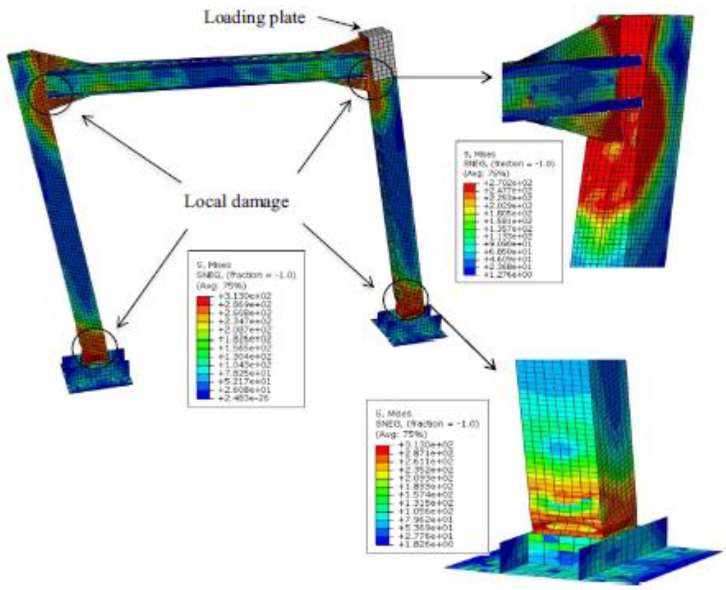

Figure 2- 15: FEM of the experimentally tested frame [10]

2.4. Cyclic Behavior of CFS Bolted Connections

Sabbagh et *al.* [11] investigated the seismic performance of CFS moment resisting frames. The aim of the study was to improve the ductility of connections and delay the local failures that may occur in the CFS of the beams and columns. The research was conducted using finite element analysis where curved and straight flanges were modelled and followed the strong column weak-beam design criteria so that the plastic deformations were limited to the beams while the column and gusset plate remained elastic. It was found that the 2mm thick flat flange CFS did not meet the ductility requirements set by AISC 341-16 [6]for IMF and SMF and showed sharp strength degradation, while curved flanges gave better results in terms of ductility. Also, Sabbagh et al. [11] investigated the optimum location of added stiffeners that would result in higher ductility which resulted in the shape described in Figure (2-16). The added stiffeners had the same plate thickness of that of the beams. It was found that the connection with the optimum added stiffeners exceed the ductility and strength required for SMF as stated by AISC seismic provisions.

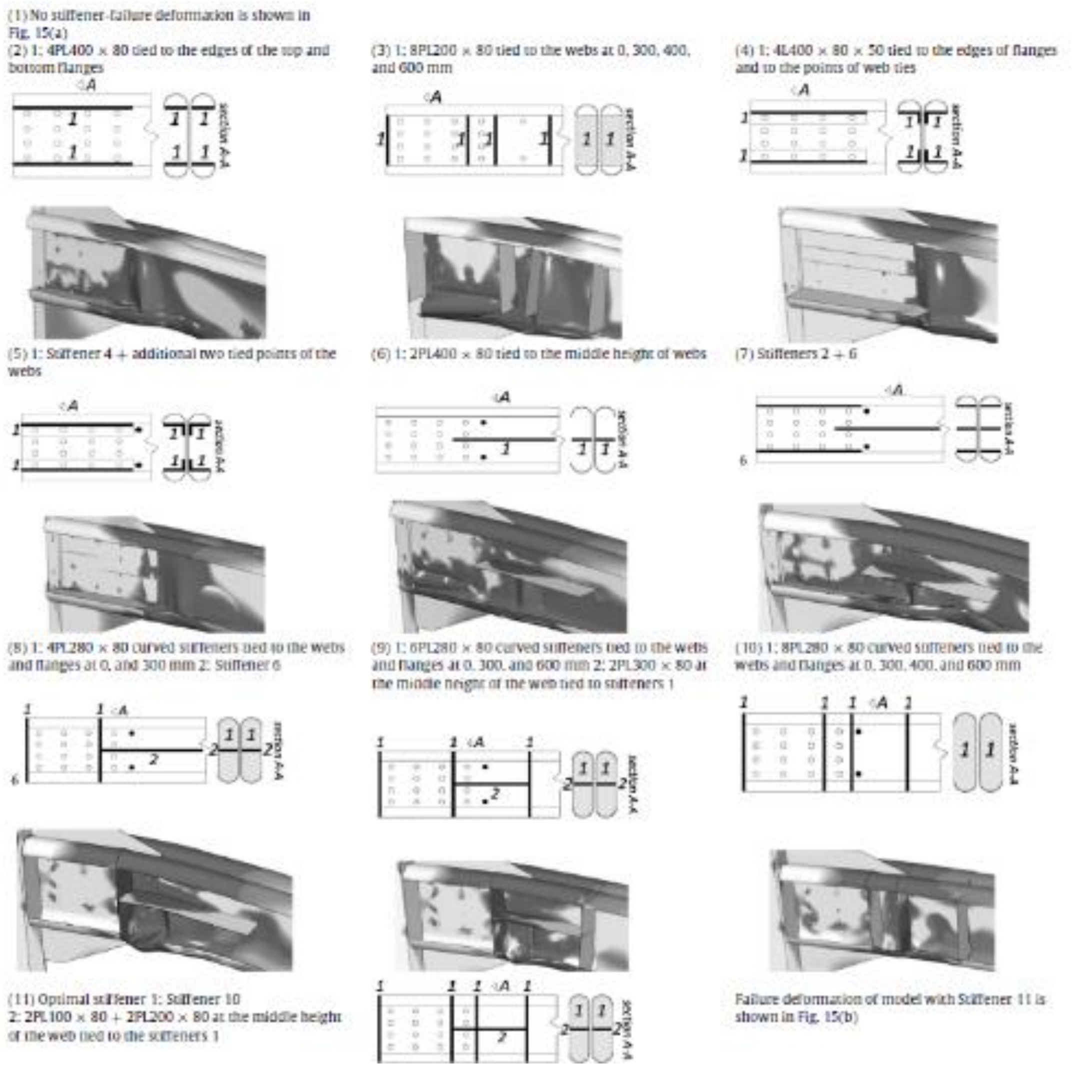

Figure 2- 16: Failure deformations with different stiffeners' locations [11]

Rinchen and Rasmussen [12] investigated the performance of cold formed steel connections of single C section. The research included analytical finite element models validated via experimental tests on a series of base, apex and eaves connections. The aim of the research was to establish non-linear moment-rotation relations and derive flexural stiffness values for these connections. Significant deformations of the connecting brackets of both the eaves and apex connection were noticed prior reaching the ultimate load of each specimen. Tearing of the CFS lips and fracture of screws triggered the collapse of the connection while the web buckling of the brackets and bending of the sections along the bolt lines were the two dominating failure modes in the study. The following Figure (2-17) illustrates the connection details presented by Rinchen and Rasmussen [12].

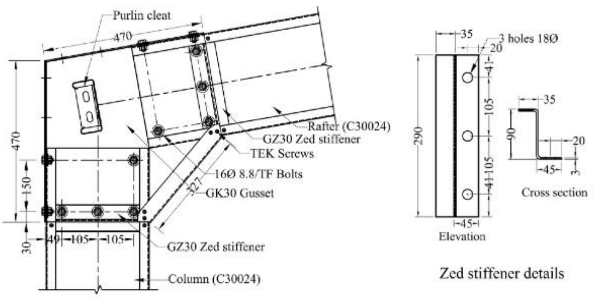

Figure 2- 17: Single c-section eave connection [12]

Shahini et *al.* [13] investigated CFS moment resisting connections prone to seismic actions. The research included FE modelling and experimental testing of slip-critical bolted joints with two different bolt group arrangement, circular and square (Figure 2-18), in order to reach larger energy dissipation capacities and higher ductility. Moreover, slotted holes (Figure 2-18) were proposed the bolts bearing action would not cause the unfavorable hardening effect. Both monotonic and cyclic testing of the connections were conducted in order to investigate the ductility of these connections and the extent to which the non-ductile local buckling of the CFS can be postponed. The connections with slip critical mechanism were able to dissipate energy 75% higher than that without slip. Moreover, It was found out that the circular bolt group had a more uniform distribution of forces that is close to the idealized solution which led to less excessive additional moment in the joint which can lead to the local buckling of the CFS.

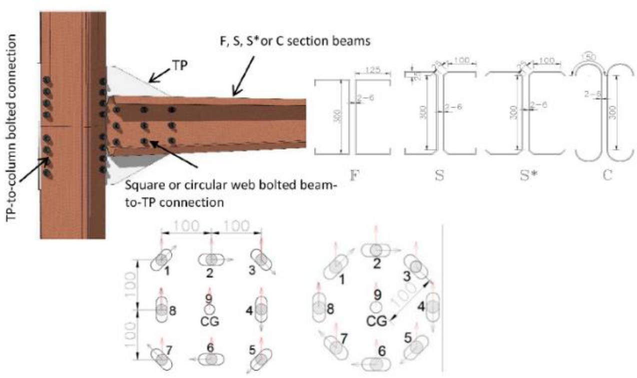

Figure 2- 18: Cross-sections and bolts arrangements tested in the study [13]

Ye et *al.* [14] studied CFS moment connections while comparing the effect of changing multiple parameters such as CFS slenderness ratios, bolt group arrangement (square, circular and diamond arrangement), flange shapes (flat, stiffened and curved flanges) and gusset plate thicknesses on the cyclic behavior of the connections. The aim of the research is to reach a reliable method for designing CFS moment resisting frames suitable for seismic applications. The study was conducted using experimentally validated finite element models and included both monotonic and cyclic loading. It was found that the curved and folded flanges performed better in terms of postponing the local buckling of the flange and hence increasing the moment capacity, however, this increase was only by 10%.

Moreover, in terms of ductility and energy dissipation, folded flanges with diamond or circular bolt arrangement managed to increase the efficiency of the connections up to 100% and 250% respectively compared to the conventional flat flange with square bolts arrangement, nevertheless, the square bolt arrangement provided higher moment capacity compared to the diamond and curved bolt arrangement.

In order to check for the adequacy of the connections for seismic design, Ye et al [14] classified the sections in accordance with the Eurocode (classes 1, 2, 3 and 4). Only classes 1 and 2 satisfied the conditions set by the AISC for special moment frames and classes 3 and 4 did not satisfy these conditions. In addition to that, the ductility and the energy dissipation were highly affected by the slenderness ratios and section class. Finally, Ye et al [14] studied the effect of the gusset plate thickness on the behavior of the connections and it was found that increasing the gusset plate thickness slightly above the thickness of the CFS is recommended in order to avoid any premature failure in the gusset plate itself rather than the CFS.

Ye et al [5] also investigated the effect of bolted connections with friction -slip mechanism on the behavior of these connections under cyclic loading for seismic applications. The research was conducted using experimentally validated finite element analysis using ABAQUS. The research also included investigating different bolt group arrangement, sections' slenderness ratio and shapes along with the friction slip mechanism. The moment capacity, ductility, energy dissipation and equivalent damping coefficient were determined for each connection. It was found that the friction slip mechanism did not affect much the moment capacity of the connection, however, the hysteric moment rotation response was shifted and the energy dissipation of the connections increased significantly especially with slender sections (class 3 and 4). The equivalent damping coefficient and the ductility of the connections increased significantly as well when class 3 and class 4 beam sections where used for the connections. Finally, class 3 and class 4 sections used for the moment connections did not satisfy the AISC regulations for intermediate moment frames and special moment frames despite using friction slip bolt mechanism that increased the ductility of the connections.

Rinchen and Rasmussen [15] conducted a research on the behavior of large scale cold formed portal frames using finite element analysis. The models presented were validated and compared with a recent research conducted by the same authors [12] on large scale cold formed portal frames using experimental testing. The CFS used were single C-sections modelled using shell elements. Semi-rigid connections were modelled for the different connections in the portal frames (eaves, apexes and base plates connections) using mesh independent point-based fasteners. Geometric and material nonlinearity were accounted for (referred to as Advanced Analysis throughout the research) in order to predict the CFS strength. Eigenvalue linear buckling analysis was performed in order to predict the different buckling modes and amplified according to the absolute imperfections measure on the tested sections Figure (2-19). It was found that the numerical models were in good agreement with the experimental tests conducted on the portal frames.

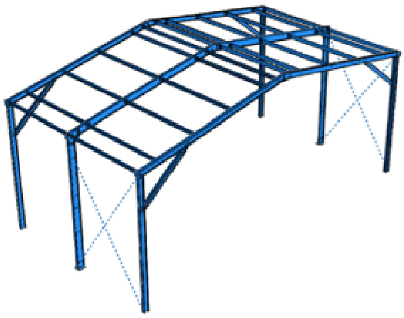

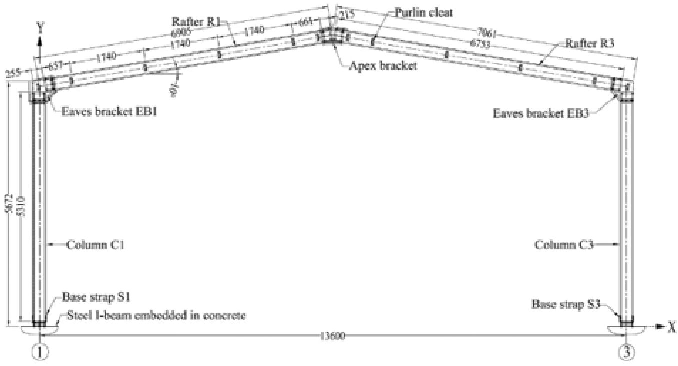

Figure 2- 19: FEM (left) and model details (right) [15]

Moreover, Rinchen and Rasmussen [15] conducted a parametric study on the different connector types offered by ABAQUS that can be used for the connections. These connector types are: Rigid Multi-Point Constraint (MPC), Beam Connector section, and a combination of CARTESIAN and CARDIAN sections denoted as "current fastener model" in Figure (2-20). It was found that the latter type of connection gave an almost identical behavior of the connection strength while the other two models overestimated the connection strength and underestimated the deflections

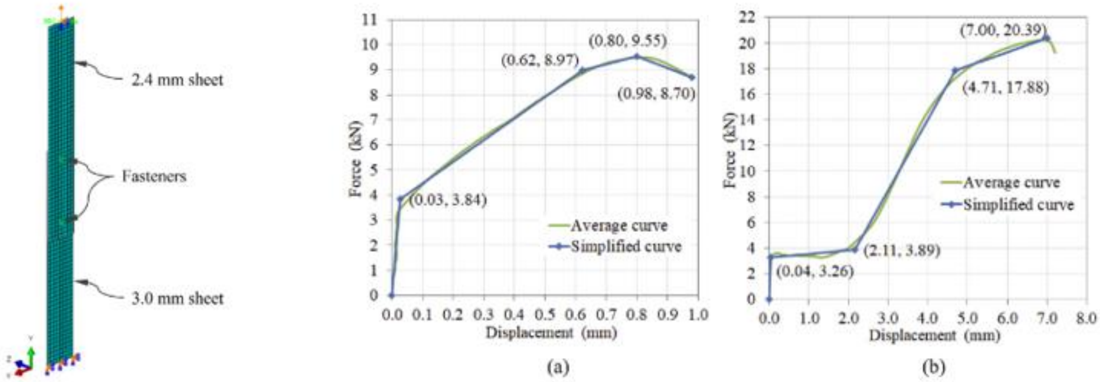

Figure 2- 20: FEM of the lap joint (left) shear force vs. displacement for (a) bolts (b) screws [15]

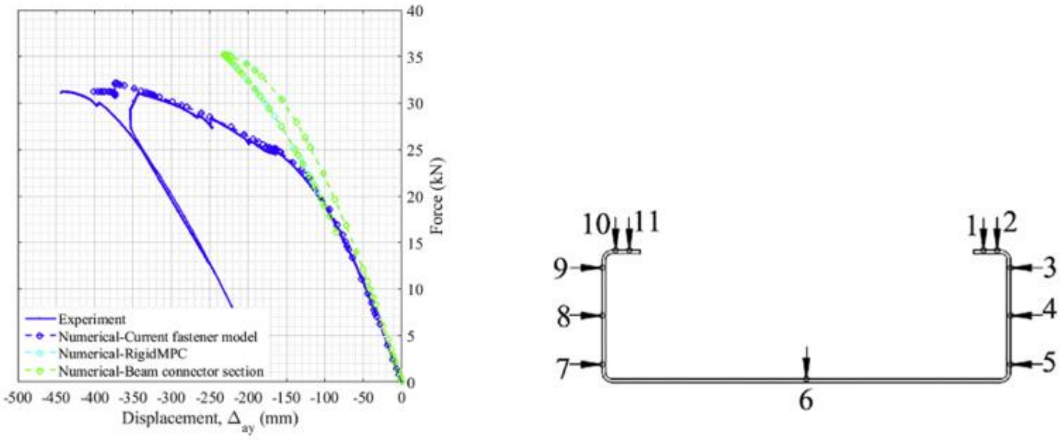

Figure 2- 21: Prediction of frame behavior with three types of connector sections (left) location of laser measurement points for geometric imperfections determination (right) [15]

Pouladi et *al.* [16] investigated the rotational stiffness of cold-formed single channel-section eave joint of steel portal frames, commonly used in New Zealand and Australia, using both experimental and finite element analysis. Both screws and bolts were used for the connection where screws were used to prevent the slip during frame erection. The sequence of failure as reported by Pouladi et al. [16] was shear failure in the screws, followed by twisting of the sections and yield line formation in the bracket. Although the screws failed first in shear, the point-based fastener approach used for modeling the screws and bolts failed to simulate any type of failure in these elements. The results of the finite element model were found to be in good agreement with the experimental results. Moreover, the results were compared with the semi-empirical formula proposed by Zaharia and Dubina (2006) and a hand calculation proposed by Crawford and Kulak (1971) for determining the rotational stiffness of joints and were also found to be in good agreement.

.

2.5. Cyclic Behavior of CFS Screw-Fastened Connections

Minh et al. [17] investigated the shear strength of self-drilling screws using experimental and numerical approaches where ABAQUS software was used for numerical modelling of the connections and the explicit solver was implemented for the analysis. Three screws aligned in a direction parallel to the direction of the applied load were used to fasten two G450 steel sheets of thicknesses 2.4 mm and 3.0 mm Figure (2-22). The diameters of the fasteners used in the study were 5.5 mm and 6.3 mm (gauges 12 and 14), moreover, the study included the effect of the number of threads per inch (TPI) on the behavior of the screws where screws of 10, 12 and 24 TPI were used in the research. The numerical model was able to simulate the behavior of the screws in terms of ductility, shear strength and stiffness Figure (2-23) and showed good correlation with the experiments. Table (2-1) summarizes shear strength obtained from the experimental and numerical investigation.

Table 2- 1: Shear Strength of Screws [17]

Screws	Experiments (kN)	FEM (kN)	From manufacturer (kN)
12 g – 24 TPI	10.1	10.1	9.0
14 g – 20 TPI	10.2	10.5	11.2
14 g – 10 TPI	12.2	12.0	n/a

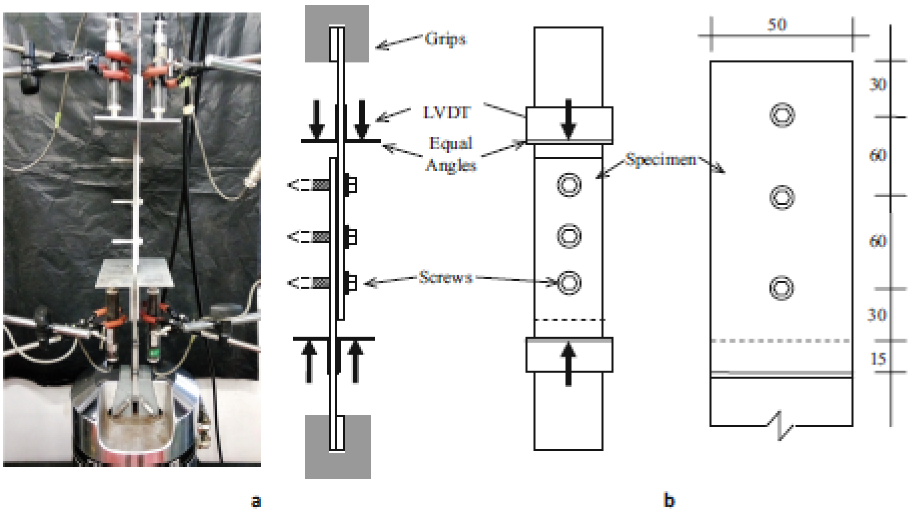

Figure 2- 22: (a) Test set-up (b) test specimen [17]

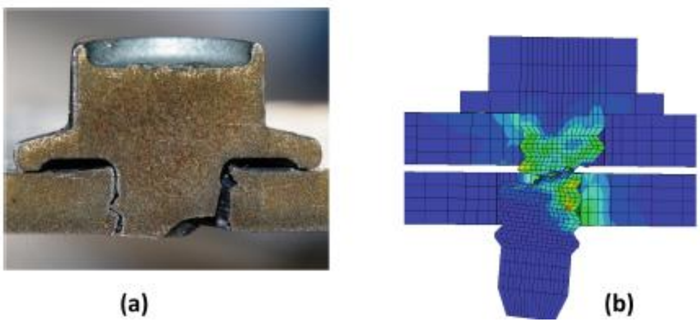

Figure 2- 23: Screw failure in (a) testing and (b) modeling [17]

Roy et al. [18] also discussed the strength of cold-formed steel connections where self-drilling screws of gauge 12 and 14 (illustrated in Figure 2-24) were used for connecting G550 steel sheets of thicknesses (1.0mm and 1.2 mm). The different failure modes of screws which includes tilting, bearing, pullout and shear failures were investigated using 25 experimental tests where the effect of screws' number, patterns and spacings were studied. Explicit non-linear finite element analysis using ABAQUS software was implement and a fracture criterion for the steel plates was implemented. It was found that the FE models were in good agreement with the experimental tests in terms of failure modes and connection strength. The explicit finite element model was capable of simulating the shear fracture, tilting, pullout and bearing failure modes resulted from the experimental tests Figure (2-24)

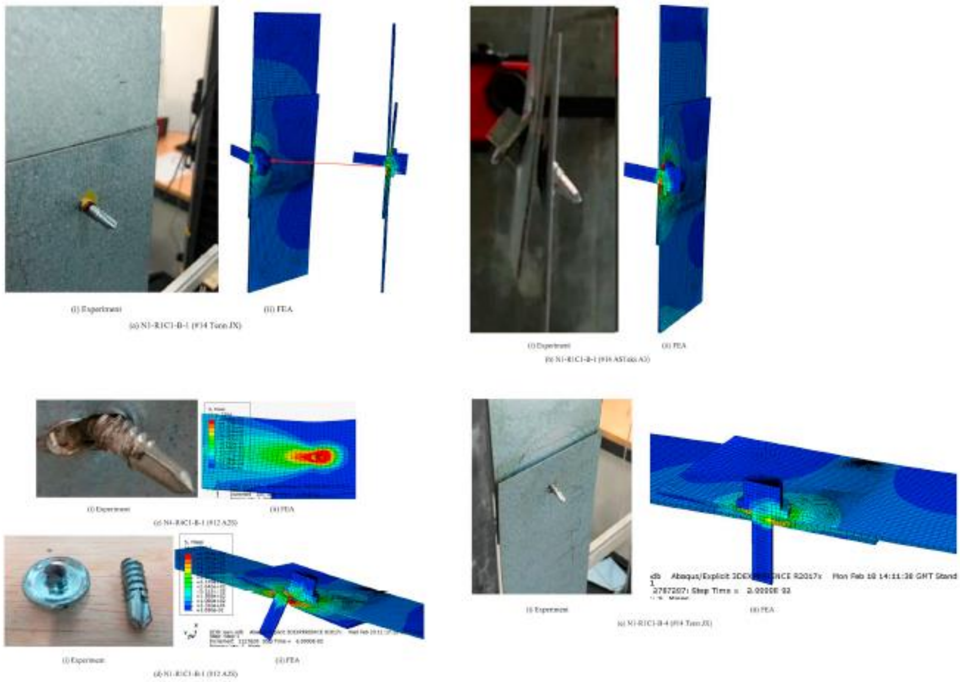

Figure 2- 24: Experimental vs. numerical failure modes [18]

Huynh et *al.* [19] investigated the behavior of self-drilling screws under shear stresses since self-drilling screws proved to be practical in terms on on-site assembly and can be drilled with ease in the thin-walled cold formed sections. Three tests per each screwed connection type were tested with screw sizes illustrated in Figure (2-25). The study included obtaining the load-deflection curves for the screw connectors, using both experimental and finite element analysis, in order to better understand their complex behavior in shear. Solid deformable elements were used for modeling the screws and the screw threads were accurately modeled. A plasticity model was employed for the steel sheets used in the connection in order to accurately capture the behavior of steel during failure as well as a damage model using fracture strain formulas. The finite element model successfully captured the different types of failure that the connection went through as described by the European Recommendations ECCS TC7 TWG 7.10 as well as the load-displacement of the specimens especially in the elastic region.

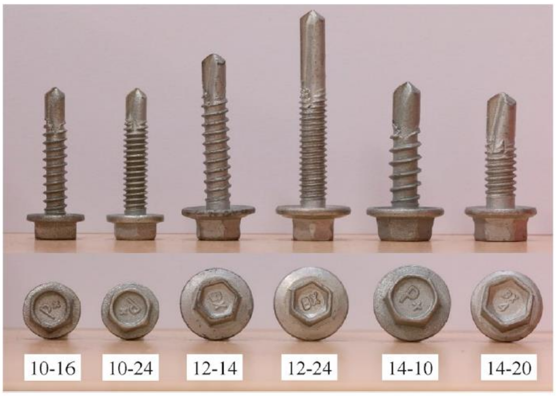

Figure 2- 25: Screws' sizes and number of threads per inch [19]

Minh et al. [20] investigated the performance of self-drilling screws against shear. The aim of the investigation was to examine the tilting and bearing failure of screw-fastened connections Figure (2-26) where 2 self-drilling screws were used to connect high strength steel plates of different thicknesses, and to compare the results against the American, European and Australian standards and specifications for design screw-fastened connections. The tests took place at the university of Sydney where a total of 51 tests were conducted and screws failed either in shear fracture or bearing and tilting of the screws. Table (2-2) provides a summary of the results for screws failing in bearing and tilting. The results of the experiments were compared to the predicted loads from the AISI S100-16, the Eurocode (EN 1993-1- 3:2006), and a set of revised design equations proposed by the research. The summary of this comparison is provided in Figure (2-27) where the ratio between the ultimate loads from the experiments were divided by the capacity predicted from the design equations in the codes. It can be noticed that only the proposed equations gave a ratio greater than 1 in all cases which reflects that the design codes, in some cases, may overestimate the capacity of the screw-fastened connections and the modifications for the design equations proposed by Minh et al. [20] may help overcome this issue.

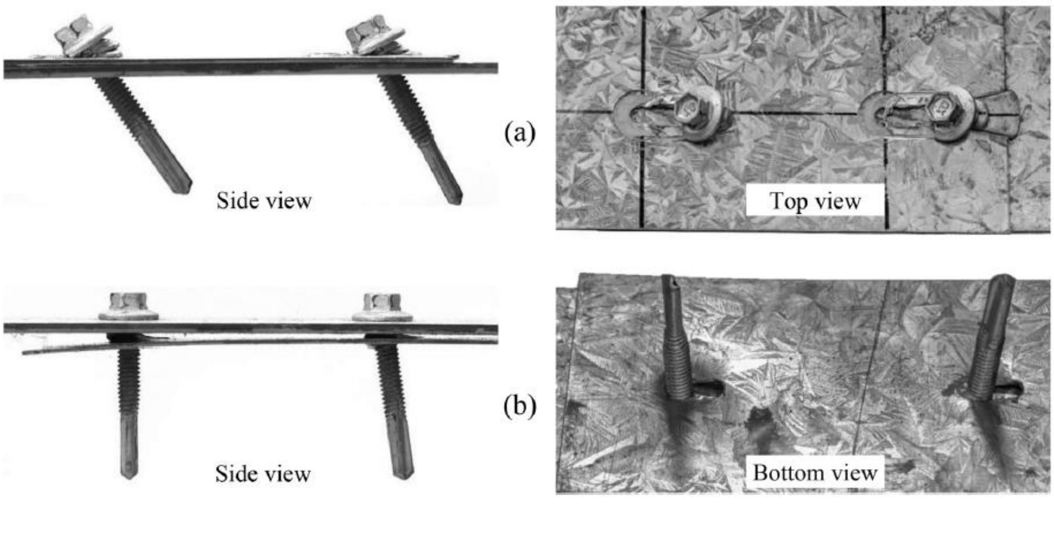

Figure 2- 26: Bearing and tilting failure for G12-24TPI screws [20]

Table 2- 2: Bearing and tilting tests results [20]

Screws	Screw Diameter d_f (mm)	Nominal steel thickness t_1-t_2 (mm)	Test results (kN)			Mean Strength V_{ut} (kN)	St. dev. (kN)	C.o.V.
			1	2	3			
G12-24TPI	5.5	0.75–1.2	6.09	5.74	6.04	5.96	0.19	3.2%
	5.5	0.75–1.9	7.94	8.06	8.14	8.05	0.10	1.3%
	5.5	1.0–1.2	7.14	7.17	6.91	7.07	0.14	2.0%
	5.5	1.0–1.5	7.89	7.85	7.56	7.77	0.18	2.3%
	5.5	1.0–2.4	11.40	11.12	11.49	11.34	0.20	1.7%
	5.5	1.0–3.0	12.27	11.23	11.54	11.68	0.53	4.6%
	5.5	2.4–1.0	7.73	8.18	8.63	8.18	0.45	5.5%
	5.5	3.0–1.0	8.73	8.07	8.43	8.41	0.33	4.0%
G14-10TPI	6.3	1.0–2.4	11.87	12.54	11.49	11.97	0.53	4.5%
	6.3	2.4–1.0	7.64	7.69	8.05	7.79	0.22	2.9%
G14-20TPI	6.3	1.0–1.5	8.36	8.04	8.40	8.27	0.19	2.3%

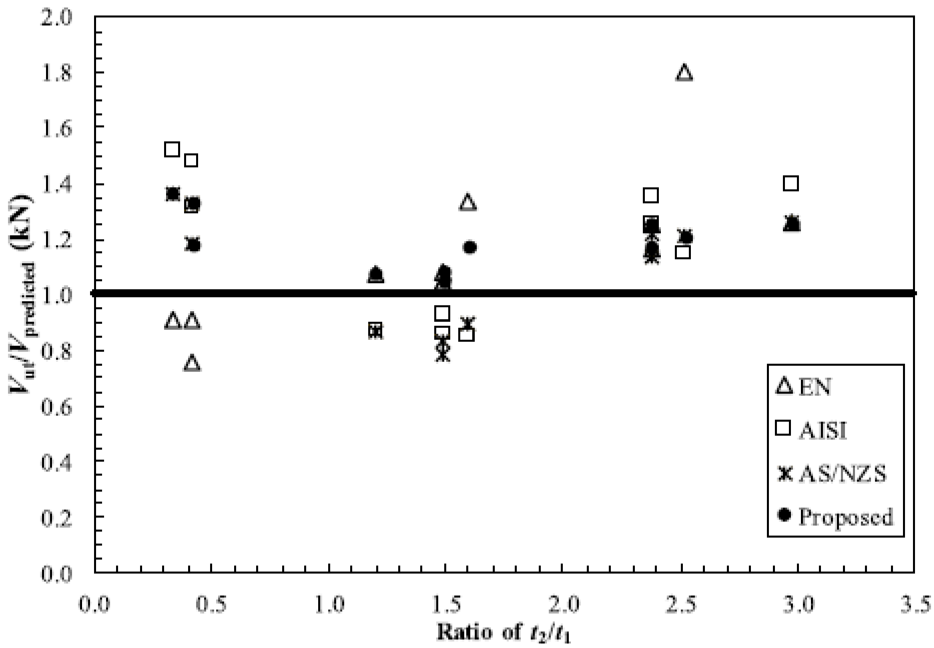

Figure 2- 27: $V_{ut}/V_{predicted}$ vs. t_2/t_1 [20]

High-fidelity finite element modelling of screw-fastened connections subjected to cyclic reversible loading on ABAQUS is very challenging even when solid elements are included. Connector sections and point-based fasteners are very good options for modelling screws but only when the screw-fastened connections are subjected to monotonic loading. Ding et al. [21] conducted a research on the FEM of self-drilling screws used in cold-formed steel framing of shear walls, subjected to monotonic and cyclic loading. A new approach for modeling the self-drilling screws was introduced by Ding et al. [21] in which an ABAQUS user element subroutine (UEL) was written in FORTRAN and used for the screws' model. The model successfully simulated the nonlinear hysteric behavior of the screw fastened CFS connections in which strength and stiffness degradation and pinching took place. OpenSees was also used for modelling the self-drilling screws and the results were verified against experimental tests fig (2-28).

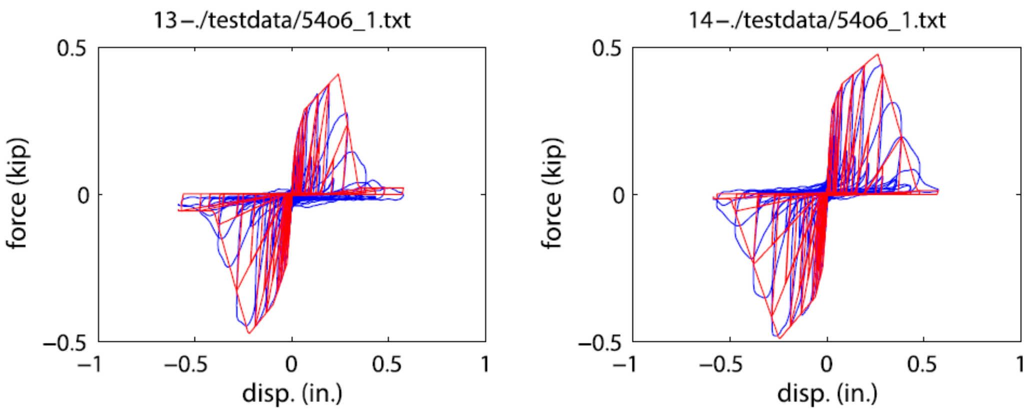

Figure 2- 28: CFS-sheathing connection test results against results against calibrated Pinching4 hysteresis Opensees [21]

In order to capture the pinching that takes place when self-drilling screws are subjected to cyclic loading, Ding et al. [21] defines four pinching states Figure (2-29): State 1, State 2, State 3 and State 4. State 1 and State 2 represent the positive and negative backbone curves respectively, and the boundaries of these curves are the maximum deformations in each direction. States 3 and 4 represent the unloading and reloading properties of the element so that the degradation of strength and stiffness are captured. The load path in states 3 and 4 can be linear, bilinear, or trilinear based on the load-deformation data. The change in states occurs when the loading direction changes as in the case of cyclic loading or when loading takes place beyond state boundaries which triggers the degradation of stiffness and strength. The state-change relationship is illustrated in figure (2-30). Figure (2-31) illustrates the positions of the UELs that were used to model the self-drilling screws, and figure (2-32) illustrates the ABAQUS load-deformation results where it can be noticed the behavior of individual fasteners affects greatly the cyclic response of the shear walls.

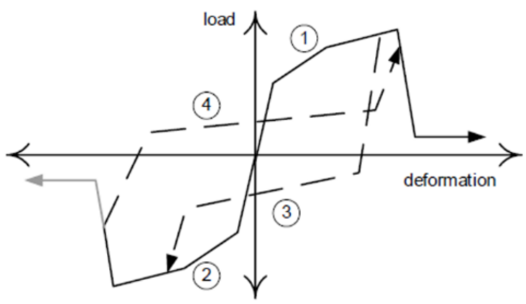

Figure 2- 29: Pinching material states [21]

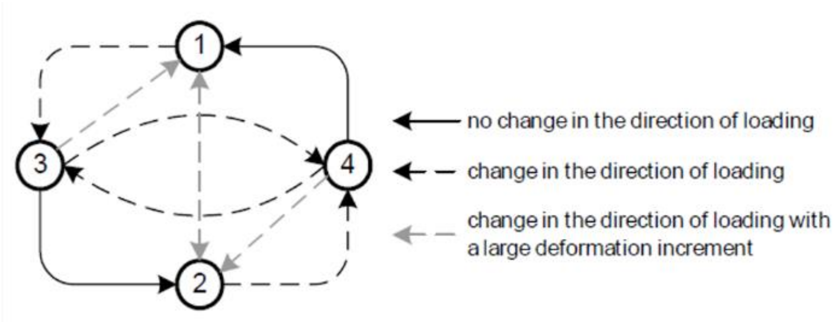

Figure 2- 30: State changes rules [21]

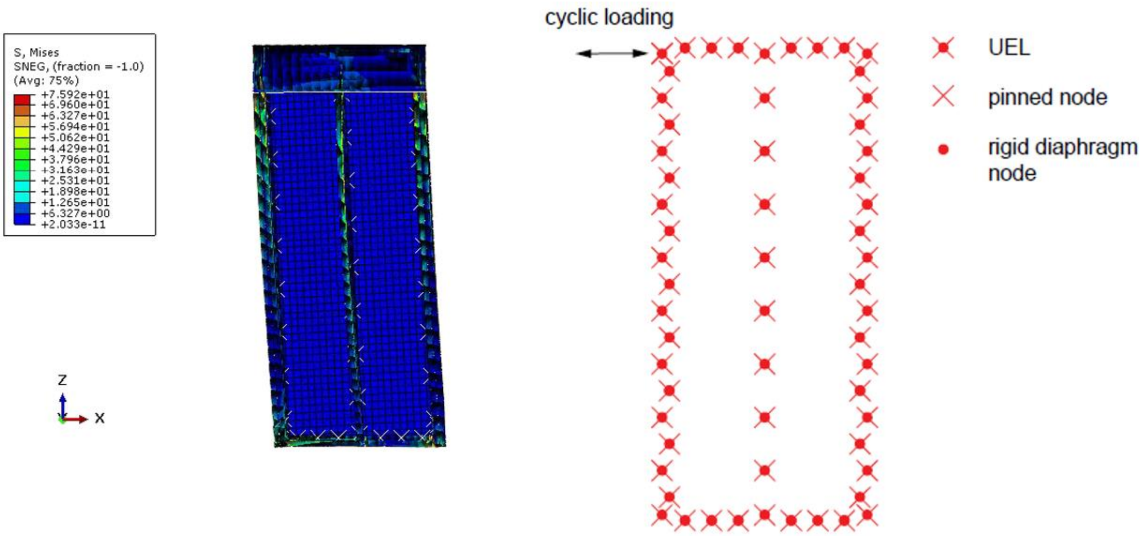

Figure 2- 31: UEL self-drilling screws' location in the model [21]

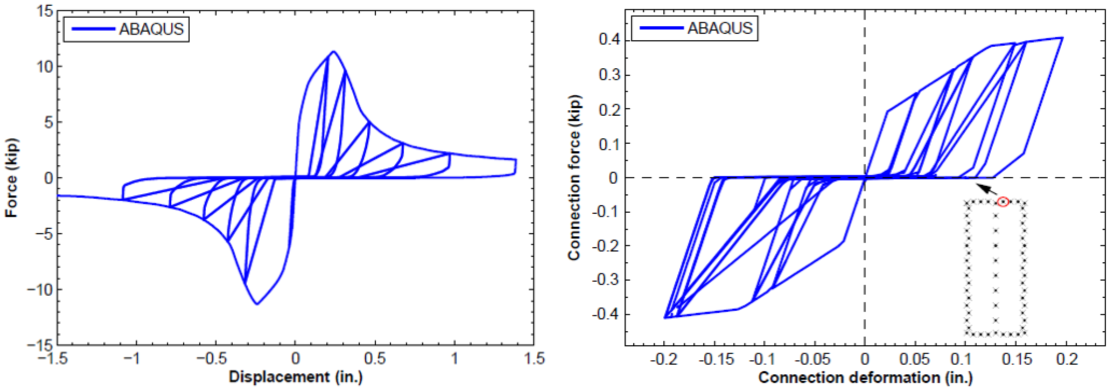

Figure 2- 32: Load-deformation relationships for (left) shear wall (right) single screw [21]

Kechidi et al. [22] investigated the modeling of CFS back-to-back C-channels fastened using self-drilling screws Figure (2-33) and subjected to axial monotonic and cyclic loading. The results of the models developed were validated against experimental tests where 17 back-to-back CFS columns were simulated. The aim of the research was to further investigate the behavior of CFS columns under monotonic and cyclic loading where self-drillings screws were used and to provide a framework for finite element modelling of built-up CFS columns using ABAQUS software. Non-linear material and geometry were included in the model where coupon tests were used to identify the true stress-strain curves for steel while laser-scanning of the column specimens were used to identify the geometric imperfections. Moreover, the User-Element subroutine developed by Ding [21] was used to model the self-drilling screws connecting the back-to-back built-up columns. The deformed shapes, collapse mechanism and load-deformation curves of the FE models were found to be in a very close agreement with those obtained from the experimental results Figure(2-34).

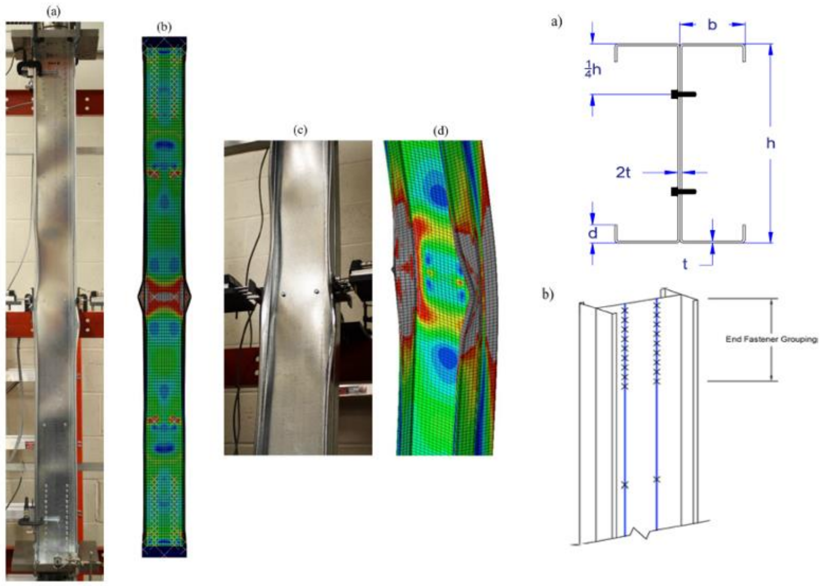

Figure 2- 33: Experimental vs. numerical deformed shapes [22]

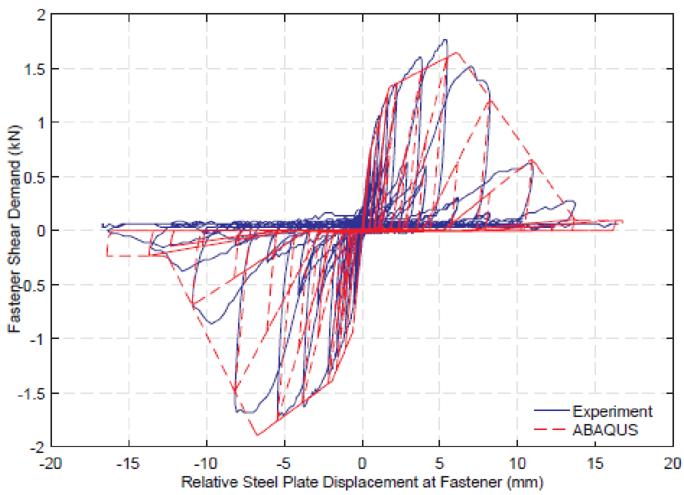

Figure 2- 34: Experimental vs. numerical load-deformation curves [22]

Previous researches mentioned in this chapter provides multiple approaches either for experimental testing or numerical modelling and analysis of the CFS members and connections. From the literature, it was found that screw-fastened connections were not used as moment connections before, therefore in this research, beam-to-column moment connections using screw-fasteners and bolts will be investigated while previous research findings from the literature is considered. Finally, the techniques adopted for numerical modelling of the specimens will be discussed in Chapter 4.

Chapter 3 : Experimental Work

3.1. Introduction

Experimental testing of steel connections is very important especially if these connections are expected to resist seismic actions. According to ASCE/SEI 41-71, a minimum of 3 tests subjected to cyclic loading should be performed for any connection expected to resist seismic forces. In this chapter, the experimental part of the research is explored where three cold-formed steel, beam-to-column moment connections are tested against quasi-static cyclic loading. The aim of the test is to provide load-deformation (moment-rotation) relationships, measure the ultimate moment capacity, obtain the energy dissipation capacity, and observe the behavior of screw-fastened and bolted connections subjected to cyclic loading. These tests will be used for verification of finite element models developed for a parametric study at a later stage.

3.2. Experimental Investigation

3.2.1. Specimens Description

Lipped cold-formed C-channel has proven to be a better choice over channels without lip (U-shaped), therefore, the cross-sections that were used for the study were the lipped back-to-back double C-section of dimensions 200x60x20x2 illustrated in Figure (3-1). The section used for beams is identical to that used for columns, however, the boundary conditions differ.

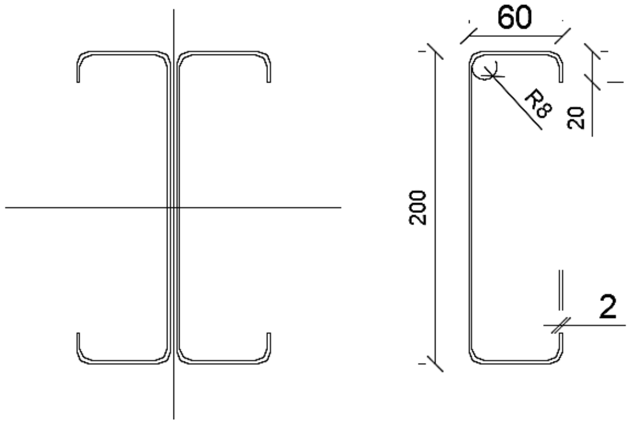

Figure 3-1: CFS cross-section dimensions

3.2.2. Material Properties

The specimens were manufactured in Engineering Metal Construction Company in Egypt (EMCON). Although the steel material properties were provided by the company before manufacturing, tension tests were performed as standard size coupons were taken from the steel plates that were used and tested in tension. Moreover, the self-drilling screws used in the tests were also tested in shear. Finally, the bolts used were grade 4.6 but no tests were performed on the bolts.

The stress-strain curve obtained from the coupon tensile testing is presented in Figure (3-4), while Figure (3-2) and Figure (3-3) illustrate the specimens during and after the test, respectively. Table (3-1) illustrates the tests output. The average values of yield stress for CFS taken as 350 MPa and the average values of ultimate stress taken as 450 MPa.

Table 3- 1: Steel Properties from tensile tests

Specimen ID	Dimensions		Yield Strength (MPa)	Ultimate Strength (MPa)	Elongation (%)
	t	b			
SP01	2.58	46.98	325	420	21
SP02	2.37	52.95	357	457	21
SP03	2.32	49.46	365	471	24

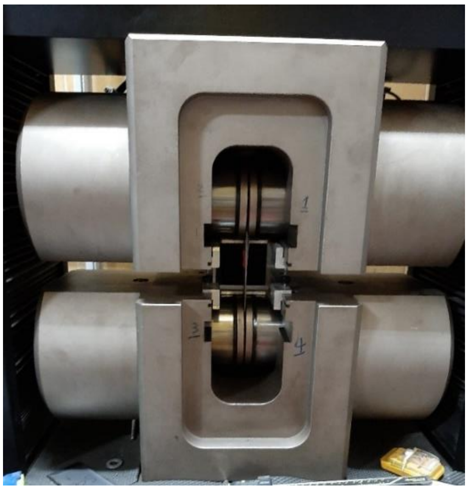

Figure 3-2: Coupon tension testing

Figure 3- 3: Specimen after tension testing

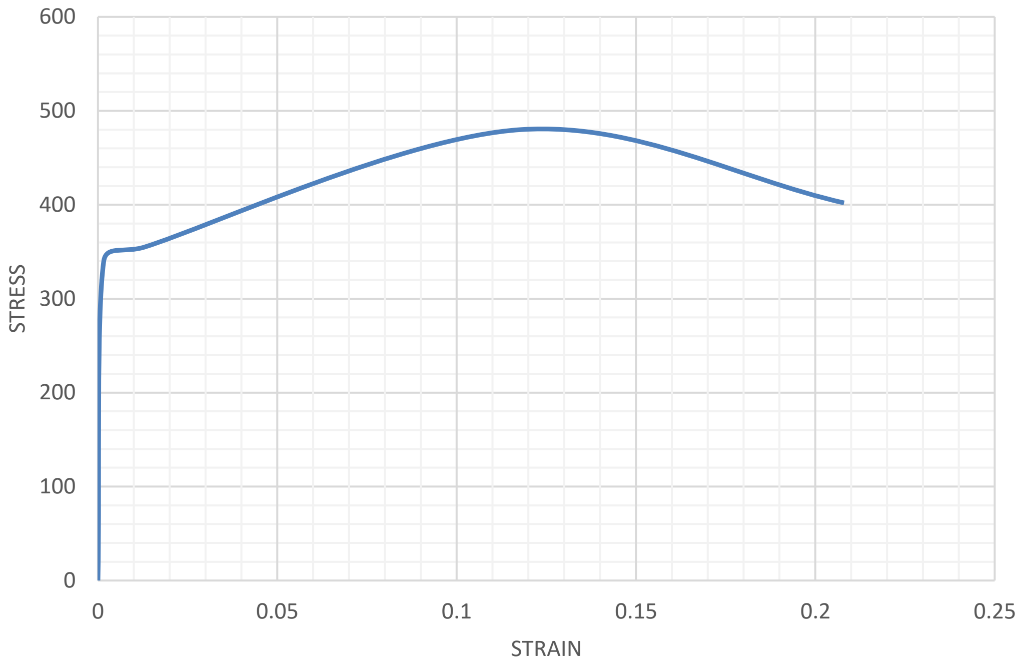

Figure 3-4: Stress-Strain relationship obtained from tension tests

Self-drilling screws were used to connect two steel plates and tested in shear as mentioned earlier. The specimen during and after the tests are presented in Figure (3-5).

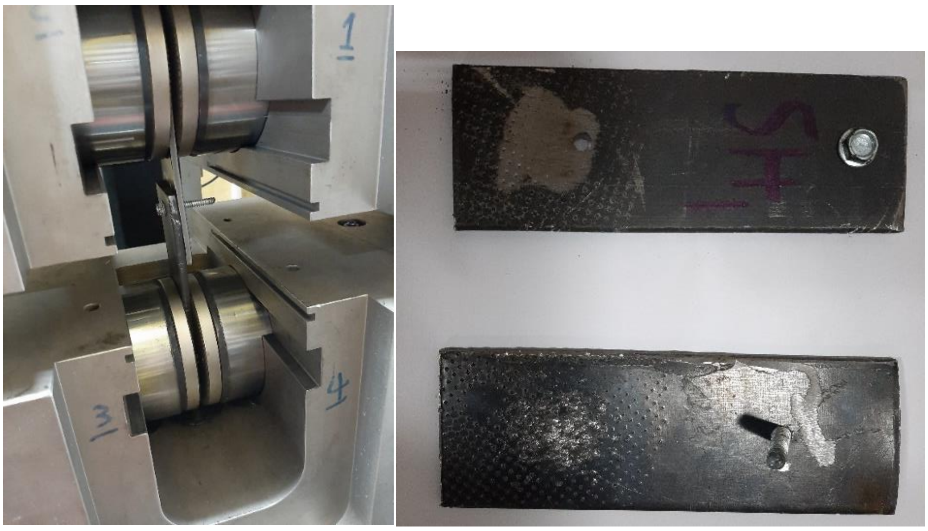

Figure 3- 5: Shear testing of self-drilling screws during (left) and after (right) testing

3.2.3. Test Configuration

As mentioned earlier, the tests are performed on beam-to-column moment connections, therefore, the specimens used in the study were cantilever frames with the same test configuration illustrated in Figure (3-6) while changing some parameters in the test.

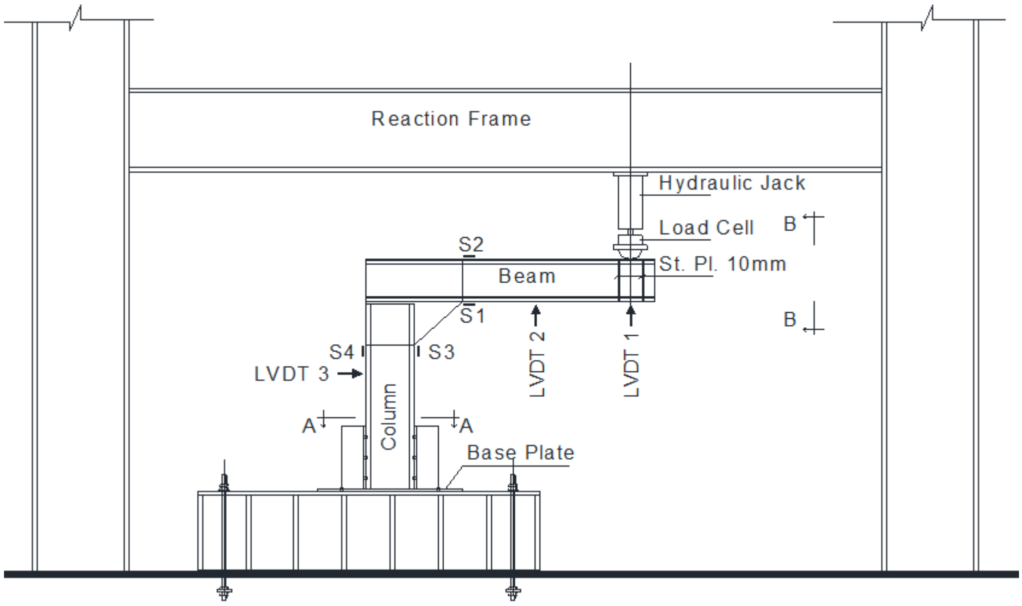

Figure 3- 6: Test configuration

The load cell that was used in the tests is capable of load reversal, therefore, the beam-to-load cell connection needs to fit this purpose as illustrated in Figure (3-8). The details of the tested specimens are provided in Figure (3-7), (3-9) and (3-11). As previously mentioned, three specimens were tested and self-drilling screws were used for two of these specimens designated as Sp-1 and Sp-2, while bolts were used for the third specimen designated as Sp-3. Sp-2 differs from Sp-1 as an additional plate connecting the column flanges to the beam top flanges was used as illustrated in Figure (3-10). Specimens Sp-1 and Sp-3 have the same layout and fasteners arrangement, the only difference is the type of fastener used. LVDTs were used to record the displacements at different locations in the specimen as noticed in Figure (3-6). Moreover, strain gages were also used to record the strains at critical locations in the beams and columns. Figure (3-13b) illustrates a sample of attaching strain gages to a specimen. The details of the tested specimens are summarized in Table (3-2).

Table 3- 2: Details of the tested specimens

Specimen ID	Fasteners Type	Fastener Diameter	Gusset Plate Thickness	Additional Top-plate
Sp-1	Screws	6	3	-
Sp-2	Screws	6	3	Yes
Sp-3	Bolts	12	2	-

Another very important element in the tests was the lateral support at mid-span of the beam. Initially, lateral supports of wooden boxes surrounding the beam cross-section and connected to posts rested on the ground were used Figure (3-13c), however, it was noticed in preliminary testing that these posts are not sufficient to act as lateral supports. Consequently, a steel lateral support manufactured specifically for the test and fixed to the ground beam was made. Figure (3-13d) illustrates the workers effort to lubricate the surface were the lateral support and the beam flanges interact so that the friction between these surfaces do not contribute to the beam resistance to vertical load.

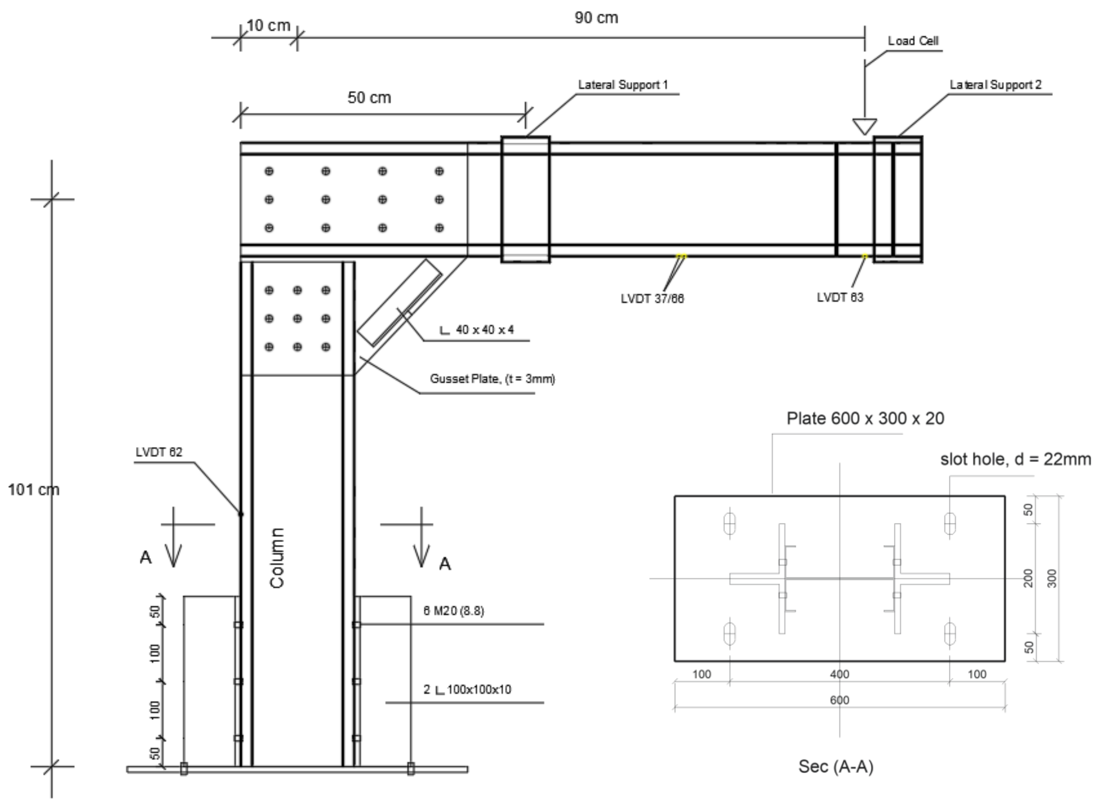

Figure 3-7: Specimen "Sp-1" details

Figure 3-8: Specimen "Sp-1" before testing

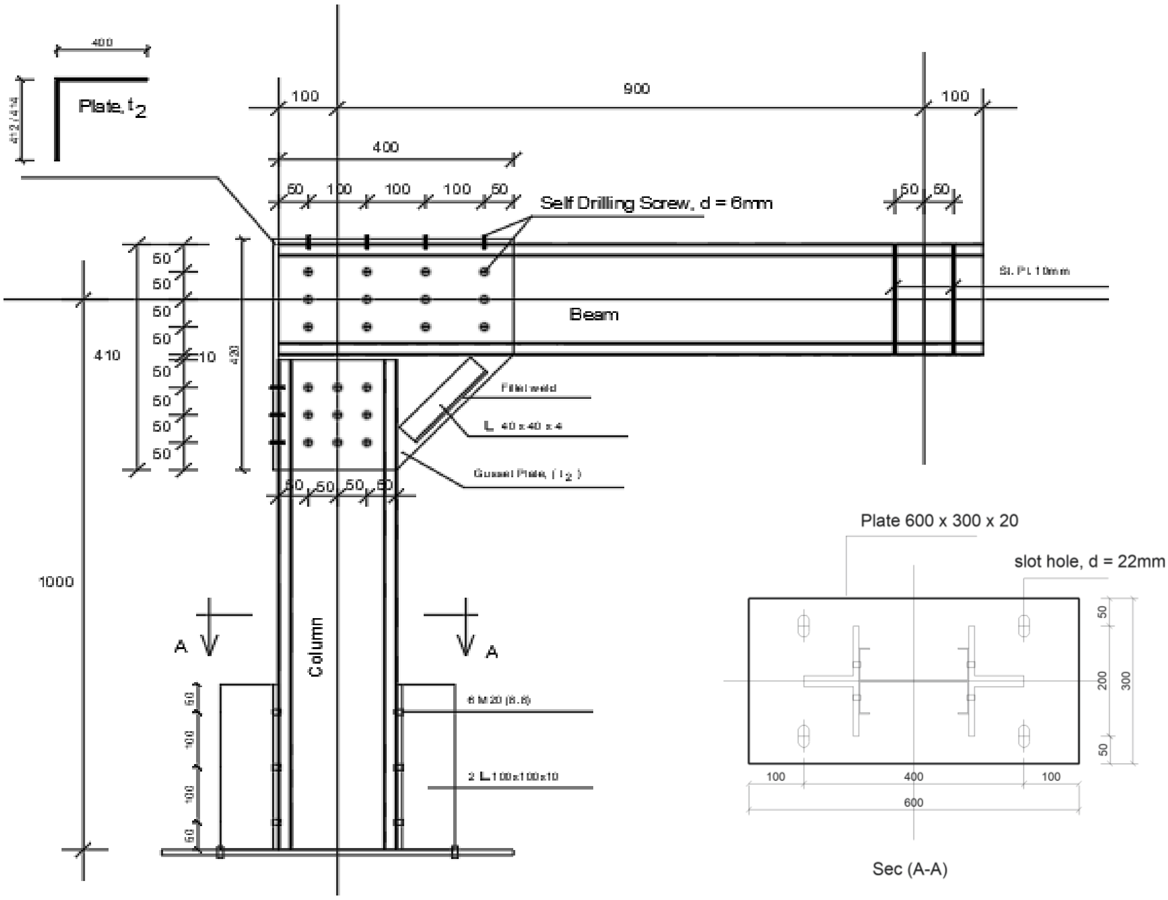

Figure 3- 9: Specimen "Sp-2" details

Figure 3- 10: Specimen "Sp-2" before testing

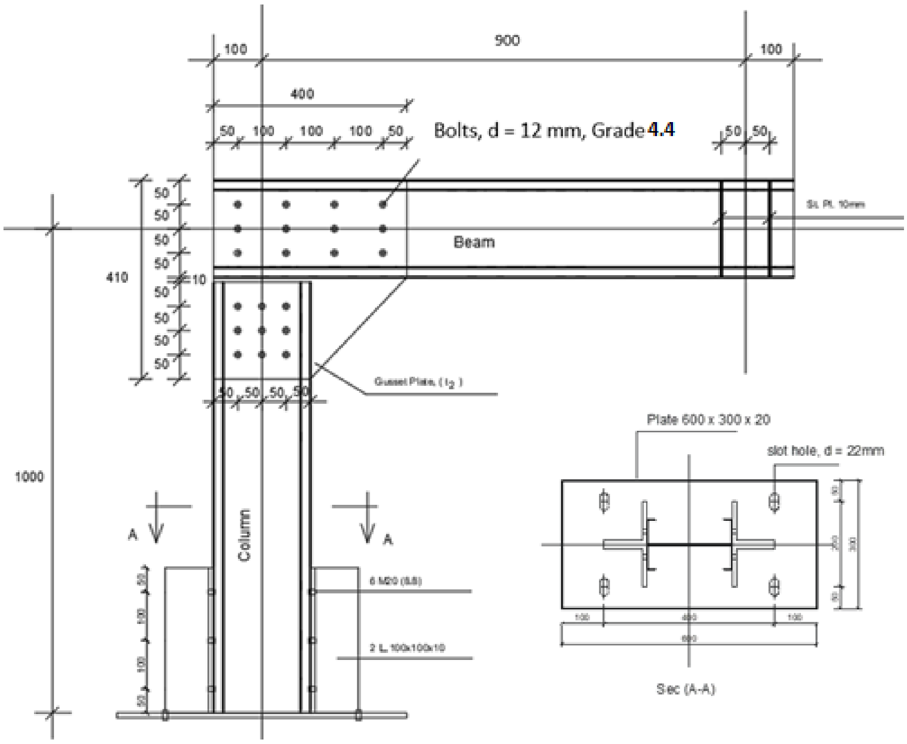

Figure 3- 11: Specimen "Sp-3" details

Figure 3- 12: Specimen "Sp-3" before testing

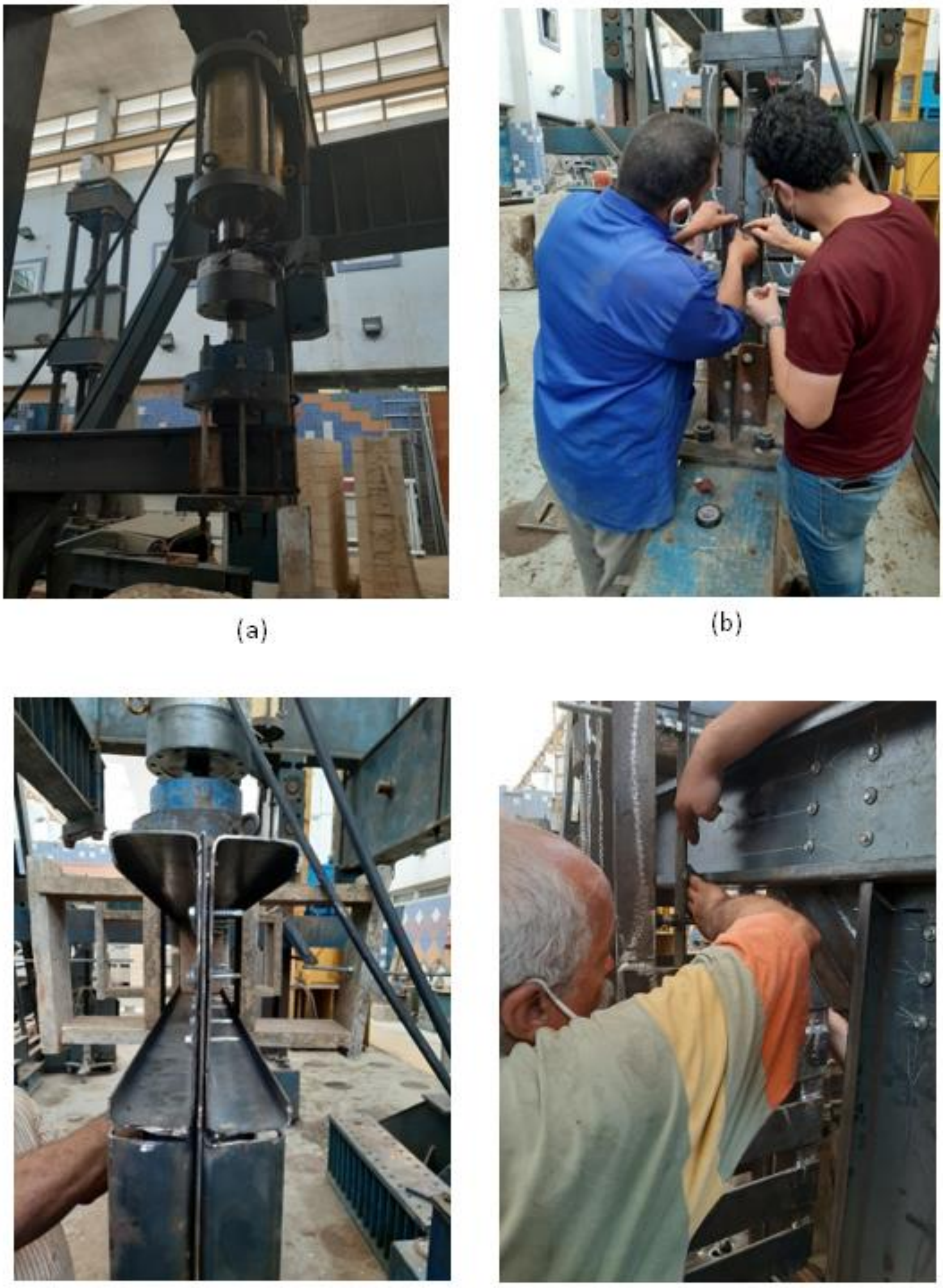

Figure 3- 13: (a) Load cell (b) strain gages installation (c) old lateral support (d) new lateral support

3.2.4. Imperfections

Initial geometric imperfections can cause a reduction in strength and stiffness in members. Measurement of plates thicknesses were done to check for any imperfections Figure (3-14), however, some imperfections were visible in the specimen. Geometric imperfections can be captured accurately using laser scanning of the members or other less accurate devices can be used such as using total station, theodolite, or tapes and vernier calipers.

Figure 3- 14: Measuring gusset plate thickness

Figure 3- 15: Measuring CFS plate thickness

3.3. Experimental Results

Cyclic loading is essential for testing structural elements prone to seismic actions. The AISC cyclic loading protocol was adopted for testing the three specimens. Figure (3-16) illustrates graphically the number of cycles and applied displacements on the specimens.

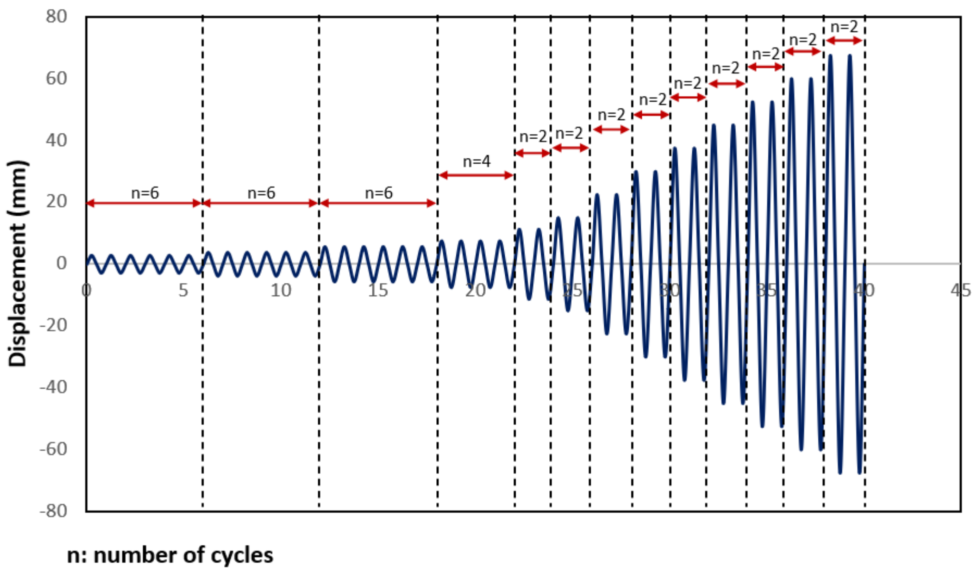

Figure 3- 16: Graphic illustration of cyclic load protocol adopted from AISC 341

As displacements were applied to the specimens through the load cell as indicated previously, the resistance of the specimens was recorded and so as the behavior of the connections tested. The load-deformation output for specimen Sp-1 is illustrated in Figure (3-17). Moreover, it was noticed that the failure mode for Sp-1 consisted of tilting in the screws connecting the column webs to the gusset, illustrated in Figure (3-18). It was also noticed that no buckling or permanent deformations took place anywhere in the gusset or the cross-sections of the beams and columns Figure (3-18).

Specimen Sp-2, where an additional plate connecting the flanges of the column to the top flanges of the beam, had a similar behavior in terms of the failure mode. Tilting of the screws can be observed in Figure (3-21b) and Figure (3-21c) though it is not obvious as screws in Sp-1. In addition, the gusset plate and the column webs began to buckle when large deformation cycles were applied. Moreover, deformation of the beam flanges under the bent plate can also be observed in Figure (3-21a) and Figure (3-21d). The hysteresis loops from the load-displacement output of the test are illustrated in Figure (3-20).

The last cyclic load test conducted was on specimen Sp-3 where ordinary bolts of grade 4.6 were used as fasteners rather than using self-drilling screws. The behavior was very different compared to Sp-1 and Sp-2, as the gusset plate buckled forcing the column flanges to buckle as well, as presented in Figure (3-23) and Figure (3-24). The load-displacement hysteresis loops for Sp-3 were remarkably different as illustrated in Figure (3-22)

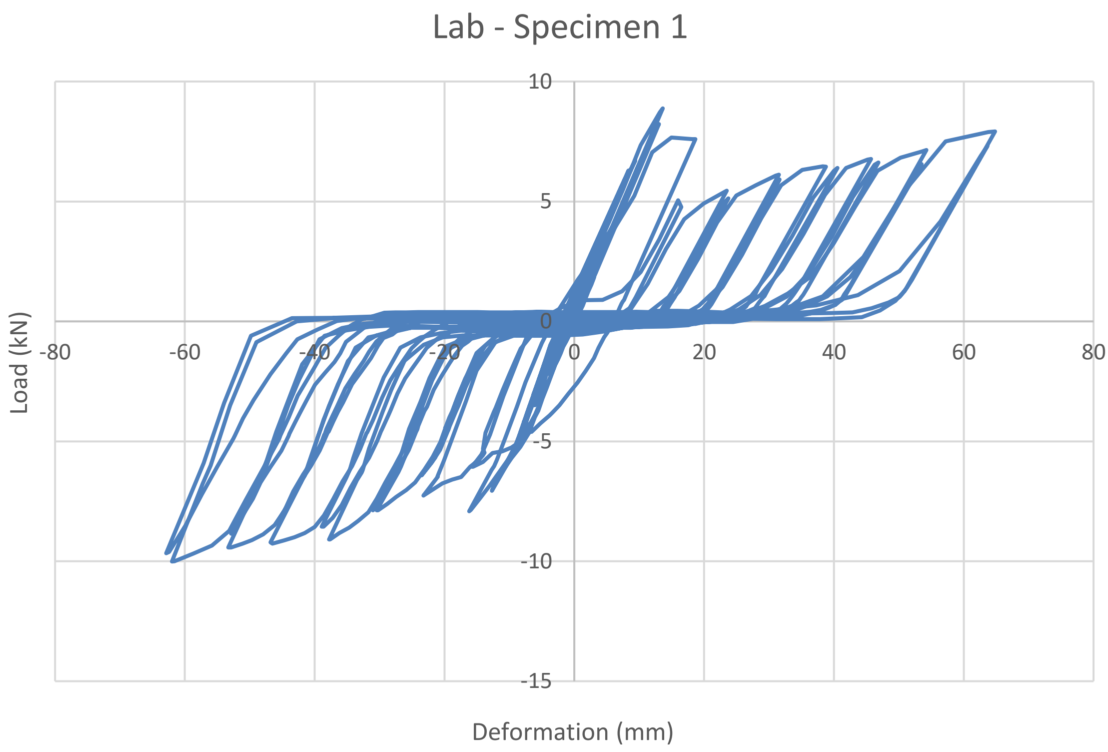

Figure 3- 17: Load-deformation hysteresis loops from "Sp-1" testing

Figure 3- 18: Deformations observed during “Sp-1” downward displacement

Figure 3- 19: Deformations observed during “Sp-1” upward displacement

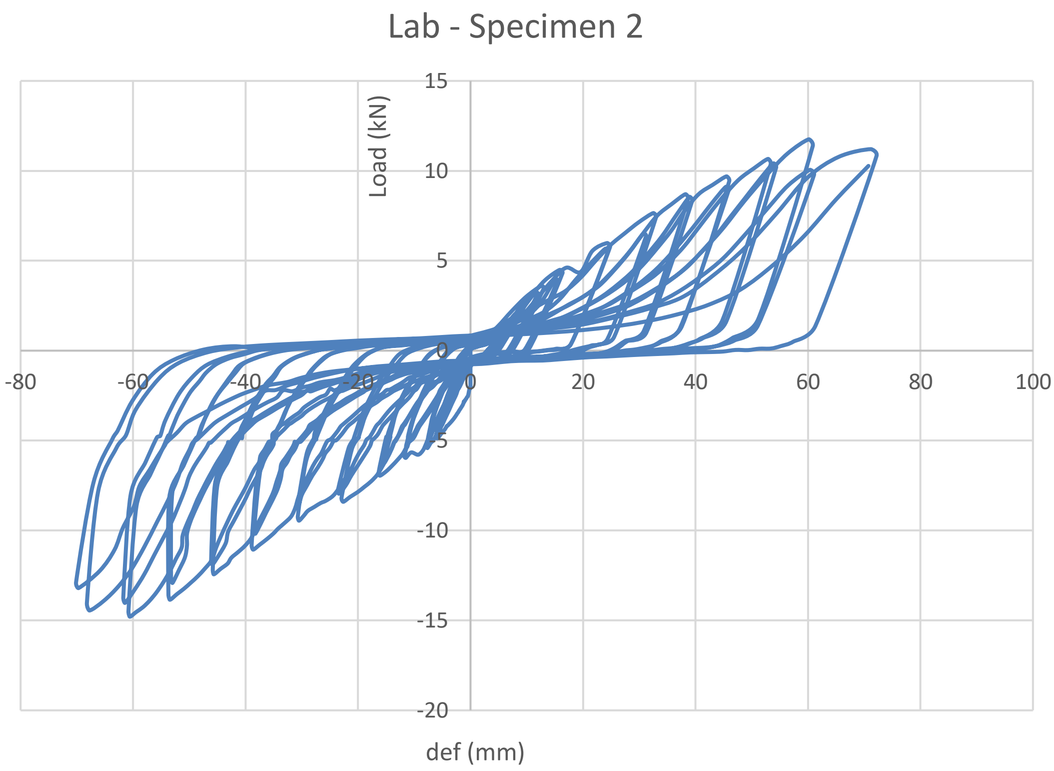

Figure 3- 20: Load-deformation hysteresis loops from "Sp-2" testing

Figure 3- 21: Deformations observed in "Sp-2" (a) beam top flange buckled under the bent plate (b) tilting in screws in the column web (c) tilting in screws of the column flange (d) slight deformation in the column web

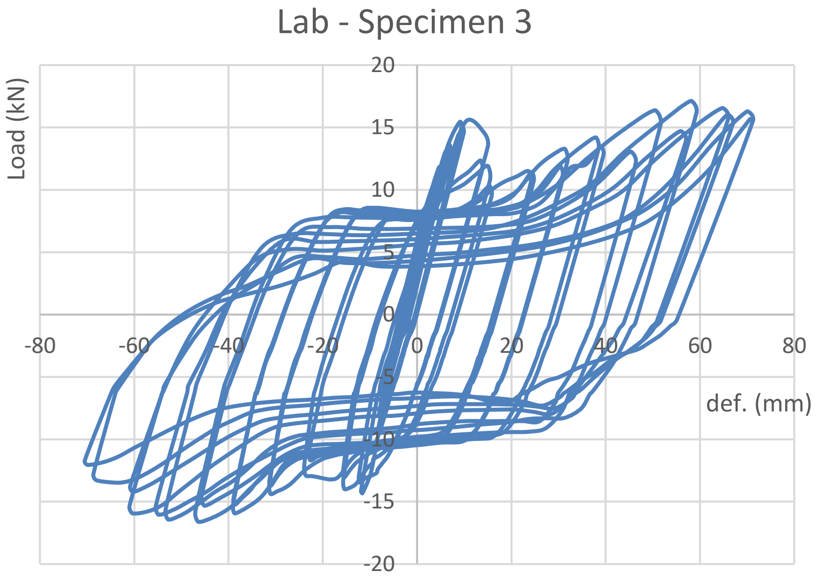

Figure 3- 22: Load-deformation hysteresis loops for "Sp-3"

Figure 3- 23: Deformations observed in "Sp-3"

Figure 3- 24: Buckling of the gusset plate in "Sp-3"

3.4. Analysis of Experimental Results

An analysis of the three tests is conducted by comparing the results of the three tests output. In Figure (3-25), the load-displacement hysteresis loops are plotted against each other to compare the shapes of these loops. First, it can be noticed for Sp-1 and Sp-3 that at the beginning of the tests, high resistance is recorded. This is attributed to the spot welds that were used for fabrication of the connections. These spot weld soon broke due to the cyclic nature of the applied load and the connection began to behave normally afterwards, therefore, the records of high resistance that were noticed at the beginning of the test were ignored in the analysis of the data.

It can be noticed that the bolted connection was superior in terms of peak reaction forces/moments recorded and plumpness of the hysteresis loops. The plumpness of hysteresis loops is an indication of the energy dissipated during the tests in addition to the area under the cyclic envelope curve of peak forces or moments. Screw-fastened connections have a unique shape of hysteresis loops as mentioned earlier in the literature and noticed in this research. This proves that the tests conducted are in conjunction with previous research done in the field of screw-fastened cold-formed steel connections. The cyclic envelopes of the three tests are also provided in Figure (3-26) to compare the peak reaction forces recorded. It can be noticed that the bolted connection provided higher resistance compared to the screw-fastened connections, while the screw-fastened connection with additional top plate provided better resistance over the first specimen. The energy dissipated during the tests was calculated as the area under the cyclic envelopes in Figure (3-26) and a summary of the results is provided in Table (3-3). The bolted connection dissipated energy the most, then the screw-fastened connection with top plate, and finally specimen Sp-1 recorded the least energy dissipation capacity.

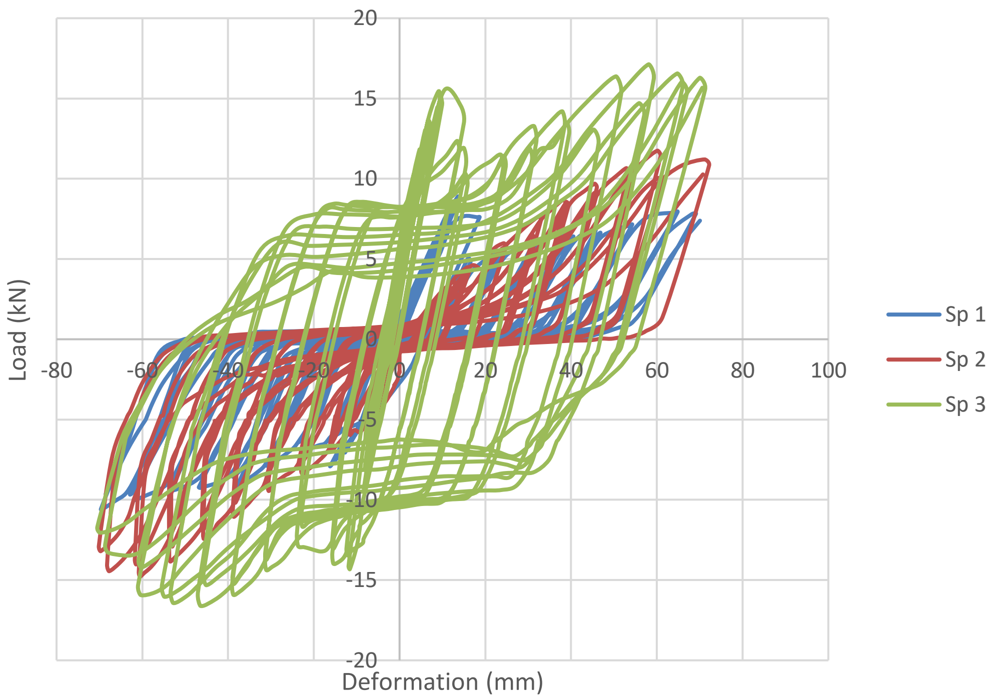

Figure 3- 25: Load-deformation hysteresis loops for the three tested specimens

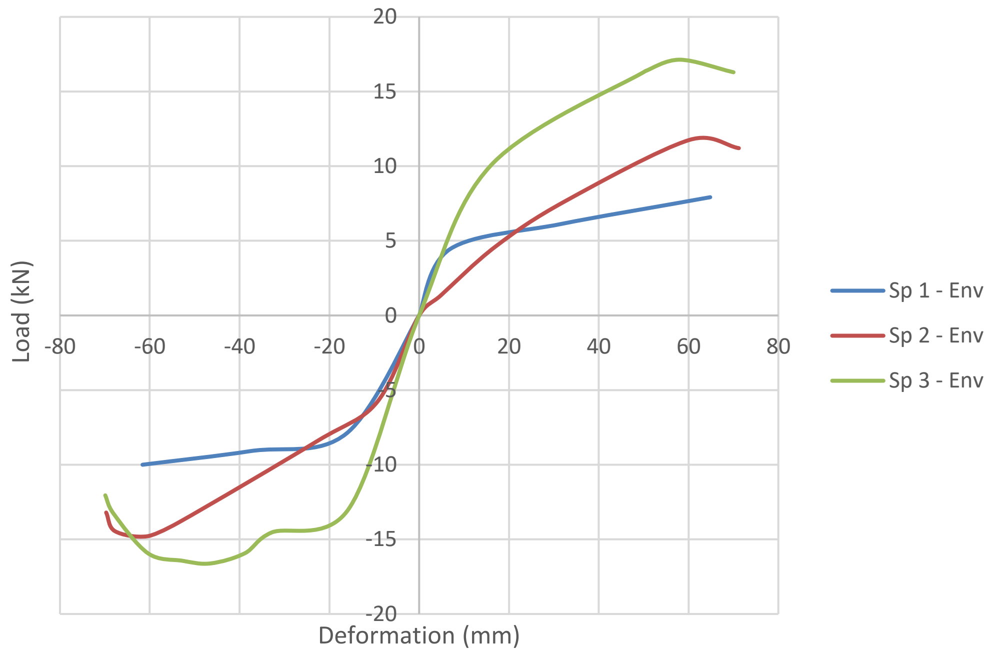

Figure 3- 26: Cyclic envelope of the curves

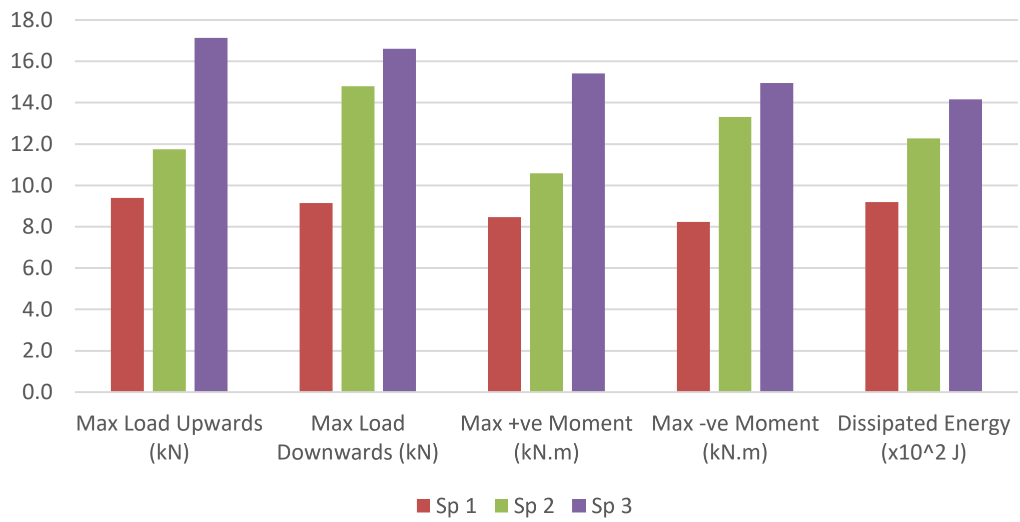

Figure 3- 27: Graphical comparison of the results

Table 3- 3: Summary of lab results

	Sp 1	Sp 2	Sp 3
Max Load Upwards (kN)	8.0	11.8	17.1
Max Load Downwards (kN)	-10.0	-14.8	-16.6
Max +ve Moment (kN.m)	7.2	10.6	15.4
Max -ve Moment (kN.m)	-9.0	-13.3	-14.9
Dissipated Energy (J)	854.4	1228.0	1779.0

3.5. Concluding Remarks

This chapter discussed the experimental work done in this research. Three cyclic tests were conducted, and the following is concluded:

- Screw-fastened connections are capable of withstanding cyclic reversible load and capable of dissipating energy in the process
- Bolted connections provided 82% higher strength over the screw-fastened connection SP1 and 45% higher than SP-2 when displacements were applied in the upward direction
- Bolted connections provided 82% higher strength over the screw-fastened connection SP1 and but only 12% higher than SP-2 when displacements were applied downwards
- Bolted connections was also superior in terms of energy dissipation as the estimated dissipated energy record for SP-3 was 54% higher than SP-1 and 15% higher than SP-2
- Consequently, adding an additional top plate to the screw-fastened connection improves the moment capacity within a range of 25% to 63%, and the energy dissipation capacity of the connection by 34%

Finite element modelling of CFS connections are discussed in the next chapter and the approaches adopted in modelling the experimentally tested connections are then presented.

Chapter 4 : Finite Element Modeling

4.1. Introduction

The finite element analysis and modelling of complex engineering systems is considered a pillar for the simulation and prediction of the behavior of these systems either in the field of research or design. Since finite element analysis (FEA) has become very popular and very essential, educational and academic engineering firms included commercial FEA packages, that have gained acceptance and trust from engineers and researchers, in the undergraduate and graduate levels to cover both the theoretical and practical aspects of the finite element analysis.

This chapter is divided into three main sections:

1. **FEM of cold-formed sections**
2. **FEM of bolted Connections**
3. **FEM of screw-fastened Connections**

Techniques adopted in previous research for modelling and analysis of CFS, bolted connections and screw-fastened connections will be briefly explored, and the tools and techniques adopted in this research will be thoroughly explained. Moreover, verification of the finite element models developed for the bolted connections and screw-fastened connections is provided where numerical models are compared to experimental results in terms of general behavior of the connections, ultimate moment capacity and energy dissipation capacity.

4.2. FEM of Cold-Formed Sections

In this section, the techniques used for modelling cold-formed steel sections (CFS) are discussed. This research follows most of the approaches adopted in previous research for modelling CFS.

4.2.1. Geometric Modelling

Developing a 3D model of the specimens require components to be generated in a certain sequence and then assembled. The beam, column and gusset plate were modeled as parts, then the whole assembly is brought together in the assembly module on ABAQUS. Finally, Bilinear material model is adopted for the CFS parts with yield stress and ultimate stress defined as obtained from the coupon tensile testing.

4.2.2. Meshing and Element Types

CFS are generally classified as thin structures compared to their other dimensions, consequently, the most suitable finite element type to be used for CFS is the shell element. A 4-noded general purpose shell element (S4R) is used for modelling beams, columns and gusset plates. A mesh size of around 25 x 25 mm can provide the adequate accuracy [23], [24], therefore, the beams and columns shells were modeled using a mesh size of 20 x 20 mm and the gussets were modeled using mesh size 10 x 10 mm.

4.2.3. Contact Modelling

Contact between different parts in the model is very essential in the behavior. "Contact pairs" are first defined then "surface-to-surface" contact type is applied. The properties of the surface-to-surface contact are then defined in two perpendicular directs. "Hard" contact properties are defined in the normal direction with slippage allowed between surfaces in the tangential direction [23], [24].

In the following sections, the finite element modelling techniques for bolted connections and screw-fastened connections are discussed. These sections include the models used for validation of the techniques adopted in this research.

4.3. FEM of Bolted Connections

Modelling of connections can be very challenging when it is required to simulate the behavior of these connections subjected to cyclic (reversible) loading protocol. There are several modelling techniques for the bolts that are commonly used for connections subject to monotonic loading. These techniques are straight forward and do not require extensive or complex procedures. One of which is the mesh independent point-based fasteners adopted by [23]–[26]. The schematic drawing shown in Figure (4-1) illustrates the idea of using the point-based fasteners where the location of the fastener need not to be at coincident with a mesh node. The ABAQUS user defines the influence radius which represents the bolt diameter, and the user can also define the linear/nonlinear elastic properties, plastic properties, fastener failure criteria, and several other properties. The location and the shape of the point-based fasteners are illustrated in Figure (4-2).

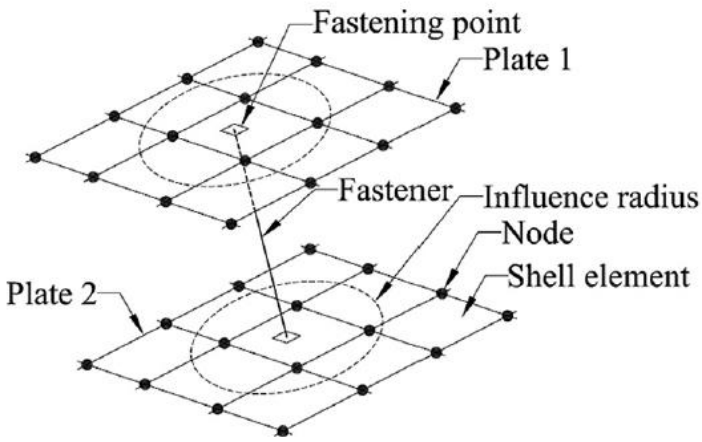

Figure 4-1: Mesh-independent fastener [23]

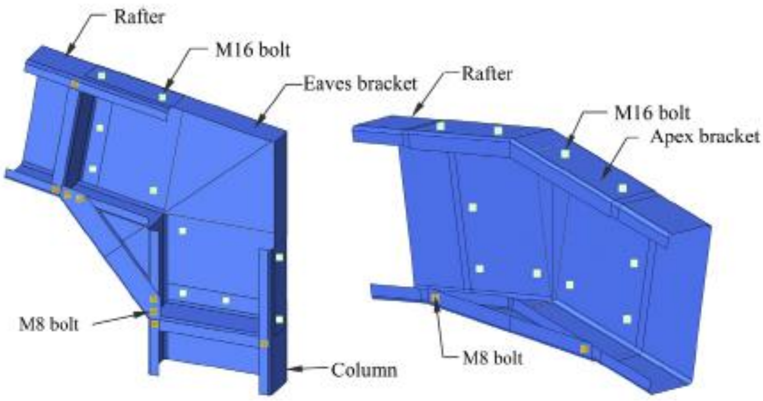

Figure 4-2: Mesh-independent deformable fasteners in steel connections [23]

Another technique that can be used for modelling bolted connection is using mesh dependent attachment line where the properties of the connector can be assigned to these lines (or wires as defined in ABAQUS) shown in Figure (4-3). This type of connector is less stiff than the point- based fasteners and in addition to the properties that can be defined for the point-based fasteners, connector sections provide other options such as STOP and LOCK, which are used in case the bolt hole diameter has some tolerance and the bolt hole is not in direct contact with the bolt shank. The use of such technique is suitable where pre-tensioned slip-critical bolts are used, and the idea is to define non-linear properties for the connector such that the load deformation relationship changes as soon as the forces exceeds the slip resistance of the bolts and the bolt shank comes in contact with the steel plates as illustrated in Figure (4-4). It can also be seen in Figure (4-3) that connectors are mesh dependent, meaning that they connect two nodes on two different meshes [14].

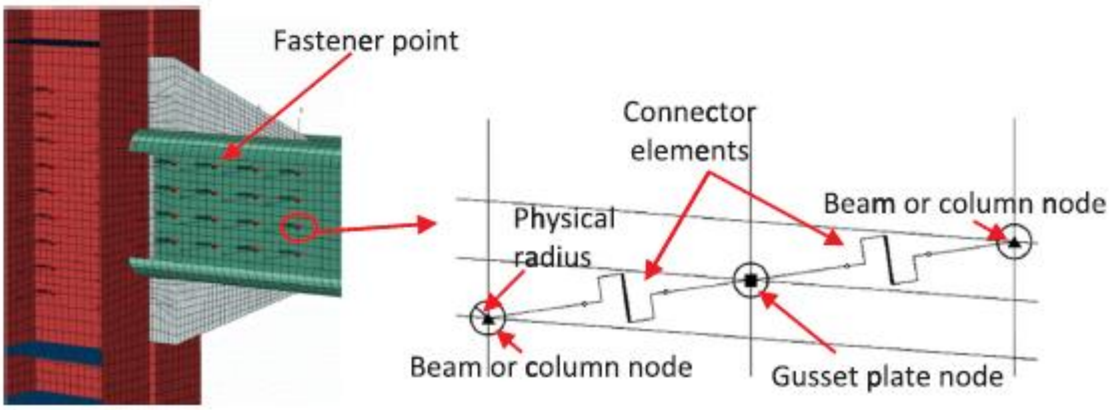

Figure 4- 3: FE model of the beam-column connection with fasteners [14]

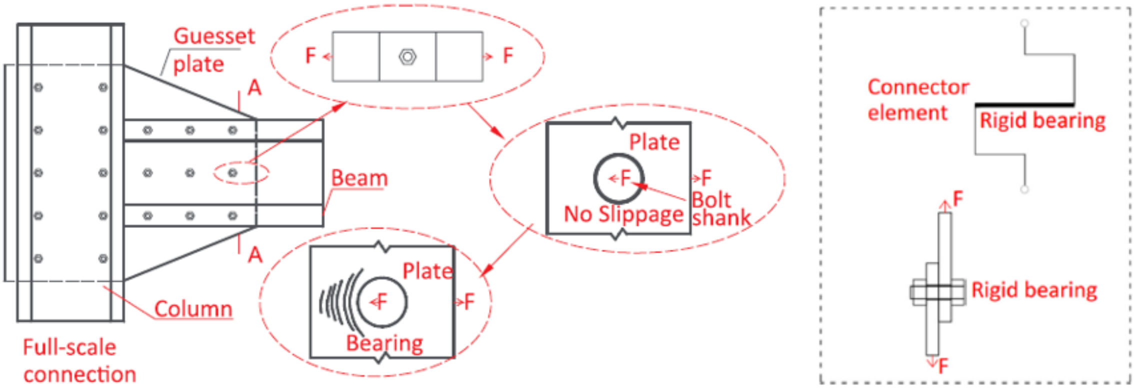

Figure 4- 4: Bolts slippage and bearing on the plates [14]

In this research, a different approach for modelling the bolted connections was adopted, which is using 4-node linear tetrahedron solid elements to make a 3D model of the bolt as shown in Figure (4-5). This is due to the fact that the connections tested were subjected to cyclic loading which may require a lot of approximations if either the mesh independent point-based fasteners or mesh dependent wire connectors were used. As illustrated in Figure (4-5), the bolt shank was modelled from the bolt head till the nut's washer rather than modelling its full length in order to reduce the number of nodes and elements in the model.

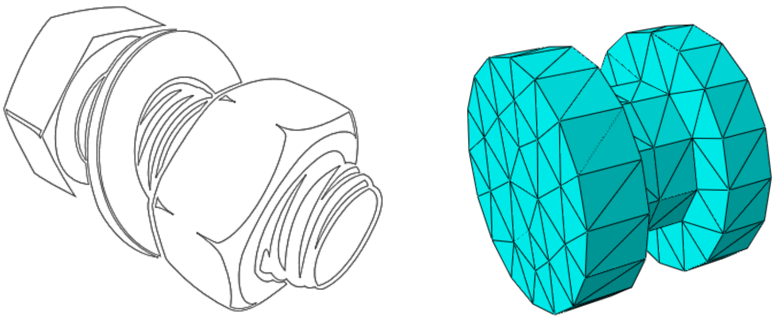

Figure 4- 5: Solid-element model for Bolts

A comparison between the point-based fasteners and full 3D solid element bolt model was conducted. A total of three models for a lap joint with two bolts spaced 100 mm between each other and with edge distances equals 50 mm were made: (1) Plates were modeled as S4R shell elements and point-based fasteners as the bolts, (2) Plates were modeled using 8-node solid elements (C3D8R) and bolts were modelled using 10-node quadratic tetrahedron (C3D10), (3) Plates were modeled as S4R shell elements and bolts were modelled using 10-node quadratic tetrahedron (C3D10).

Most of the previous research work in the field of cold-formed steel uses the point-based fasteners due to the fact that it is mesh independent, and it is straight forward in defining the properties of the bolts, however, it may require some calibration to capture the behavior of the bolted connection. Figure (4-6) shows the Von Mises stress contours from the lap joint simulated on ABAQUS, and figure (4-7) illustrates the load-deformation curve resulted from the same model. The material properties used for the plates were those obtained from the coupon testing of the cold-formed sections mentioned in Chapter 3, and the properties of the point-based fasteners were defined as elastic-rigid fasteners since no deformation or failure was noticed in the bolts when the experimental work was performed, the deformations noticed were in the plates only. It is worth mentioning that not only the modelling part is straightforward as mentioned earlier, but also the simulation time is the fastest among the three models made for this study.

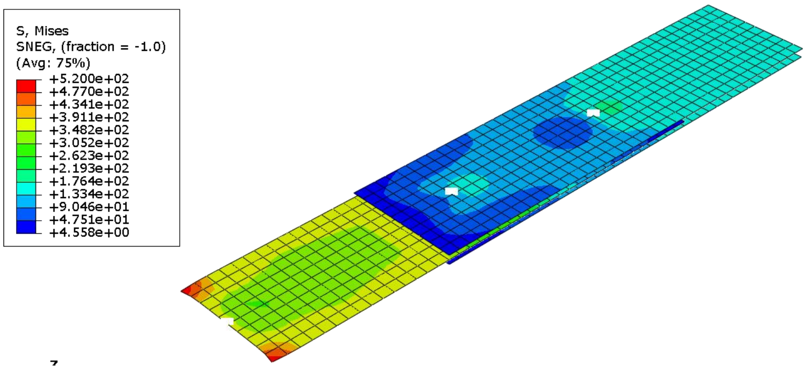

Figure 4- 6: Lap joint model (1)

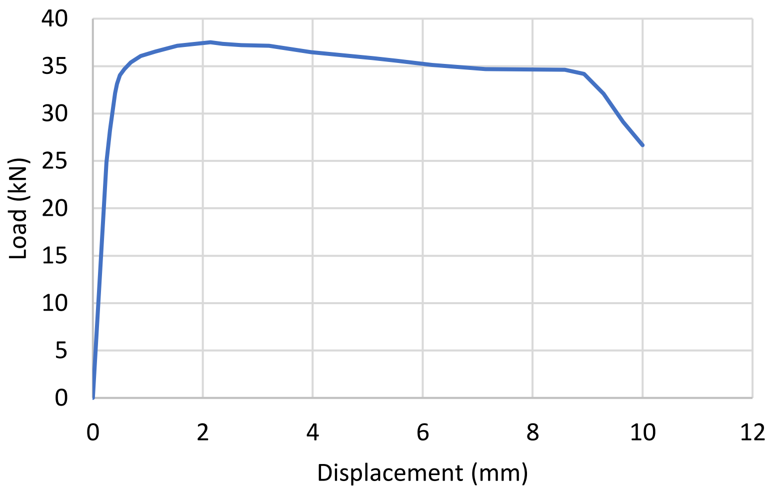

Figure 4- 7: Load-displacement relationship from model (1)

The second model used depends fully on solid elements either for the plates or the bolts. As mentioned earlier, 8-node solid elements (C3D8R) were used to model the plates and while 10-node quadratic tetrahedron (C3D10) were used to model the bolts. Figure (4-8) show the full model and shows the model with the bolts hidden from view to better show the Von Mises stresses. Figure (4-9) illustrates the load-displacement curve obtained for the same model. The advantage that this model gives over the previous method is that the bolt hole is presented in the model with two millimeters of tolerance, other than the fact that solid elements give more accurate results over shell elements in general.

It can be noticed from Figure (4-9) that at a load equals 15.2 kN, a flat plateau appears. This happens because a pretension force was introduced in the bolts causing friction between plates and when the acting forces reaches a certain limit, the plates start to slip until the bolt shank touches the inner surface of the holes and bearing between the bolts and the plates takes place. Although this phenomenon can be simulated using point-based fasteners, it will require further approximations to the model especially if these connections are subjected to cyclic loading and may result in convergence errors while running the simulation. The disadvantage of using this method is the simulation time which may reach double the time required for the previous model to run and if bigger models are considered, using solid elements will be computationally expensive and very time consuming.

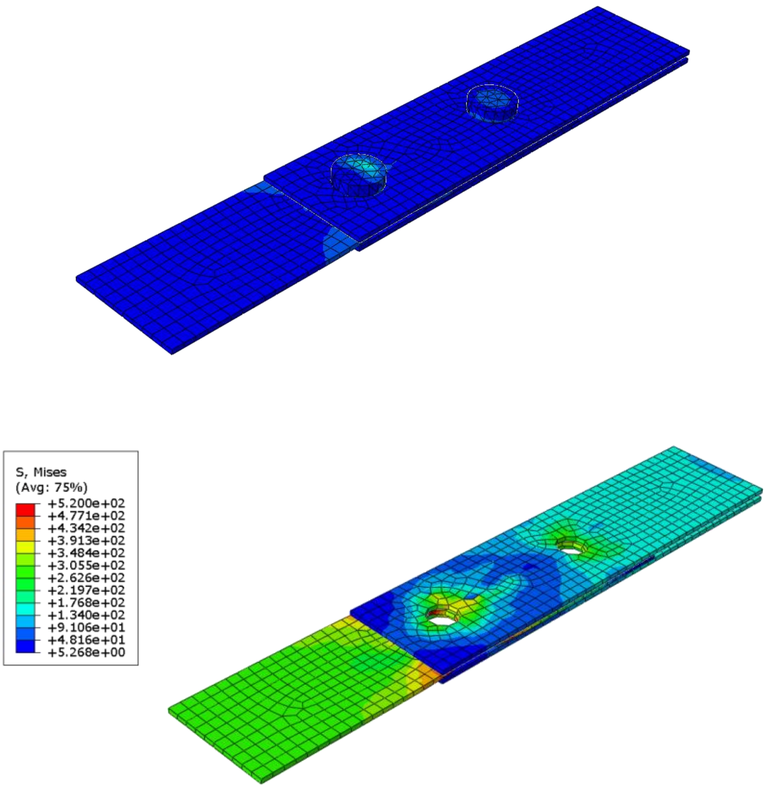

Figure 4- 8: Lap joint model (2)

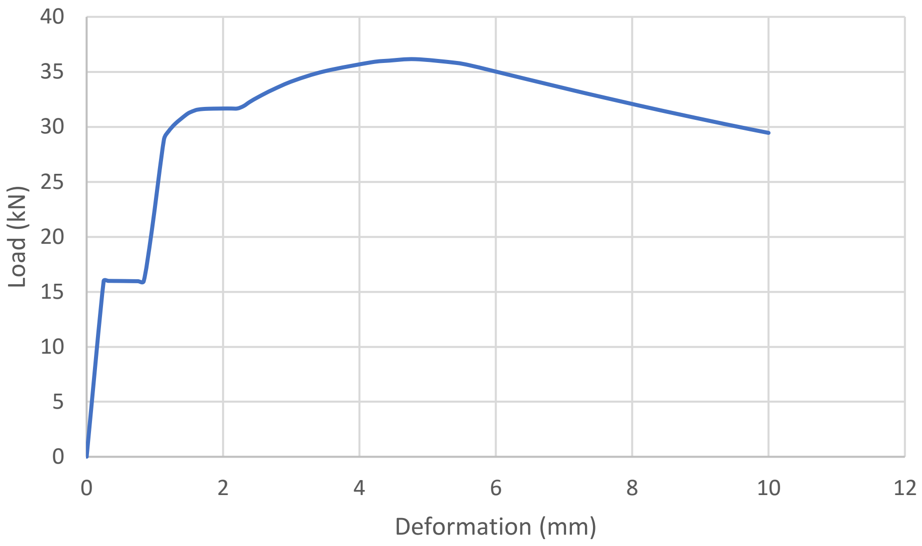

Figure 4- 9: Load-displacement relationship from model (2)

The third method uses the strength points of both methods. S4R shell elements were used to model the plates while 10-node quadratic tetrahedron (C3D10) were used to model the bolts. Using shell elements instead of solid elements to model the plates reduces the number of nodes and increases the simulation time, while using solid elements for the bolts captures the behavior of the connection required to be simulated. Figure (4-10) show the full model while figure (4-11) shows the model with the bolts hidden from view to better show the Von Mises stresses. Figure (4-12) illustrates the load-displacement curve obtained for the three models. It can be noticed that the second and third methods of modelling the connection gave very close results in terms of force at slippage and ultimate load. The third method gave better performance in terms of simulation time over the second method and was successful in simulating the behavior of the connection as desired. Therefore, the third method, where shell elements were used for the plates and solid elements were used for the bolts, is adopted in this research to model bolted connection subjected to cyclic loading.

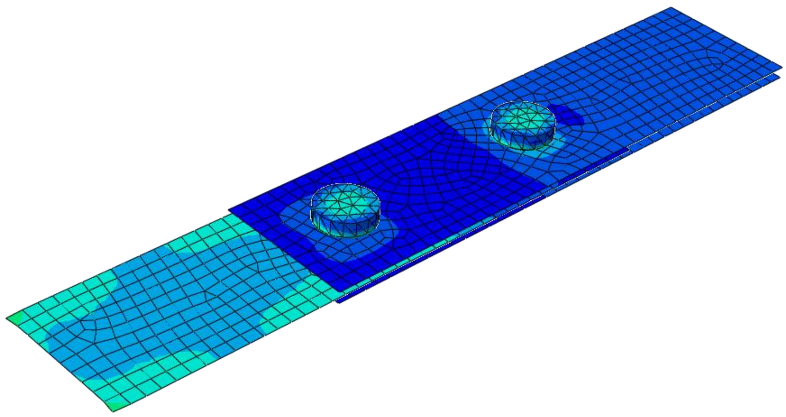

Figure 4- 10: Lap joint model (3) undeformed

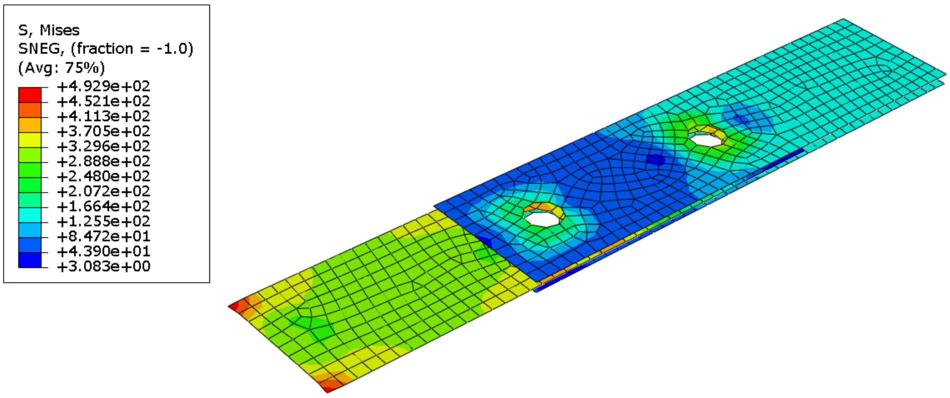

Figure 4- 11: Lap joint model (3) deformed shape

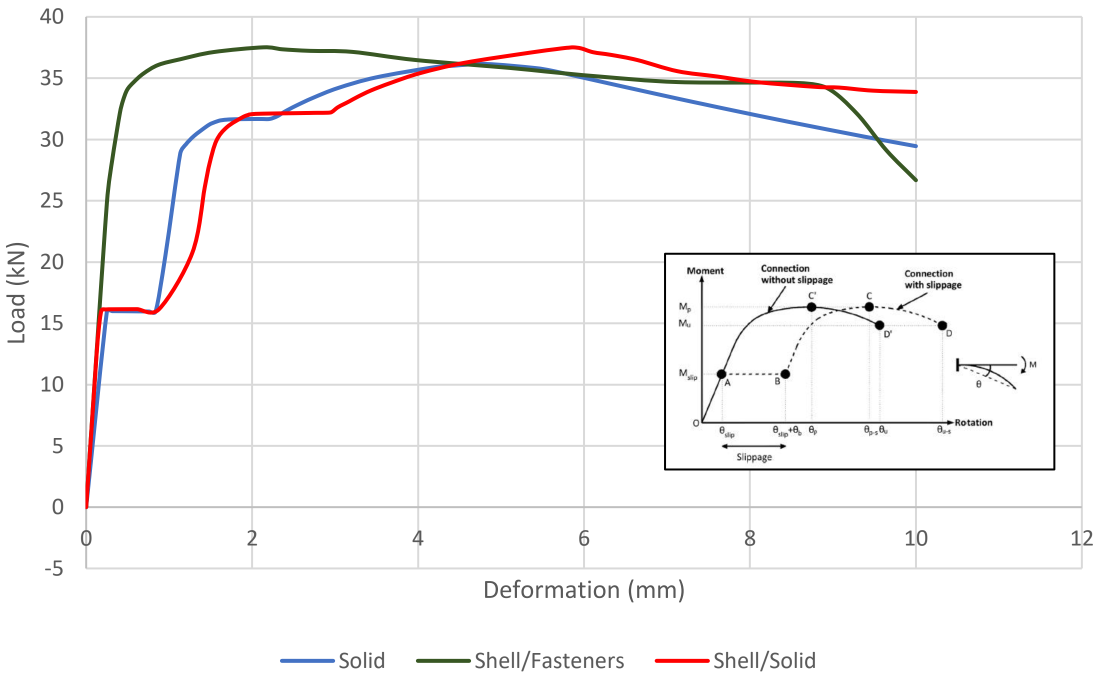

Figure 4- 12: Load-displacement relationships for the three models

Model Verification of Bolted Connections

In this section, the experimental testing of the bolted connection used in the study is compared with the ABAQUS finite element model. First, the deformed shape of the specimen and the model are compared. From the experimental tests, it can be noticed from Figure (4-13) that buckling of the gusset plate occurred first, then, plastic deformation in the column inner flange took place. Moreover, it can also be noticed that no failure in the bolts took place. This behavior is also captured by the finite element model. Buckling of the gusset plate and deformation of the inner flange can also be noticed in Figure (4-14) and (4-15).

Figure 4- 13: "Sp-3" deformed shape showing buckling in the column flange

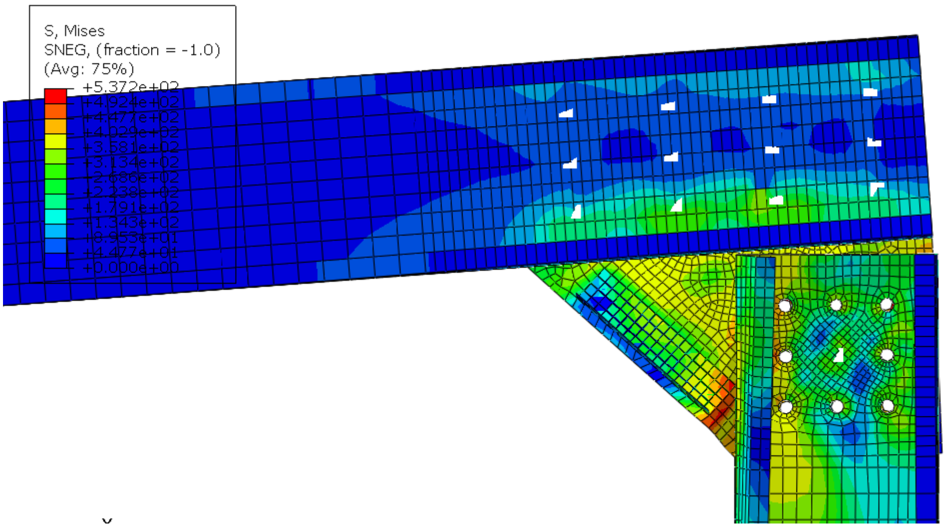

Figure 4- 14: "B-G2-R" deformed shape showing buckling in the column flange

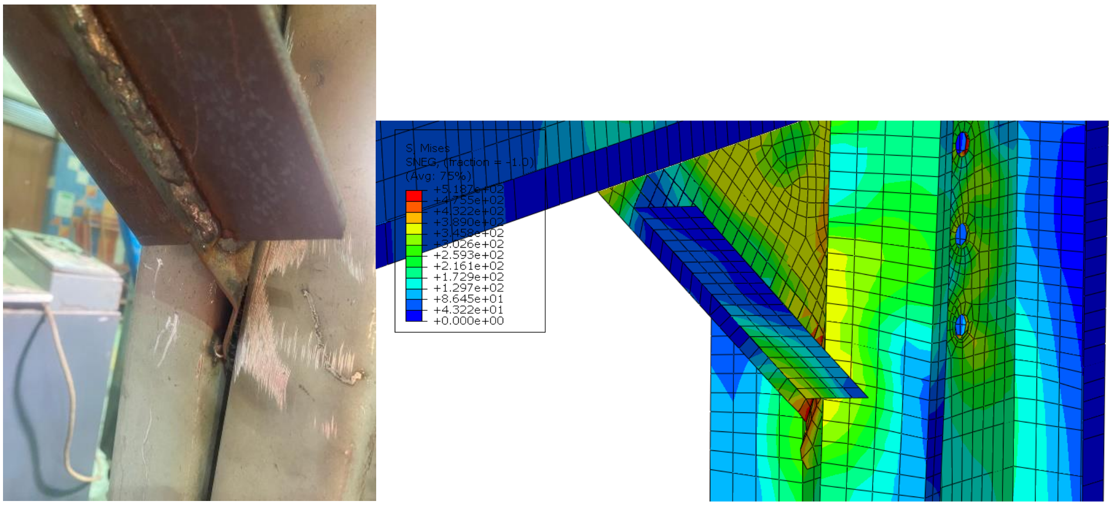

Figure 4- 15: Buckling in the gusset plate (left)"Sp-3" (right)"B-G2-R"

The second aspect of the comparison is the load-displacement relationship at the location of the load cell. An LVDT is located at the bottom flange of the beam where the load is applied so that the displacements of the beam are recorded. It can be noticed in Figure (4-16) that the hysteresis loops from the experimental and numerical are in very good agreement provided that the hysteresis loops at the beginning of the experimental test is ignored as mentioned earlier in Chapter 3. The envelopes of the curves are provided in Figure (4-17) in order to better analyze the results. The peak loads recorded from the experimental and numerical specimens when the displacements were downwards are -16.6 kN and -15.8 kN respectively, while that recorded for upward displacements are 17.1 kN and 16 kN respectively. The magnitude of the energy dissipated is calculated as the area under the envelope curve. The energy dissipated by the lab specimen was calculated as 1779 Joules, while the energy dissipated calculated from the numerical model was 1548 Joules, indicating an 13% difference between the two. Table (4-1) provide summaries for the comparison.

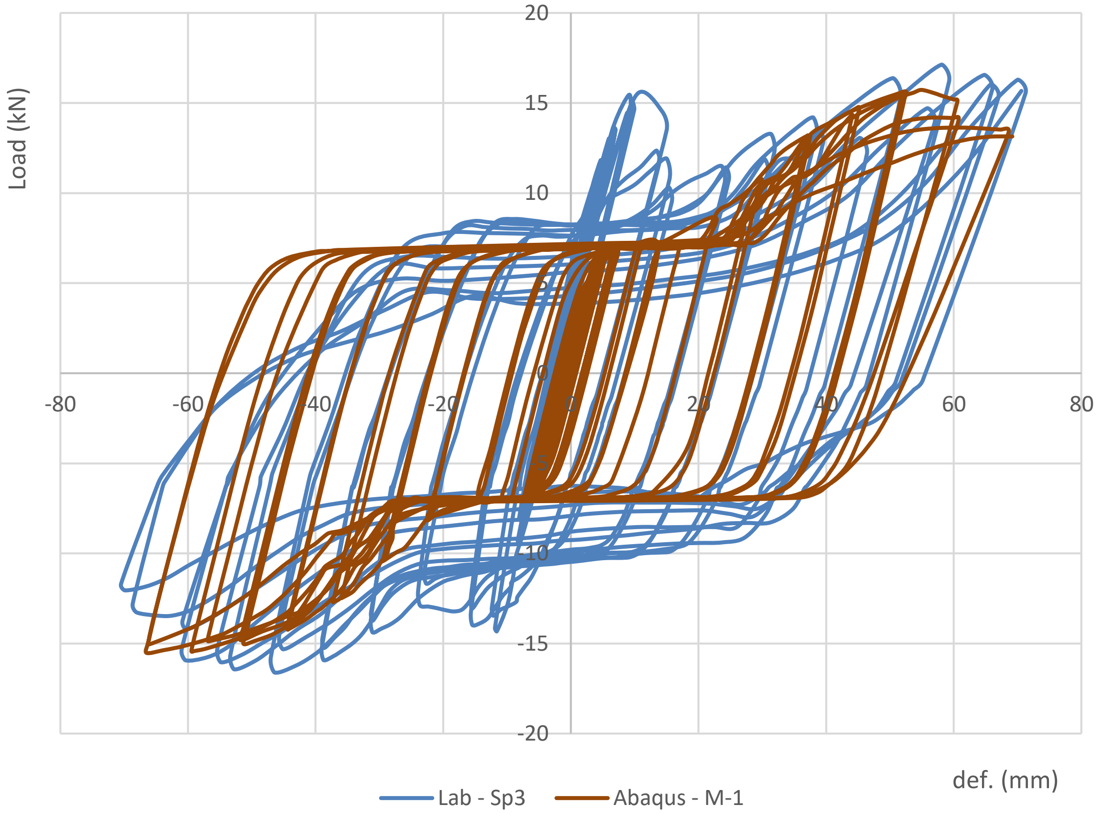

Figure 4- 16: Load-deformation hysteresis loops for "Sp-3" and "B-G2-R"

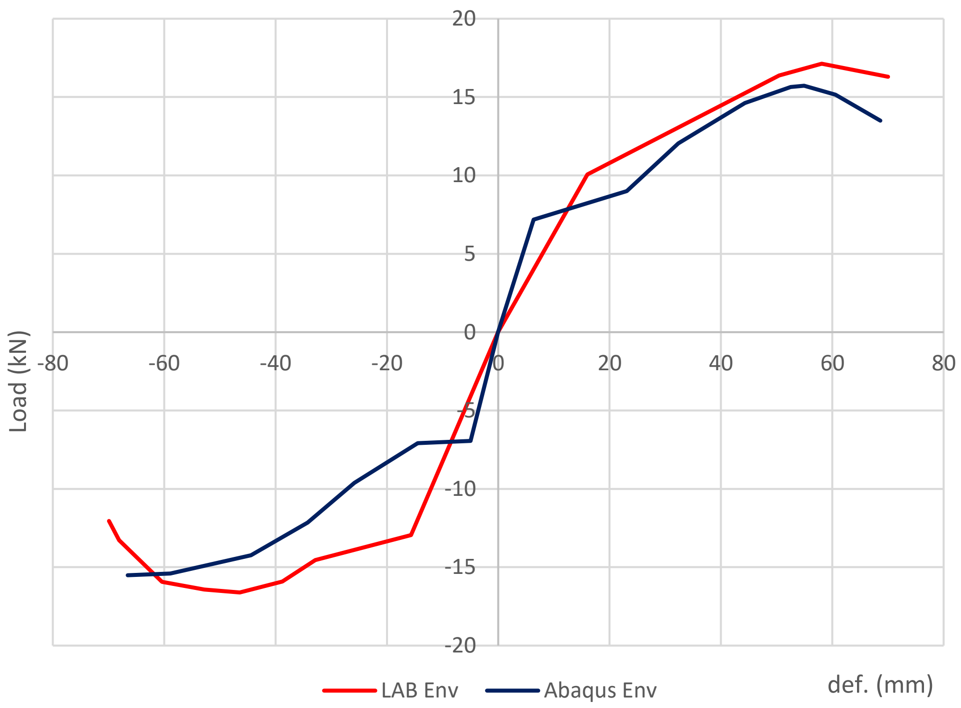

Figure 4- 17: Cyclic envelope for "Sp-3" and "B-G2-R"

Table 4- 1: Experimental "Sp-3" vs. numerical "B-G2-R" summary of results

	Lab	ABAQUS	Diff (%)
Max Load Upwards (kN)	17.13	16.05	6
Max Load Downwards (kN)	-16.61	-15.83	5
Max +ve Moment (kN.m)	15.4	14.4	6
Max -ve Moment (kN.m)	-14.9	-14.2	5
Dissipated Energy (J)	1779	1548	13

4.4. FEM of Screw-Fastened Connections

Simulating steel connections subjected to cyclic loading can always possess some challenges for researchers. Modelling bolts using solid elements is a good choice putting into consideration the accuracy, convergence, and simulation time. The techniques used to model screw-fastened connections subjected to monotonic loading are not very different from those used for bolts. Mesh-independent point-based fasteners or mesh-dependent line connectors can also be used for screws while different properties are defined for the screws. Also, screws can be modelled using solid elements as in [19] and illustrated in Figure (4-18).

In case that connections are subjected to cyclic loading, modelling bolts using solid elements is a good choice putting into consideration the accuracy, convergence, and simulation time as mentioned in the previous section, however, this is not the case for screws. Unlike bolts, threads in the screws are very crucial in their behavior and using an approach similar to the bolted connection models may be inefficient as it will neither be the most accurate, nor the most time efficient, and convergence errors are very probable given that at cycles that reaches high deformations, some screws are expected to fail and stop carrying any loads. This was noticed while conducting the experimental tests on the screw-fastened specimens which did not occur for bolted connections.

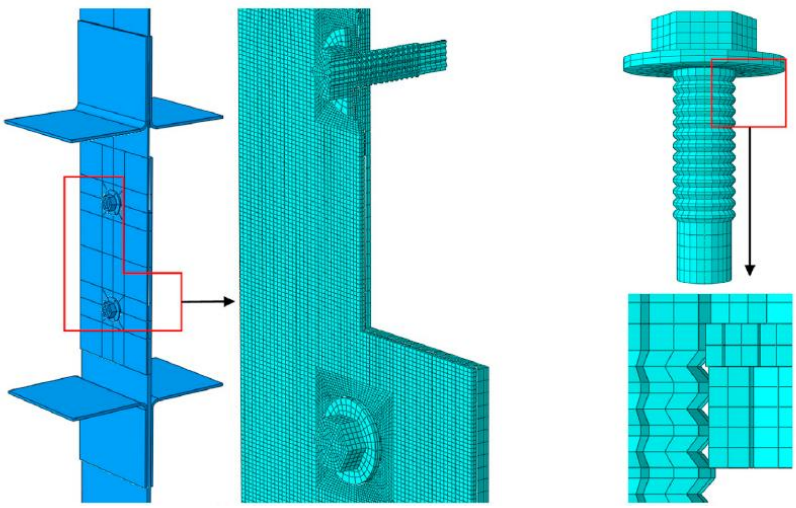

Figure 4- 18: FEM of self-drilling screws using solid elements

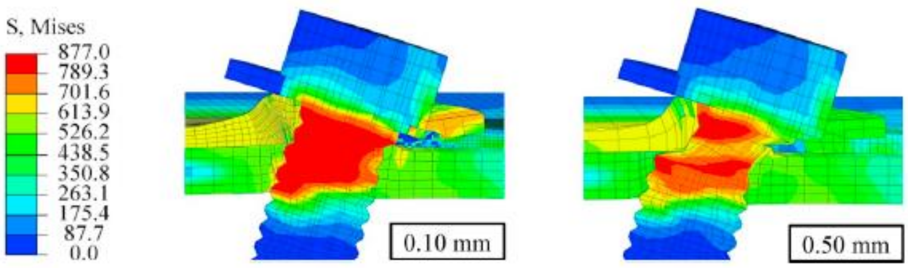

Figure 4- 19: Von-mises stresses for the self-drilling screws

Defining the plastic properties, damage, and failure criteria for a screw model using solid elements will increase the simulation time drastically and convergence error may occur, therefore, it is more convenient to use other methods that cause less problems to the model. Screws have a unique behavior when subjected to cyclic loading, that is, when load is reversed after reaching a certain displacement in one direction, no load carrying capacity is recorded until the screw returns close to its original position. Figure (4-20) shows how the screws tilt when subjected to direct shear from the plates connecting them, and Figure (4-21) illustrates the behavior of the connection when the load is reversed. Phase “1” indicates that the connection is subjected to direct shear and behave in a plastic manner. Phase “2” indicates the load reversal after reaching a certain displacement. It can be observed that once the plates translate back the elastic displacement, no significant load carrying capacity is noticed until the screw tilts back to its original position. As soon as the screw returns close to its original position, phase “3” starts and the connection regains its load carrying capacity as illustrated in Figure (4-21).

Figure 4- 20: Screws subjected to single shear [20]

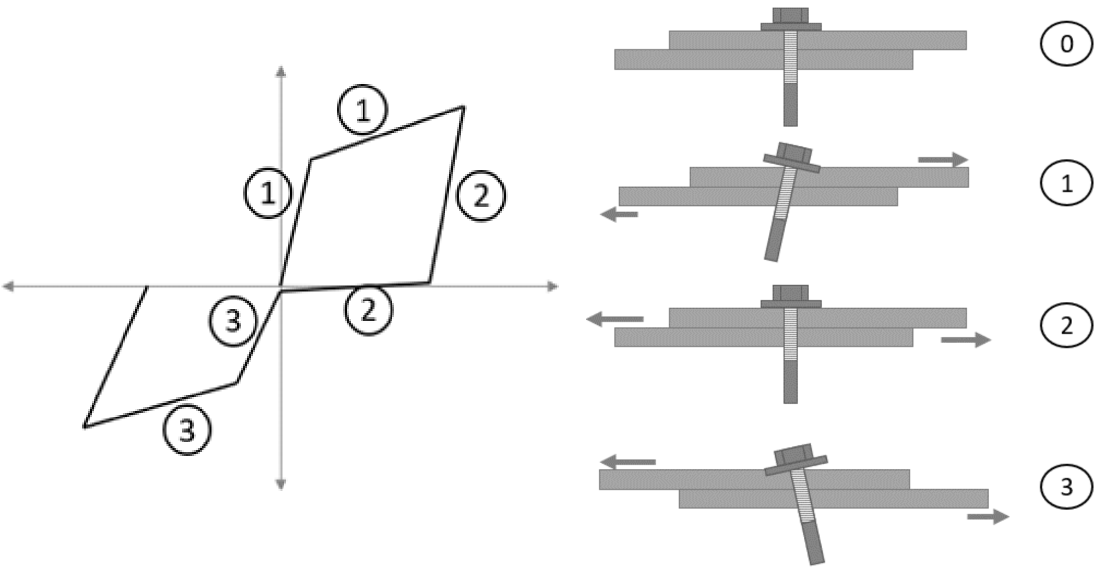

Figure 4- 21: The phases that screw-fastened connections undergo when subjected to reversible shear forces

As mentioned earlier, using solid element model for the screws is computationally expensive, therefore, the first alternative is to use point-based fasteners as in the case of monotonically loaded connections. Defining nonlinear plastic properties for the point-based fasteners is possible, however, the cyclic behavior of screws is unique and cannot be defined using the stress-strain curve directly. The second alternative is to use springs instead of fasteners. Stiffness of the spring elements in ABAQUS can be defined in X, Y or Z directions or using SPRINGA elements which are 2-node axial spring elements that consider geometric nonlinearity, meaning the line action of the spring is rotated following the boundary conditions instead of stiffness of the springs being defined in certain fixed directions.

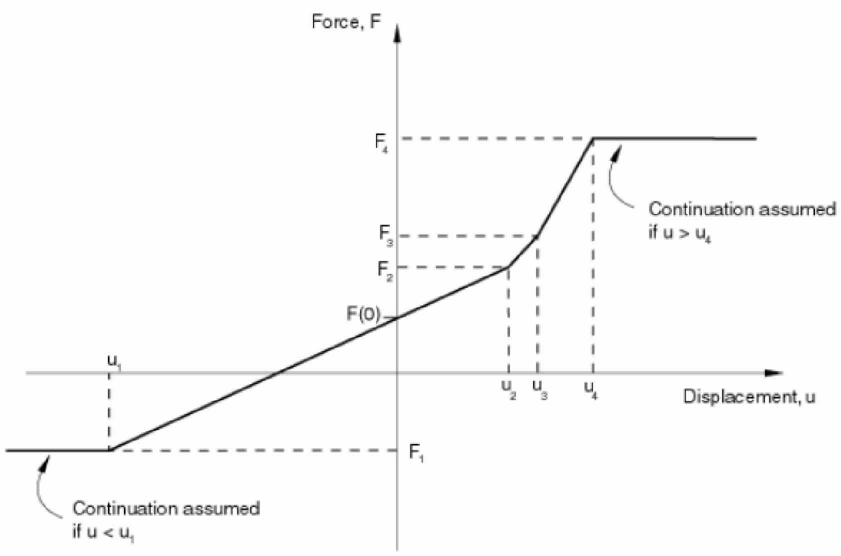

Figure 4- 22: Non-linear behavior of connectors in ABAQUS

Nonlinear load-displacement relationship can also be defined for the SPRINGA element as shown in Figure (4-22). Trial models were made to experiment using SPRINGA elements for modeling screw-fastened connections. The idea was first to model the plates with screw holes at the location of the screws, then, use springs connecting the hole edge with the center of the hole. These springs are modeled as "compression-only" springs using SPRINGA elements, meaning that these springs are incapable of carrying any tension forces. Finally, the center of each the screw hole in each plate is connected to the other hole centers of parallel plates using attachment lines and connectors.

The model gave promising results at first in terms of the behavior of the connection and the characteristic hysteresis loops that results from cyclic loading of screw-fastened connection was presented in the model, however, the major setback is the convergence errors that results at high deformations of the beam

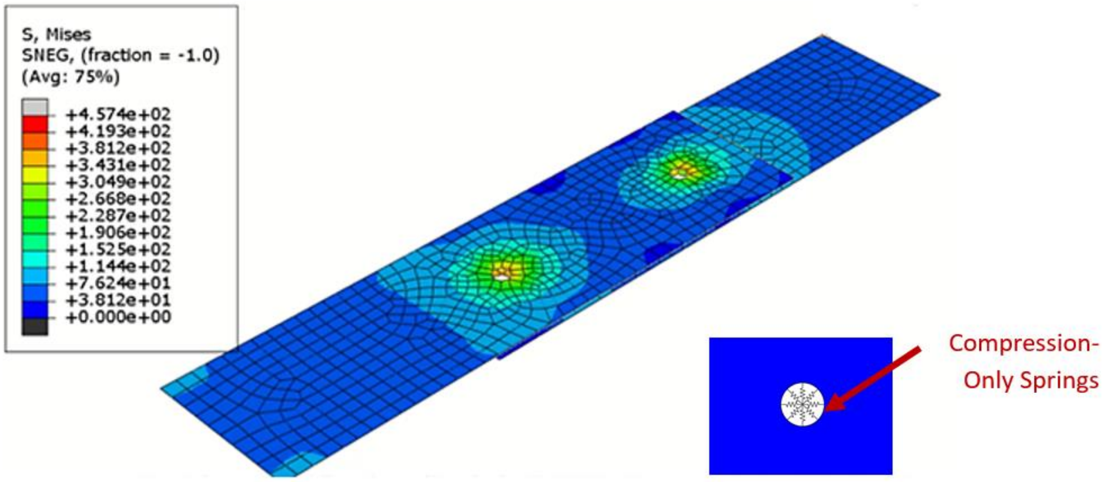

Figure 4- 23: SPRINGA elements for modelling self-drilling screws

The third alternative for modelling self-drilling screws is the one presented by Ding [21]. A breakthrough for modelling self-drilling screws using User Element Subroutines (UEL) in ABAQUS as explained in Chapter 2. This approach proved to be very successful and in close agreement with the lab results, however, the only disadvantage is it is not as straight forward as any other approach used before and requires experience with the ABAQUS software. This approach is adopted for modelling the self-drilling screws where the behavior of the screws is coded using Ding [21] Fortran code, and linked to the numerical model. The model is provided in appendix B

Model Verification of Screw-Fastened Connections

In this section, the experimental testing of the screw-fastened connections used in the study is compared with the ABAQUS finite element model. The screw-fastened connections tested in the lab were 2 specimens as illustrated earlier. In the following, the verification of the models is presented.

Screw-Fastened Connection: Specimen “Sp-1” vs Model “S-G3-R”

First, the deformed shapes are compared to each other. During the cyclic testing of the specimen Sp-1, no deformations in the cold-formed sections or the gusset were observed, however, tilting of the screws in the column was observed as illustrated in Figure (4-24). This tilting is translated into concentration of stresses in the ABAQUS model as shown in Figure (4-25).

The load-deformation relationships are also compared. From Figure (4-26), it can be seen that the curve from the experimental program and the numerical program are in close agreement. Table (4-2) summarizes the differences between the experimental and numerical results. The difference between the maximum load in the upward direction was 18%, while the difference in the downward direction is 9%. The difference between the dissipated energy calculated as the area under the envelope curve is 8%. Consequently, this modelling approach was used for the parametric study.

Figure 4- 24: Deformation of screws in "Sp-1" testing

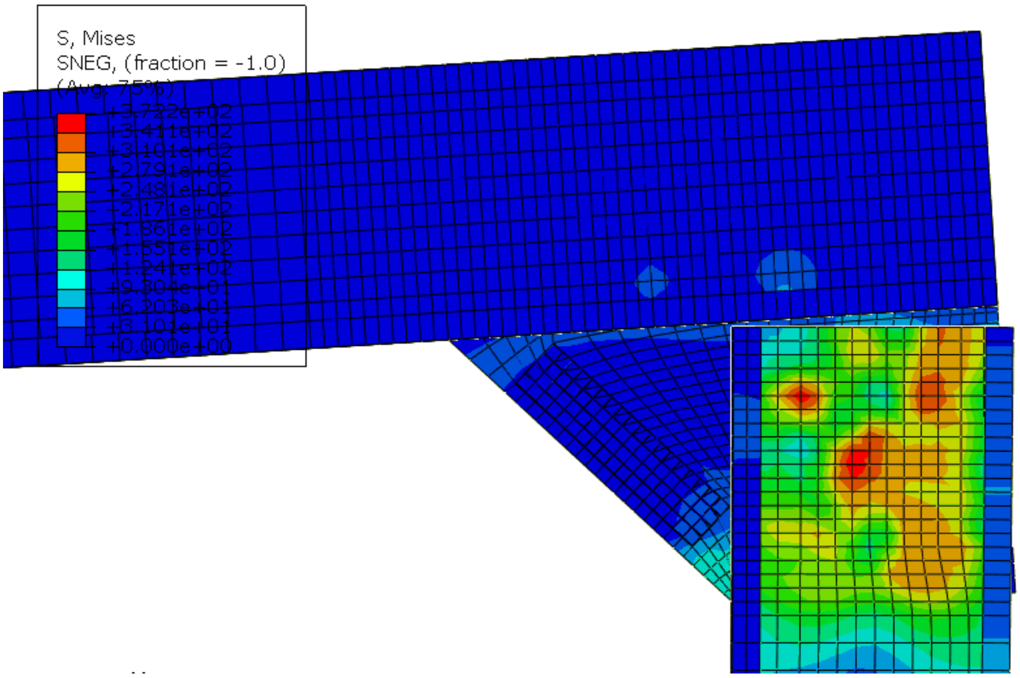

Figure 4- 25: Stress concentrations at the location of screws in the numerical model

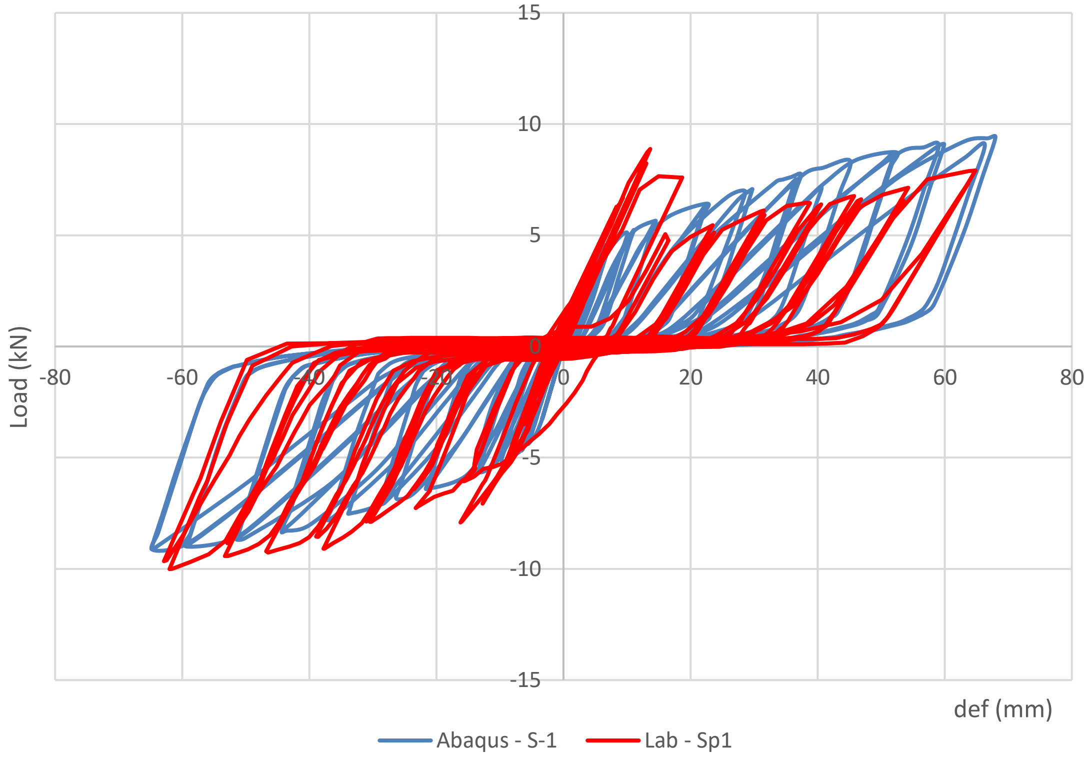

Figure 4- 26: Experimental vs. numerical results for "Sp-1" and "S-G3-R" respectively

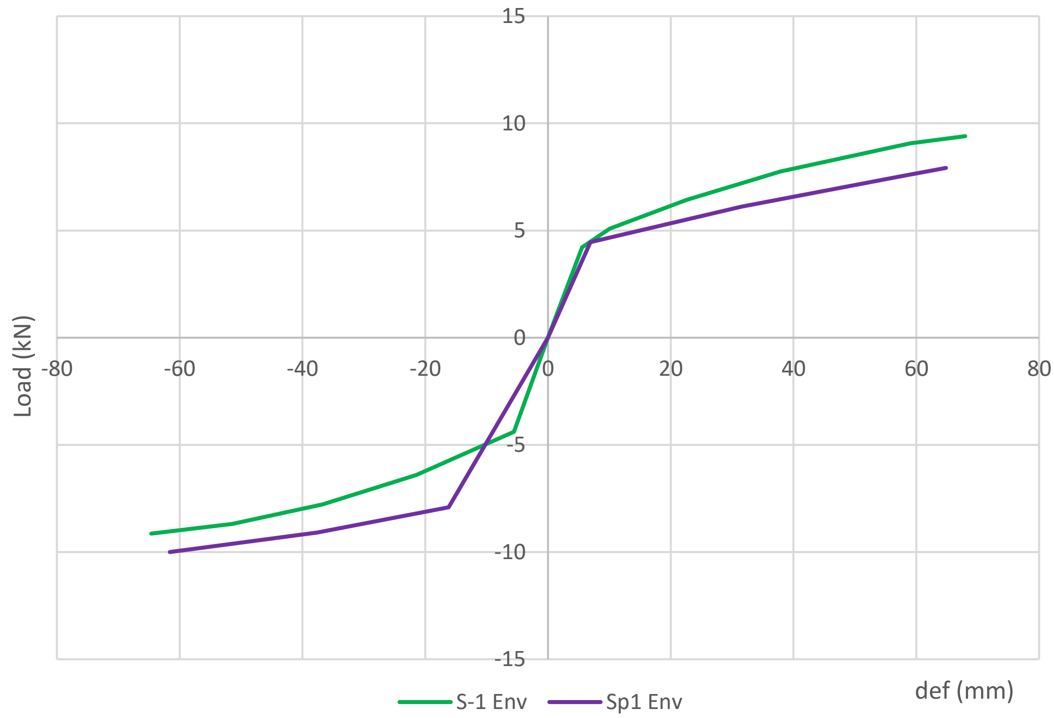

Figure 4- 27: Cyclic envelope for "Sp-1" and "S-G3-R"

Table 4- 2: Experimental "Sp-1" vs. numerical "S-G3-R" results summary

	Lab	ABAQUS	Diff (%)
Max Load Upwards (kN)	8	9.4	18
Max Load Downwards (kN)	-10.0	-9.1	9
Max +ve Moment (kN.m)	7.2	8.5	18
Max -ve Moment (kN.m)	-9.0	-8.2	9
Dissipated Energy (J)	854	919	8

Screw-Fastened Connection: Specimen "Sp-2" vs Model "ST-G3-R"

The deformed shapes are compared to each other. During the cyclic testing of the specimen Sp-2, some deformations were noticed in the top plated and flanges of the beam, moreover, tilting of the screws in the column was observed as illustrated in Figure (4-28). In a similar manner, the beam flanges slightly deformed in the numerical model and tilting is translated into concentration of stresses as shown in Figure (4-29).

The load-deformation relationships are also compared. From Figure (4-30), it can be seen that the curve from the experimental program and the numerical program are in close agreement. Table (4-3) summarizes the differences between the experimental and numerical results. The difference between the maximum load in the upward direction was 12%, while the difference in the downward direction is 5%. The difference between the dissipated energy calculated as the area under the envelope curve is very low as it reached 1%.

Figure 4- 28: Deformation in screws observed in "Sp-2"

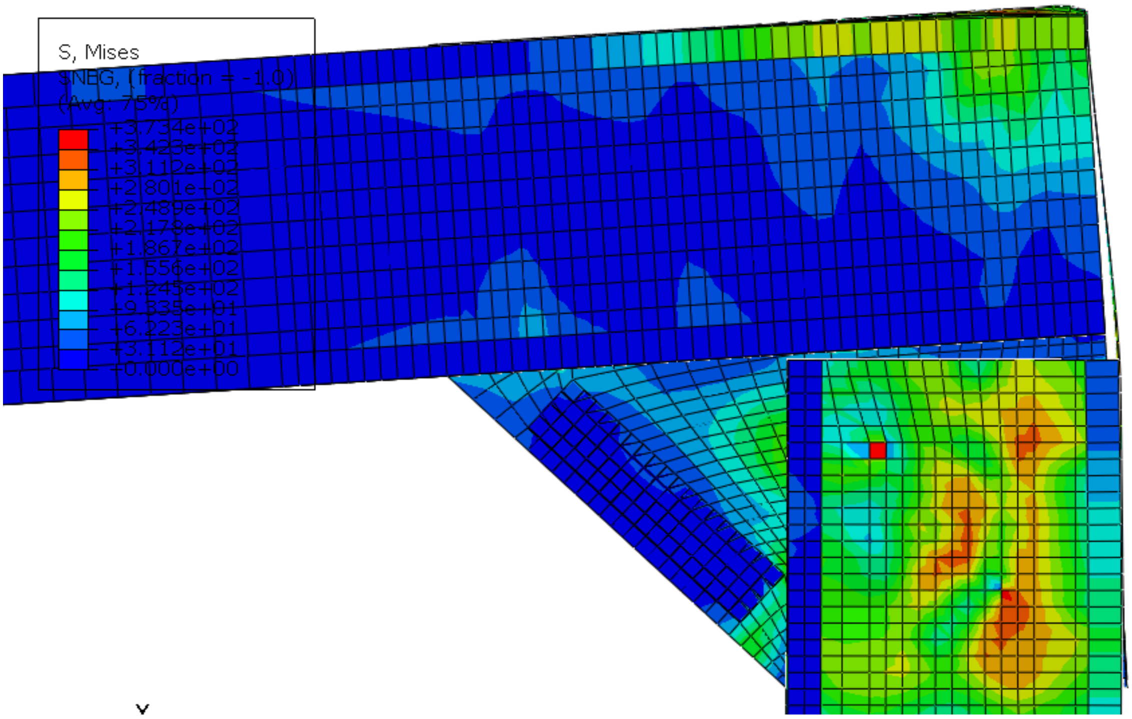

Figure 4- 29: Stress concentration at the location of screws observed in "ST-G3-R"

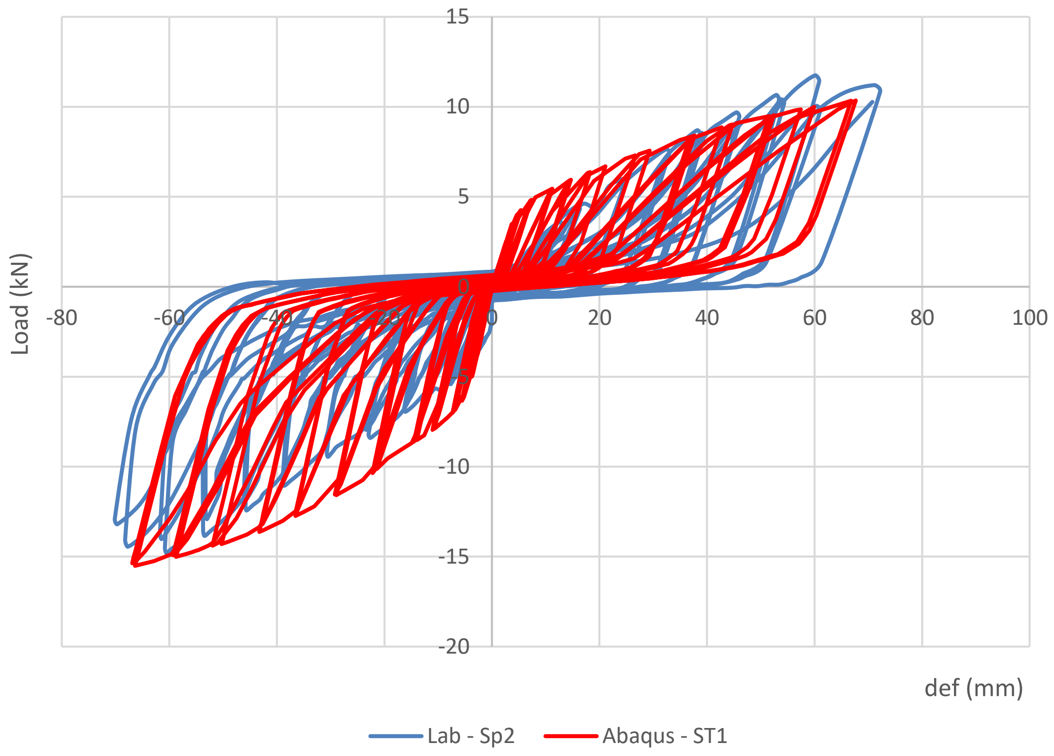

Figure 4- 30: Experimental vs numerical results for "Sp-2" and "ST-G3-R"

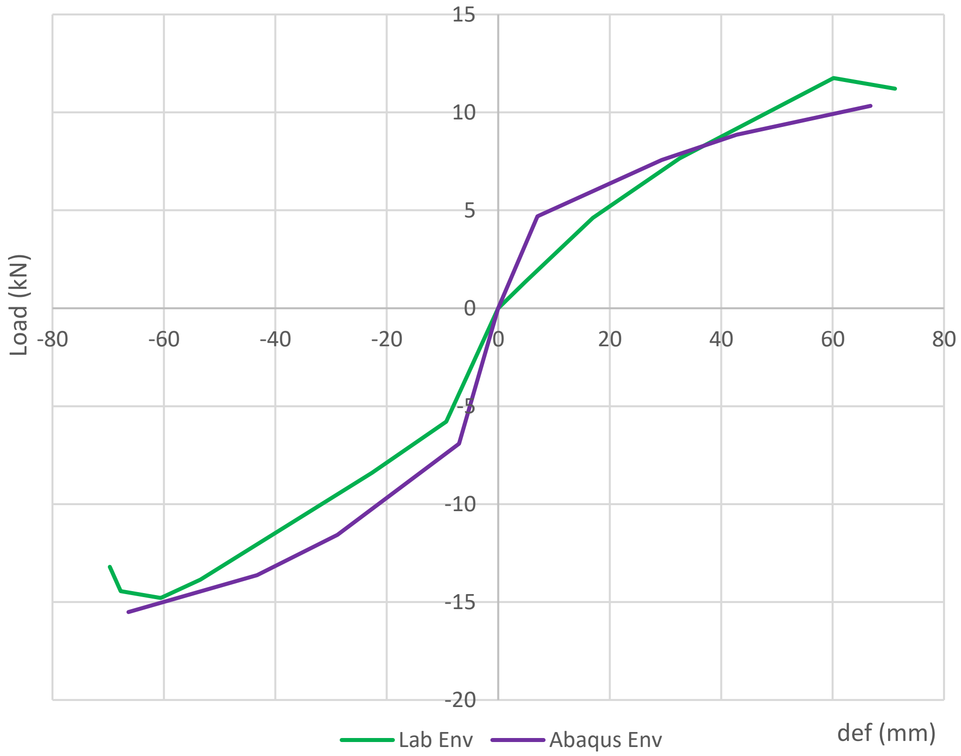

Figure 4- 31: Cyclic envelope for "Sp-2" and "ST-G3-R"

Table 4- 3: Experimental "Sp-2" vs. numerical "ST-G3-R" results summary

	Lab	ABAQUS	Diff (%)
Max Load Upwards (kN)	11.8	10.3	12
Max Load Downwards (kN)	-14.8	-15.51	5
Max +ve Moment (kN.m)	10.6	9.3	12
Max -ve Moment (kN.m)	-13.3	-14.0	5
Dissipated Energy (J)	1228	1238	1

4.5. Concluding Remarks

This chapter discussed the finite element models techniques that can be used for modelling bolted and screw-fastened connections. Bolts were modeled using solid elements while screws were modeled using User Element Subroutine (UEL). The finite element models were found to be in good agreement with the experimental work conducted as explained in the following:

- The difference in maximum load in the upwards direction between specimen "Sp3" and model "B-G2-R" was 6%, while in the downwards direction the difference was 5%. The difference in energy dissipated by the connection was 13%.
- Model "S-G3-R" for screw fastened connection recorded 18% higher than specimen "Sp1" in terms of maximum load in the upwards direction, while 9% difference was recorded for the maximum load downwards. In terms of energy dissipation, 8% difference between model "S-G3-R" and specimen "Sp1" was recorded.
- The screw-fastened connection with additional top plate model "ST-G3-R" recorded a 12% difference with the specimen "Sp2" in terms of maximum load in the upwards direction, while a 5% difference in terms of maximum load downwards was recorded. Only 1% difference between the dissipated energy calculated for "Sp2" and "ST-G3-R" was recorded.

The verified models discussed in this chapter were then used to develop other models while changing some parameters and a parametric study was conducted. The parametric study is discussed in the next chapter.

Chapter 5 : Parametric Study

5.1. Introduction

The behavior of cold-formed steel moment connections subjected to cyclic loading is assessed through three main parameters: strength, ductility, and energy dissipative capacity. Ductility is a measure of how far the connection can carry loads before it loses completely its load carrying capacity, while energy dissipative capacity can be expressed in more than one form. This chapter provides a parametric study where different parameters of the experimentally verified model is altered and the effect of this change is studied and compared to other changes on the model. The aspects of comparison include the ultimate strength, ductility, energy dissipation and viscous damping coefficient which is another approach of expressing the energy dissipative capacity of certain element. As mentioned earlier, the numerical models were developed using ABAQUS software as both material and geometrical nonlinearity were included. The chapter starts with a general overview of the models developed and aspects of the comparison between models, then three parametric studies are discussed as follows:

- **Parametric Study 1**: Screw-Fastened Connections
- **Parametric Study 2**: Screw-Fastened Connections with Top Plate
- **Parametric Study 3**: Bolted Connections

5.2. Parametric Study

5.2.1. Detail Configuration

Three configurations for the bolts/screws, used to fasten the gusset plate with the column webs, were used in this study. The first is the ordinary square arrangement presented in Figure (5-1) with spacings between bolts/screws' centers equal 50 mm. The second configuration investigated was the circular arrangement for the bolts/screws with radius of circle equals 50 mm illustrated in Figure (5-2). The third and last configuration is the diamond configuration presented in Figure (5-3) with spacings between bolts/screws in the vertical and horizontal directions equal 50 mm. The same number of screws and bolts were used in all the bolts/screws arrangements.

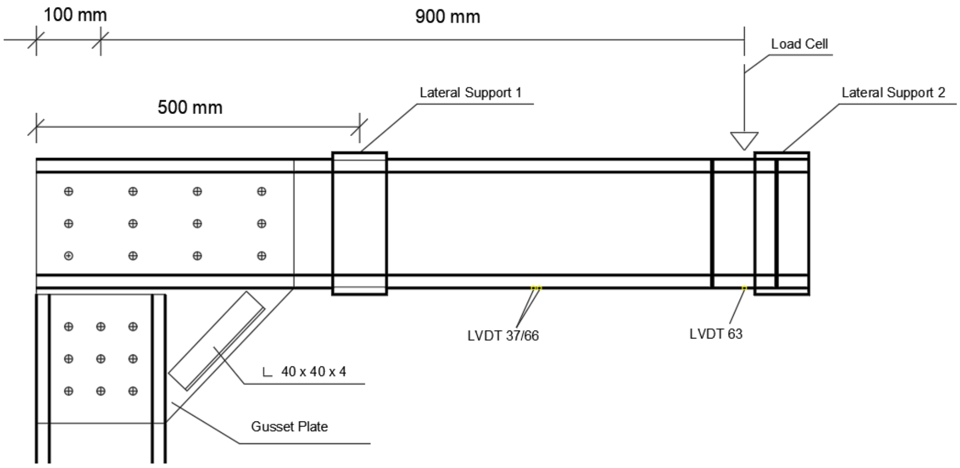

Figure 5- 1: Dimensions for rectangular arrangement of bolts/screws

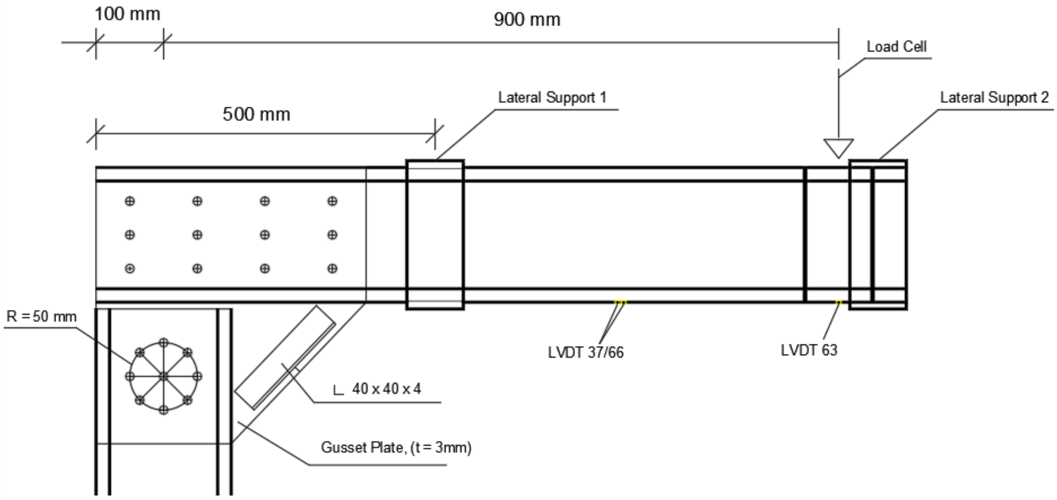

Figure 5- 2: Dimensions for circular arrangement of bolts/screws

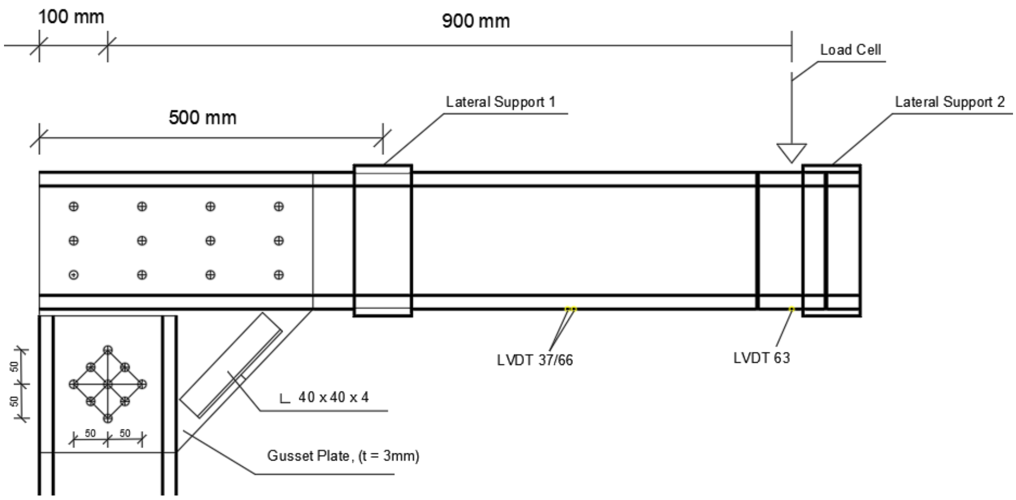

Figure 5- 3: Dimensions for diamond arrangement of bolts/screws

The second parameter used in the study is the gusset plate thickness. While square bolts/arrangements were used in the study, the gusset plate thickness varied in order to investigate the effect of changing the gusset plate thickness on the connection behavior.

5.2.2. Models Description

As mentioned earlier in Chapter 3, three experimental tests were conducted and numerical models were made and verified using the experimental results. The first specimen tested was the screw-fastened connection and the model used for this specimen is denoted as “S-G3-R”. The second specimen tested was the screw-fastened connection with a top plate connecting the column outer flanges with the beams’ top flanges, and the model used for this specimen is denoted as “ST-G3-R”. The third and last specimen tested was the bolted connection and the model used for this specimen is denoted as “B-G3-R”. The parameters used for this study are the gusset plate thickness and the bolts/screws arrangements. Finite element models with gusset plate thickness equals 3 mm, 2 mm and 4 mm are denoted with the numbers 1, 2 and 3 respectively, i.e., the model for screw-fastened connection with gusset plate equals 4 mm is denoted as “ST-G4-R”. Models with circular and diamond bolt/screw arrangement are denoted with the numbers 4 and 5 respectively. The following table (5-1) provides a summary of the models used for the parametric study.

Table 5- 1: Summary of the FEM models

Model ID	Type of Fasteners used	Fasteners’ arrangement	Gusset Plate Thickness	Top Plate
S-G3-R	Screws	Rectangular	3 mm	-
S-G2-R	Screws	Rectangular	2 mm	-
S-G4-R	Screws	Rectangular	4 mm	-
S-G3-C	Screws	Circular	3 mm	-
S-G3-D	Screws	Diamond	3 mm	-
ST-G3-R	Screws	Rectangular	3 mm	**Used**
ST-G2-R	Screws	Rectangular	2 mm	**Used**
ST-G4-R	Screws	Rectangular	4 mm	**Used**
ST-G3-C	Screws	Circular	3 mm	**Used**
ST-G3-D	Screws	Diamond	3 mm	**Used**
B-G3-R	Bolts	Rectangular	3 mm	-
B-G2-R	Bolts	Rectangular	2 mm	-
B-G4-R	Bolts	Rectangular	4 mm	-
B-G2-C	Bolts	Circular	2 mm	-
B-G2-D	Bolts	Diamond	2 mm	-

5.2.3. Parametric Study Aspects

In chapter 2, several papers discussed the parameters for comparing the strength and ductility of different connections, and their behavior when subjected to cyclic loading. These aspects will be used in this research to investigate the strength, stiffness, ductility, and energy dissipative capacity of the connections. The equations and procedures are as follows:

1. **Moment Capacity:**

   Using the experimentally verified models, the ultimate moment capacity of the connections when subjected to monotonic gravity point load is recorded using the finite element model. The ratio between the connection moment capacity to the nominal cross-section moment capacity is also calculated to evaluate the efficiency of the connection. The nominal cross-section moment capacity is calculated according to the AISI S100-16 standard code of practice. Finally, the maximum moment capacity recorded when the connection is subjected to cyclic loading and compared to the ultimate moment capacity of the connection. The nominal flexural moment capacity subjected to bending about a principal axis for doubly symmetric section, according to AISI S100-16, is calculated and presented in appendix C.

2. **Ductility:**

   As mentioned earlier, the key parameter for elements and components design to resist seismic load actions is the ductility. The ductility ratio can be used as a measure of the connection ductility, and it is calculated as the ultimate displacement (or strain) divided by the yield displacement (strain). The idealized bilinear FEMA curves can be used to determine the values for yield and ultimate displacements.

3. **Code Requirements:**

   AISC 341-16 classify moment resisting frames resisting seismic loads into three main categories, Ordinary Moment Resisting Frames (OMF), Intermediate Moment Resisting Frames (IMF) and Special Moment Resisting Frames (SMF). SMF, IMF and OMF must accommodate over 4% (0.04 rad), between 2% (0.02 rad) and 4% (0.04 rad), and less than 2% (0.02 rad) inter-story drift, respectively, with less than 20% degradation in strength. This classification will be used in the parametric study using cyclic moment-rotation envelope.

4. **Energy Dissipation:**

   Energy dissipation is typically calculated as the area under the load-displacement curve or the area under the moment-rotation curve. For cyclic loading, the FEMA idealized bilinear curves can be used or the envelope for the cyclic loads can be obtained and a more accurate area under curve can be obtained using trapezoidal rule.

5. **Viscous Damping Coefficient:**

As previously mentioned, the plumpness of the hysteresis loops can be obtained using this approach of calculating the equivalent viscous damping coefficient which provides another measure of the energy dissipated in the system. The equivalent viscous damping coefficient is calculated using the following formula:

$$C_e = \frac{1}{2\pi}\frac{S_{ABC} + S_{CDA}}{S_{OBE} + S_{ODF}}$$

5.2.4. Parametric Study 1: Screw-Fastened Connections

The first parametric investigation conducted is the screw-fastened connection. As mentioned earlier, the study includes different gusset plate thicknesses and different screw arrangements, and certain aspects of the connection is investigated. Model S-G3-R is the experimentally verified model, and different parameters varied afterwards. The following table summarizes the models' information for this study:

Table 5- 2: Parametric Study 1 data

Model ID	Type of Fasteners used	Fasteners' arrangement	Gusset Plate Thickness
S-G3-R	Screws	Rectangular	3 mm
S-G2-R	Screws	Rectangular	2 mm
S-G4-R	Screws	Rectangular	4 mm
S-G3-C	Screws	Circular	3 mm
S-G3-D	Screws	Diamond	3 mm

A monotonic gravity displacement is applied to the specimens and the moment-rotation relationship is recorded as shown in Figure (5-10). The deformed shapes for each model are illustrated in Figure (5-4)-(5-9). From the deformed shapes, it can be seen that the failure modes are different from one model to another. For S-G3-R, failure occurred in the screws, which can be noticed as stress concentrations at the location of the screws, while slight deformation in the column webs is also noticed Figure (5-4). When the gusset plate thickness is reduced to 2 mm in model S-G2-R, the failure mode significantly changed as the gusset plate buckled causing the column flange to deform out of plane Figure (5-5). The gusset plate was increased to 4 mm in model S-G4-R and it can be noticed that the failure mode is similar to that in S-G3-R where the self-drilling screws were the first to fail Figure (5-7). but unlike S-G3-R, no deformation in the column webs were noticed.

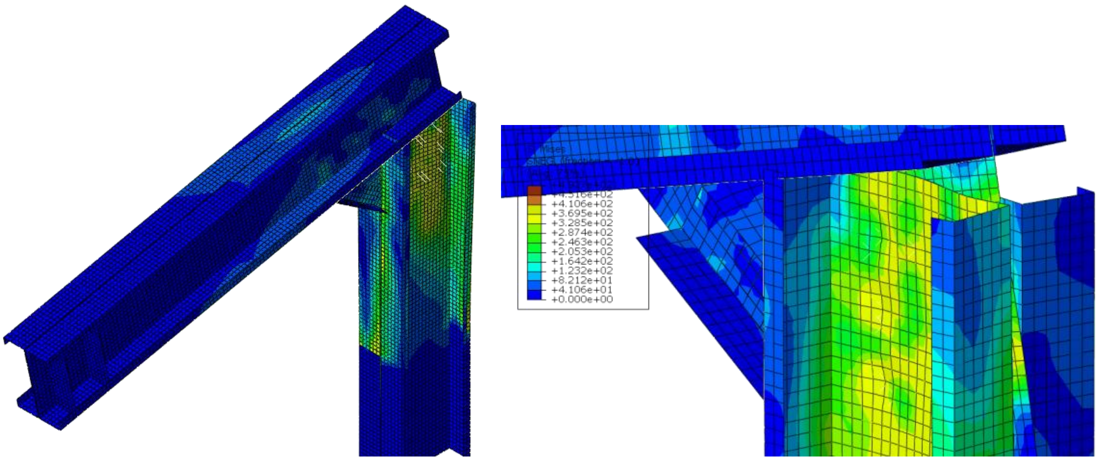

Figure 5- 4: Deformed shapes for S-G3-R

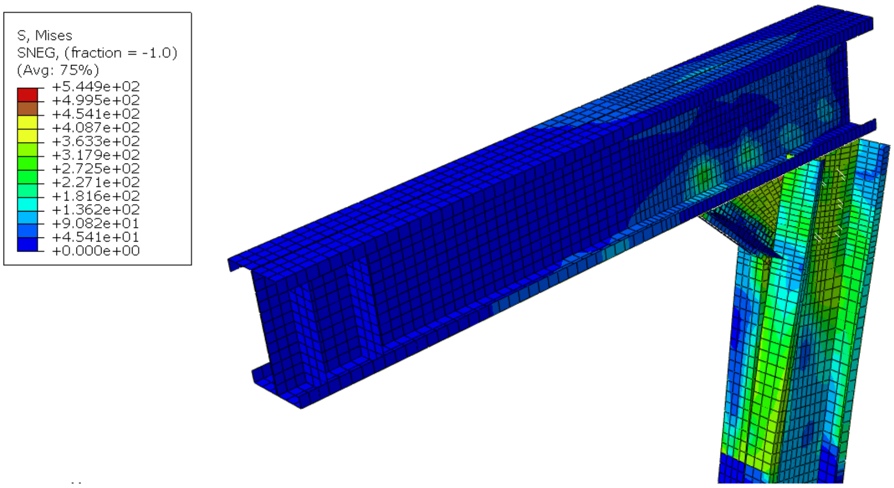

Figure 5- 5: Deformed shape for S-G2-R

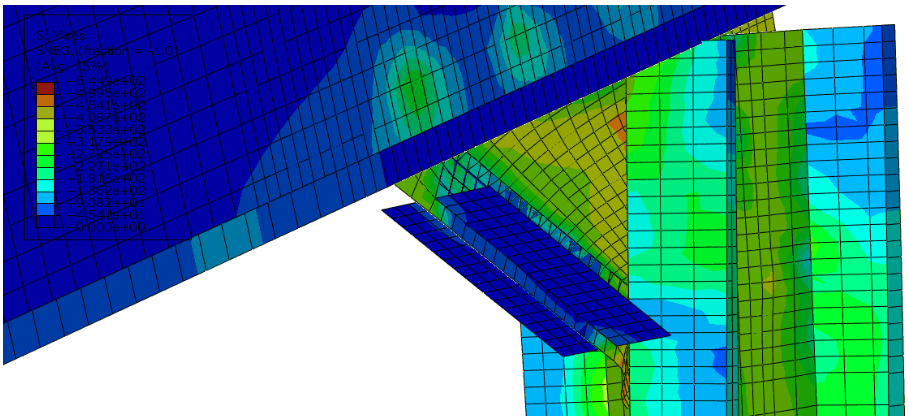

Figure 5- 6: Deformed shape for S-G2-R

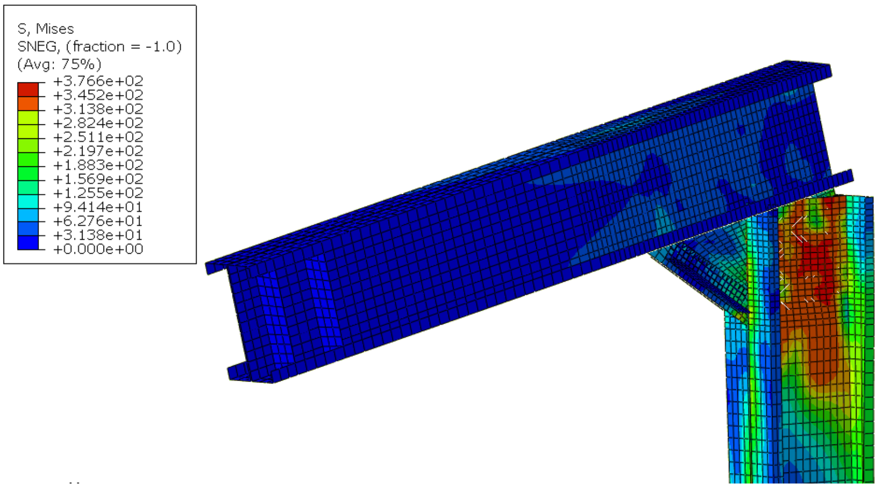

Figure 5- 7: Deformed shapes for S-G4-R

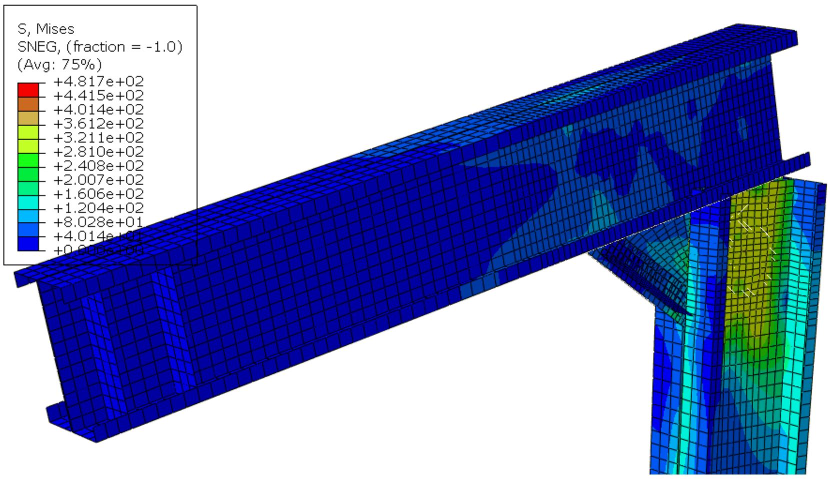

Figure 5- 8: Deformed shapes for S-G3-C

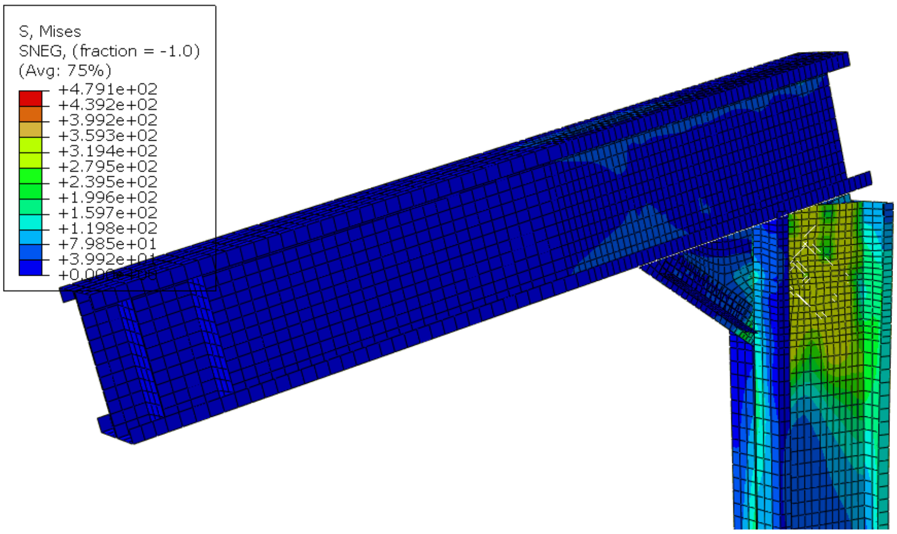

Figure 5- 9: Deformed shapes for S-G3-D

From the moment-rotation relationship illustrated in Figure (5-10)., it can be noticed that model S-G4-R provided the highest moment capacity equals to 10 kN.m at rotation equals 0.16 rad. Model S-G3-R provided the second highest moment capacity equals to 9.64 kN.m at rotation equals 0.173 rad. The third highest was model S-G2-R (gusset = 2mm) with moment capacity equals 9 kN.m at rotation equals to 0.162 rad. Model S-G3-D provided the worst performance in terms of strength when subjected to monotonic gravity load with moment capacity equals 6.3 kN.m at rotation equals 0.17 rad. The circular screws arrangement provided better results over the diamond arrangement with moment capacity equals 8.54 kN.m at rotation equals 0.177 rad. In order to provide better insight for the connection strength and behavior, the connections' moment output data were divided by the cold-formed section's nominal flexural strength and provided in Figure (5-11).

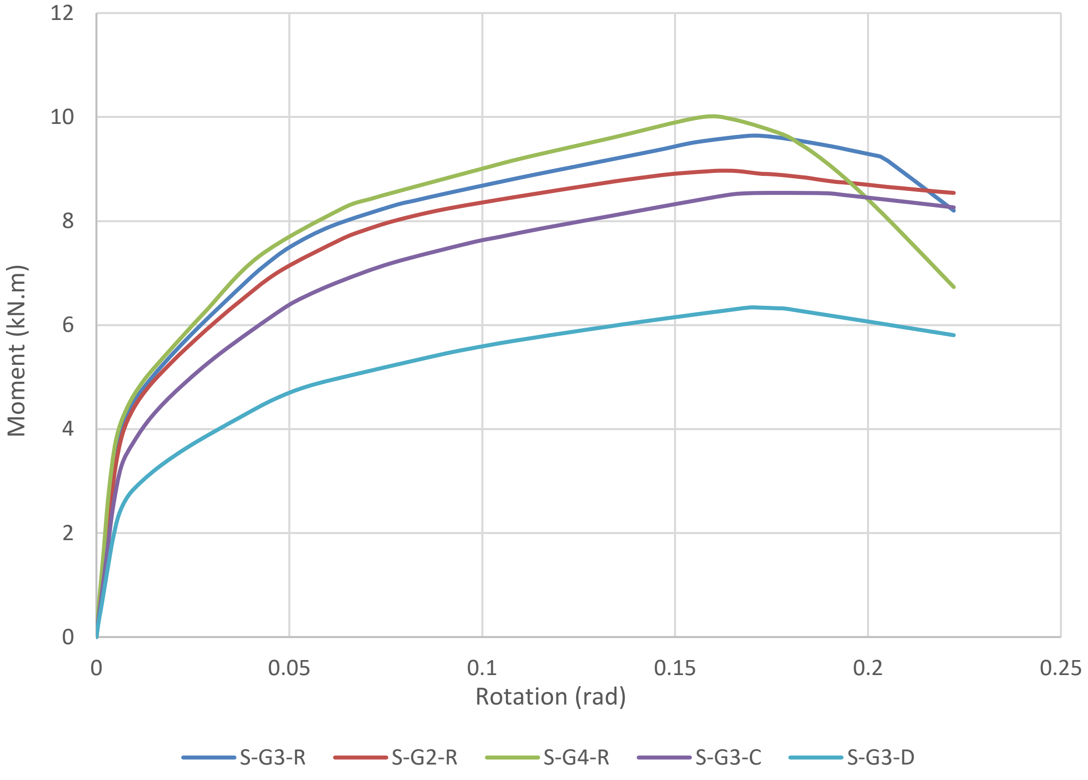

Figure 5- 10: Moment-rotation curves for monotonically loaded models

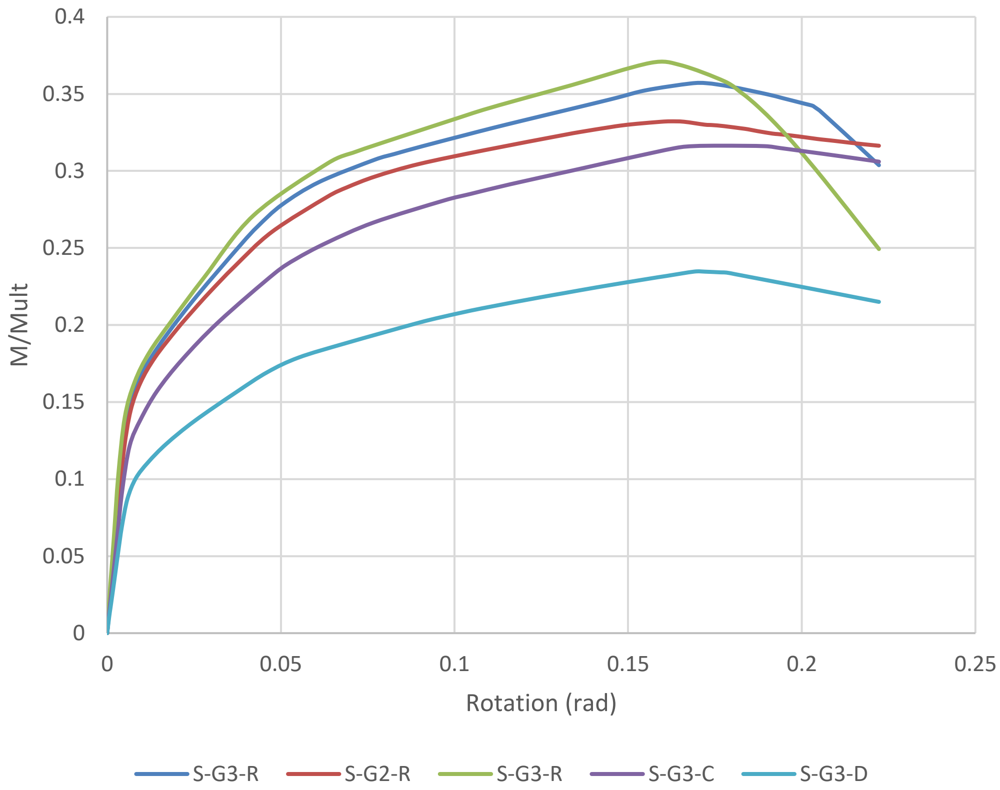

Figure 5- 11: Moment/Section Capacity-rotation curves for monotonically loaded models

As mentioned earlier in ASCE/SEI 41-17, the cyclic envelope of the load-displacement (or Moment-rotation) relationship is very essential for the assessment of ductility. A number of 40 cycles were applied to each specimen in the models similar to the experimental program even though the models have shown that the specimens can still carry more loads Figure (5-12). It can also be noticed from Figure (5-12) that the hysteresis loops of the connections where similar in behavior and in agreement with the general behavior of screw-fastened connections mentioned earlier in the literature review chapter. The curves for the hysteresis loops for the models are presented separately in appendix A.

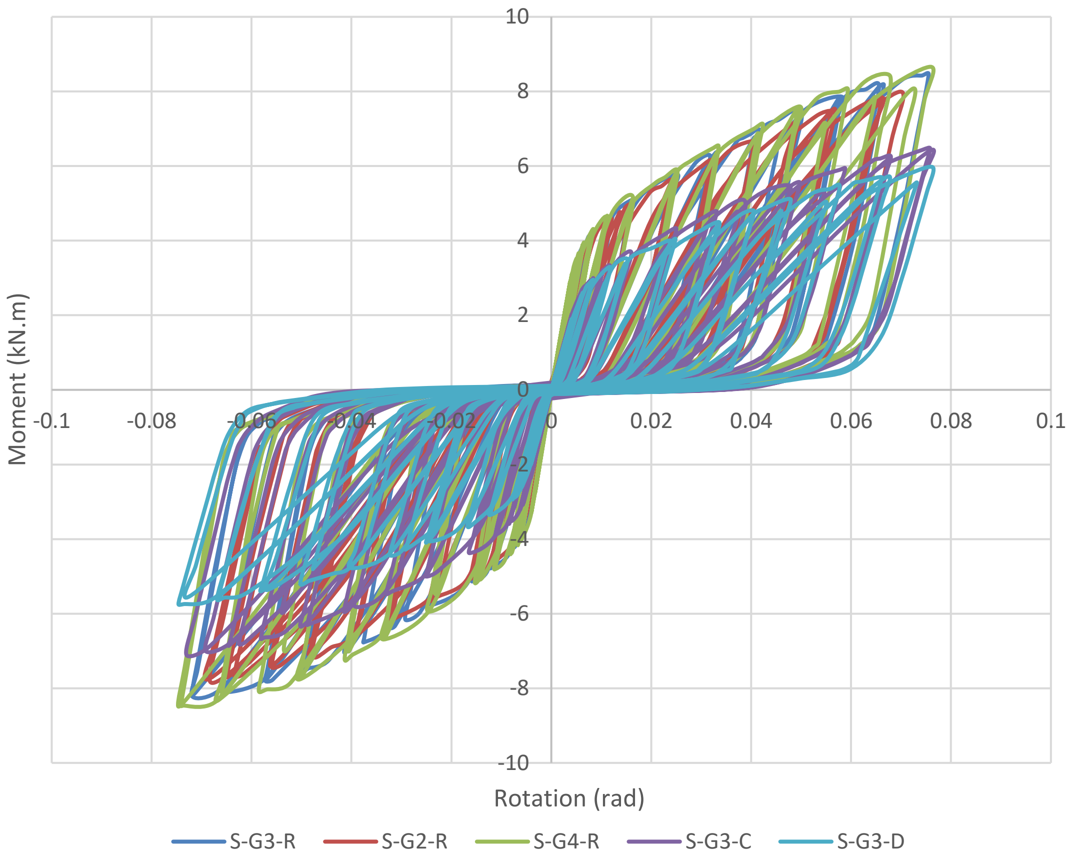

Figure 5- 12: Moment-rotation curves for cyclic loaded models

The envelope of the curves is obtained and presented in Figure (5-13) for further analysis of the results. Moreover, the envelope of the half-cycles in the downward displacement side is separated and compared with the monotonic moment-rotation relationships for all the specimens. The monotonic moment-rotation relationships represent the backbone curve which the cyclic envelope of the same specimens are expected not to exceed. It can be noticed from Figure (5-14) that the cyclic envelopes of the curves are almost coincident, however, due to the fact that 40 cycles were applied to the specimens with maximum applied displacement equals 67.5 mm, the ultimate capacity of these connections were not reached. Therefore, the monotonic backbone curve was used to calculate the ductility ratio for each specimen and the FEMA idealized bilinear curves approach were used. As illustrated in Figure (5-15) for model S-G3-R, the secant slope of the curve was assumed to intersect the curve at 60% of the yield capacity (M_y) and consequently, the M_y and its corresponding rotation are obtained. Table (5-3) illustrates the values for the rotations at yielding and ultimate stages.

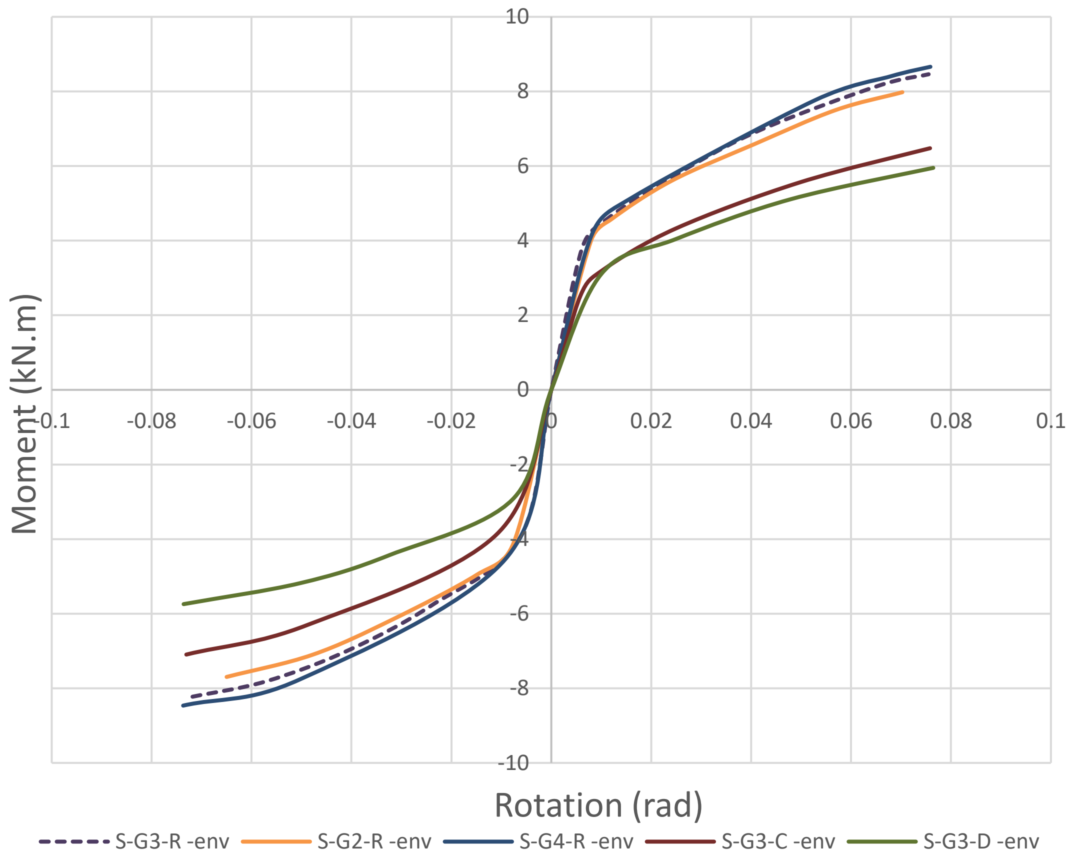

Figure 5- 13: Cyclic envelopes of models

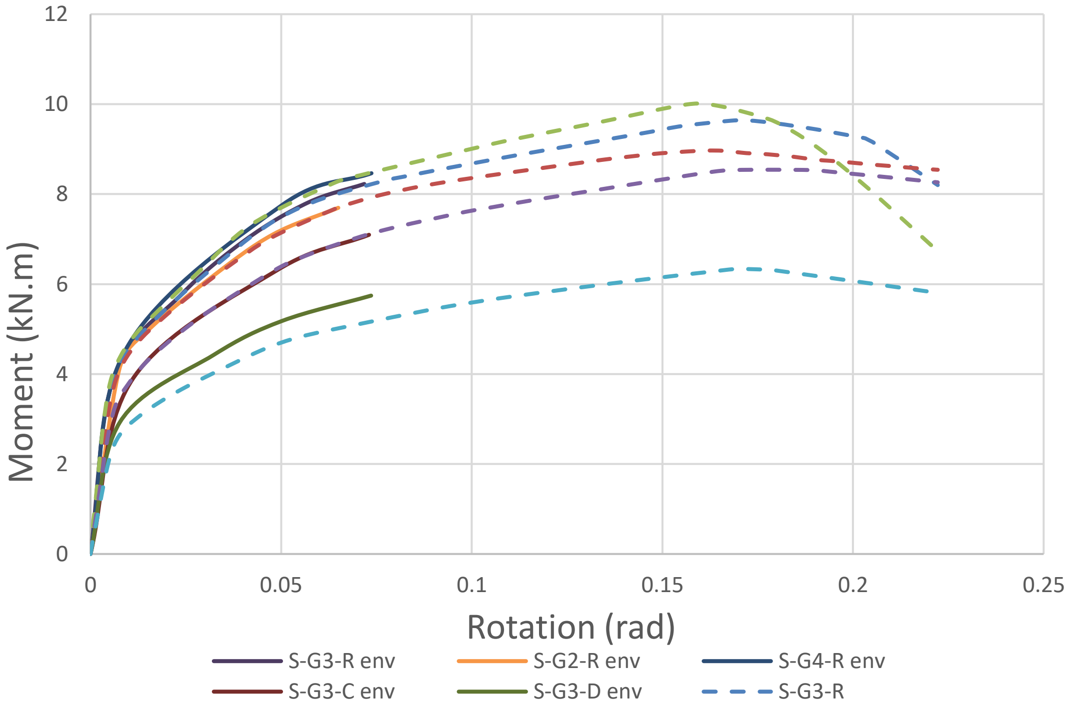

Figure 5- 14: Moment-rotation curves for monotonically and cyclic loaded models

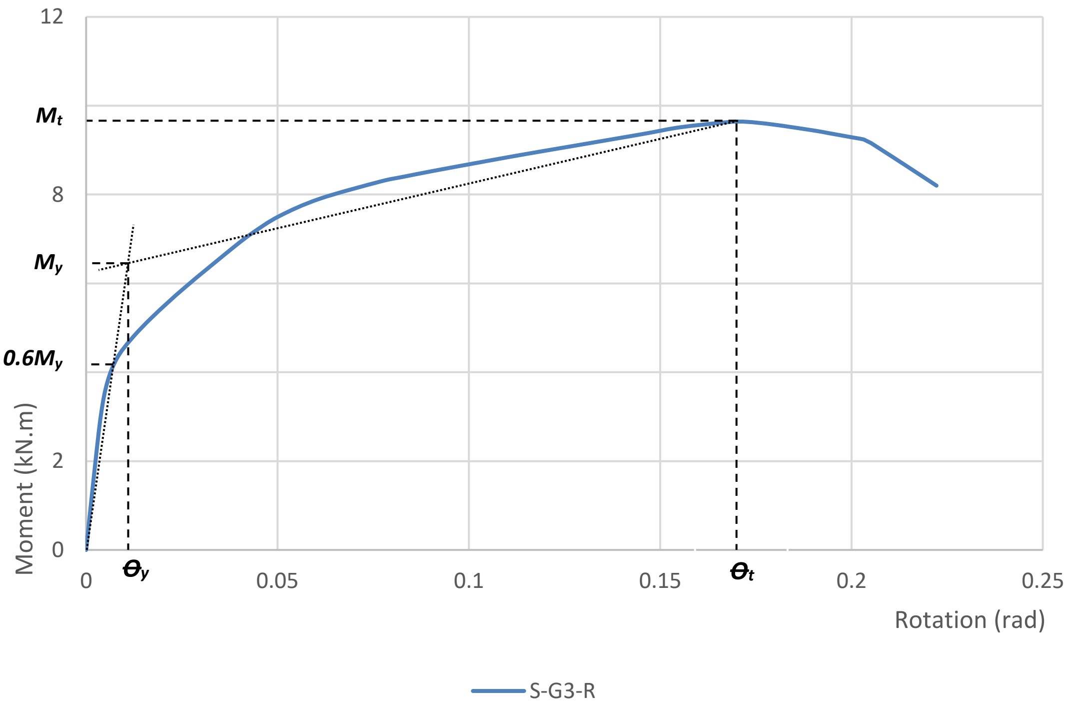

Figure 5- 15: Ductility ratio calculations for model S-G3-R

Table 5- 3: Ductility ratio calculations

Model ID	θ_y	θ_t	Ductility ratio $\mu = \theta_t/\theta_y$
S-G3-R	0.01	0.173	17.3
S-G2-R	0.012	0.162	13.5
S-G4-R	0.01	0.156	15.6
S-G3-C	0.0105	0.177	16.6
S-G3-D	0.011	0.17	15.5

It can be noticed from table (5-3) that the values for ductility ratios are close except for S-G2-R, where the gusset plate thickness is 2 mm. Specimen S-G3-R provided the highest ductility ratio while S-G2-R provided the lowest ductility ratio, which reflects the effect of the gusset plate thickness on the ductility of the connections when using self-drilling screws.

Another measure of the adequacy of using such connections in certain seismic zones is the classification of moment resisting whether they are OMF, IMF or SMF. It was found that all the specimens mentioned above satisfy the conditions to classify as SMF. These frames were capable of accommodating a rotation of 0.04 rad with degradation in strength less than 20%.

The energy dissipation capacity of structural elements is one of the most important aspects of seismic resistant design. The energy dissipated by the connections is calculated as the area under the cyclic envelope using numerical integration (trapezoidal rule). As illustrated in Figure (5-16), the curve is divided into partitions and the trapezoidal rule was used to get the area under each curve of the five models.

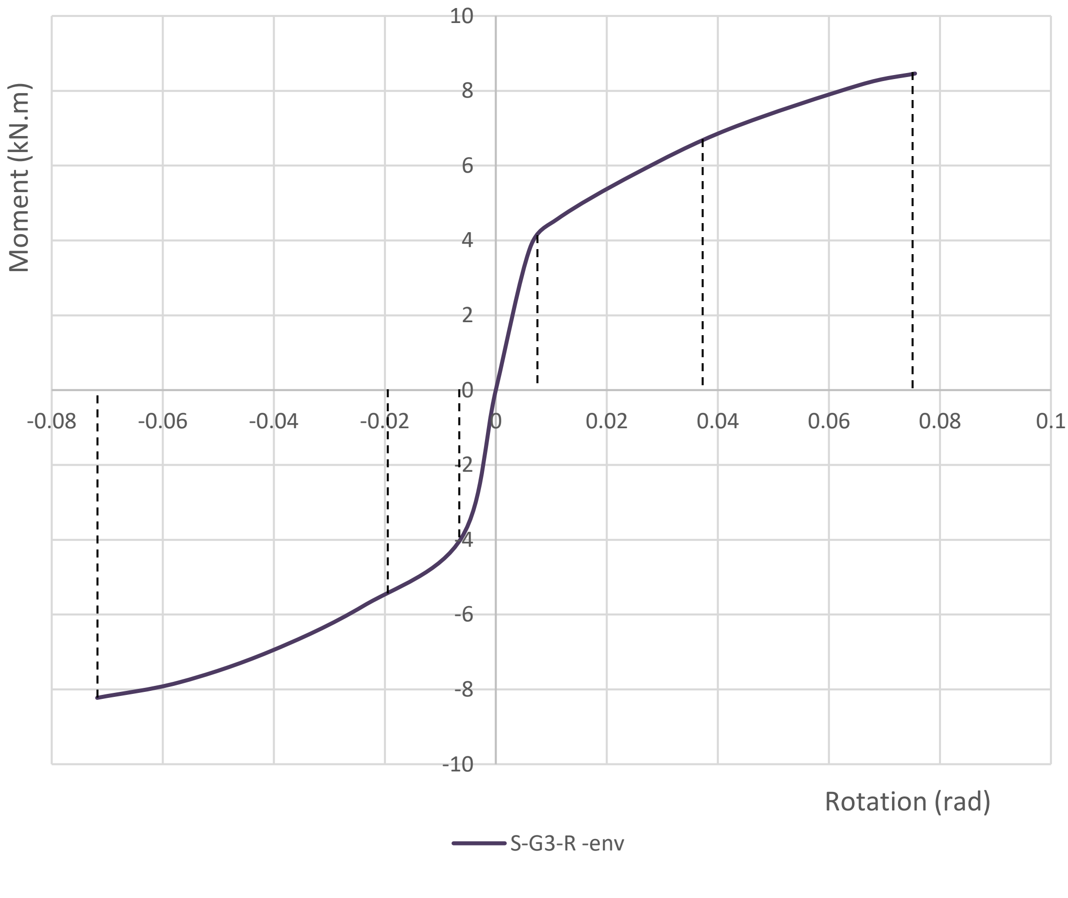

Figure 5- 16: Calculations of energy dissipation using trapezoidal rule

Another measure of the energy dissipative capacity of the connections is the viscous damping coefficient. The damping coefficient considers the peak moment loops where the energy dissipated by the peak moment cycle (area shaded in blue in Figure 5-17) is divided by the total strain energy (area shaded in red in Figure 5-18) and calculated using the following equation:

$$\boldsymbol{C_e = \frac{1}{2\pi}\frac{S_{ABC}+S_{CDA}}{S_{OBE}+S_{ODF}}} \qquad \textbf{\textit{Eq. 2-2}}$$

$$C_e = \frac{1}{2\pi} \times \frac{364.1}{617.8} = 0.094$$

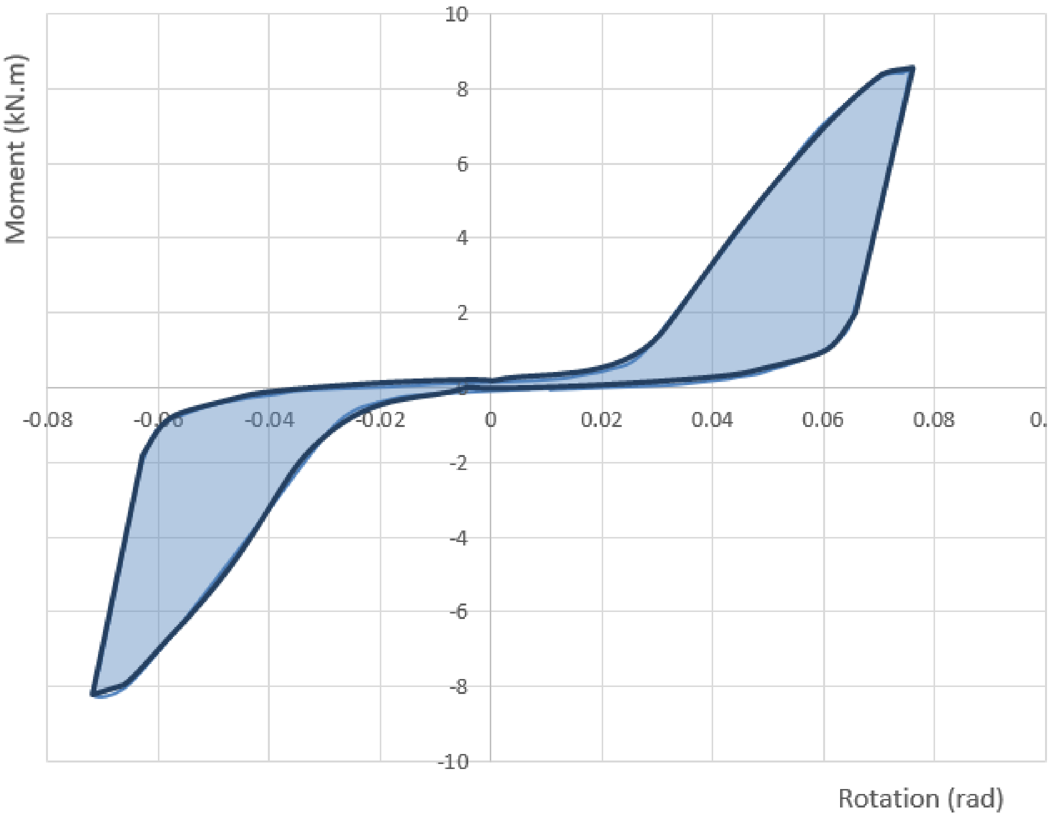

Figure 5- 17: Calculations of energy dissipated during the peak cycle for S-G3-R

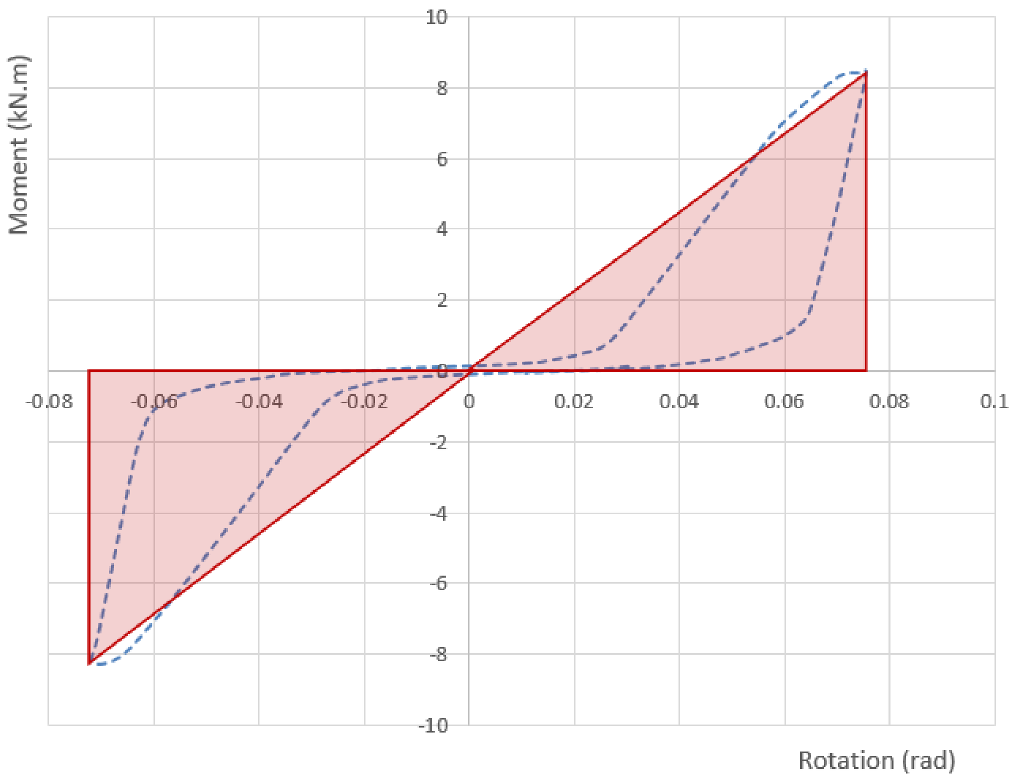

Figure 5- 18: Calculations of the strain energy from the peak cycle for S-G3-R

A summary of the results of the area under the cyclic envelopes for calculating the energy dissipation capacity and the values for the damping coefficient are presented in table (5-4).

Table 5- 4: Comparison of results

	S-G3-R	S-G2-R	S-G4-R	S-G3-C	S-G3-D
Max Load Upwards (kN)	9.4	8.9	9.6	7.2	6.0
Max Load Downwards (kN)	-9.1	-8.6	-9.4	-7.9	-5.7
Max +ve Moment (kN.m)	8.5	8.0	8.7	6.5	5.4
Max -ve Moment (kN.m)	-8.2	-7.7	-8.5	-7.1	-5.2
Dissipated Energy (J)	919	790	945	731	583
Damping Coefficient	0.094	0.094	0.087	0.094	0.096

5.2.5. Parametric Study 2: Screw-Fastened Connections

The second parametric investigation conducted is the screw-fastened connection with an additional top plate. As mentioned earlier, the study includes different gusset plate thicknesses and different screw arrangements, and certain aspects of the connection is investigated. Model ST-G3-R is the experimentally verified model, and different parameters varied afterwards. The following table summarizes the models' information for this study:

Table 5- 5: Parametric Study 2 data

Model ID	Type of Fasteners used	Fasteners' arrangement	Gusset Plate Thickness
ST-G3-R	Screws	Rectangular	3 mm
ST-G2-R	Screws	Rectangular	2 mm
ST-G4-R	Screws	Rectangular	4 mm
ST-G3-C	Screws	Circular	3 mm
ST-G3-D	Screws	Diamond	3 mm

A monotonic gravity displacement is applied to the specimens and the moment-rotation relationship is recorded as shown in Figure (5-23). The deformed shapes for each model are illustrated in Figure (5-19)-(5-22). From the deformed shapes, it can be seen that the failure modes are different from one model to another. For ST-G3-R, failure occurred in the screws, which can be noticed as stress concentrations at the location of the screws, while slight deformation in the beam flange is also noticed Figure (5-19). When the gusset plate thickness is reduced to 2 mm in model ST-G2-R, the failure mode did not change much Figure (5-20). Finally, ST-G3-C and ST-G3-D showed an increase in the stresses in the top plate as the circular and diamond arrangements are more flexible that their rectangular counterpart.

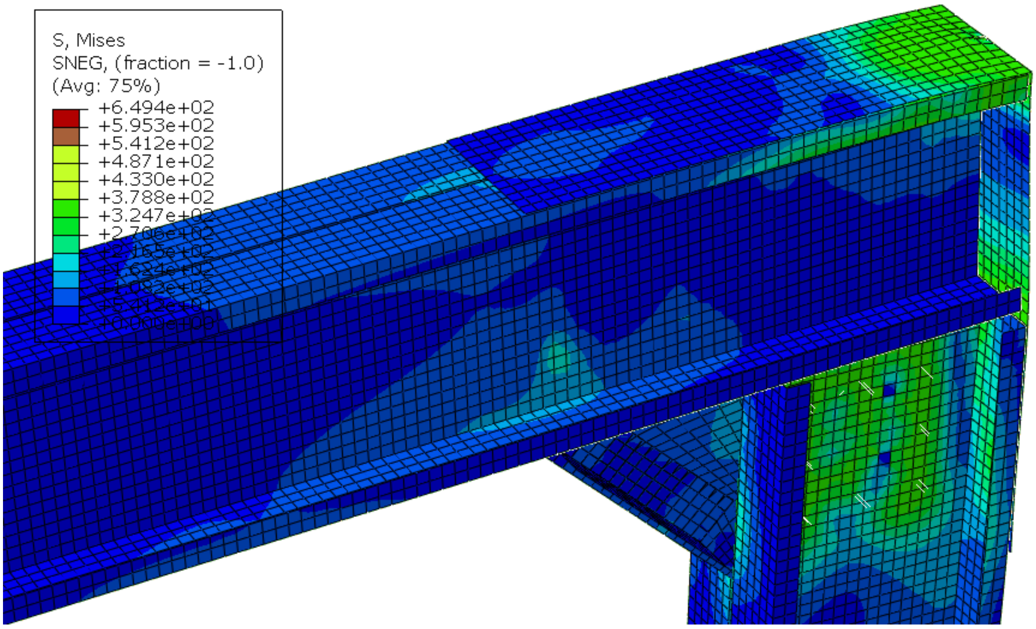

Figure 5- 19: Deformed shape for ST-G3-R

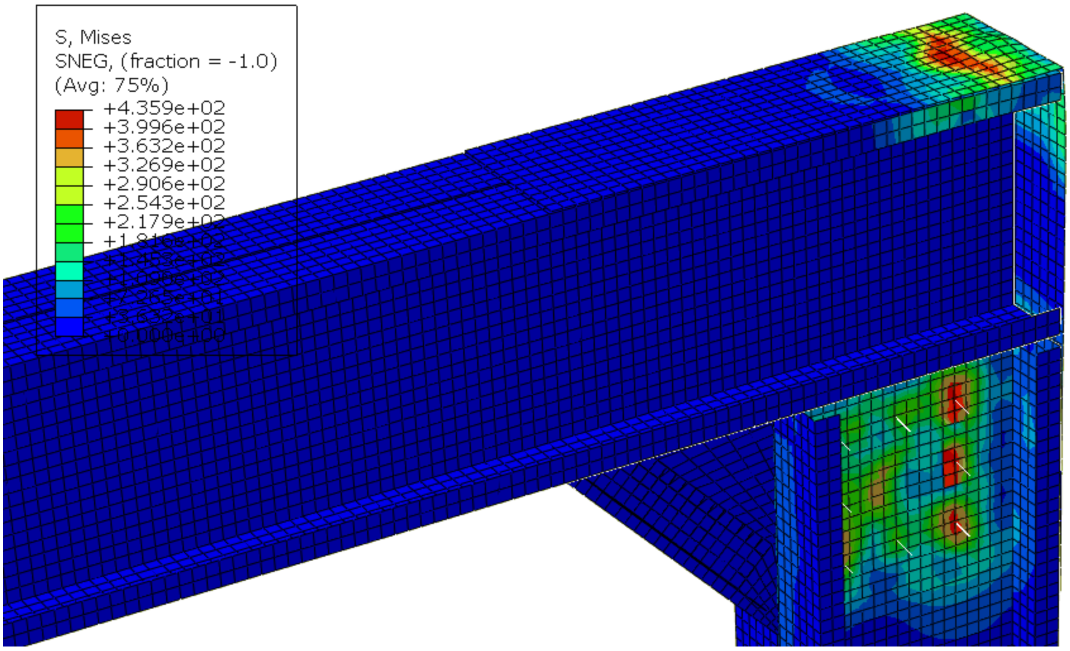

Figure 5- 20: Deformed shape for ST-G2-R

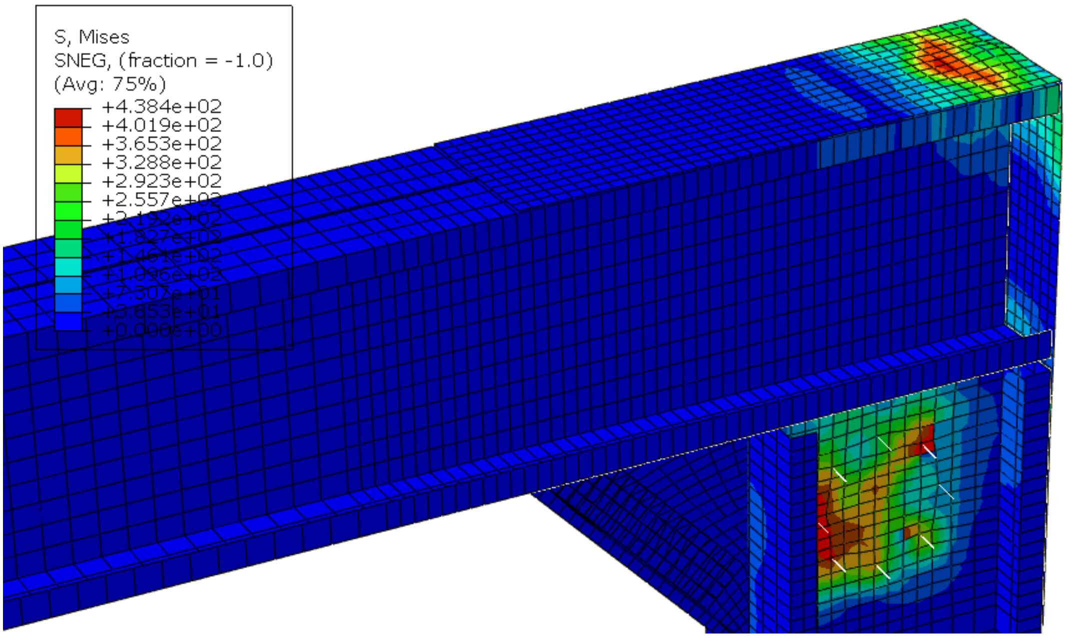

Figure 5- 21: Deformed shape for ST-G3-C

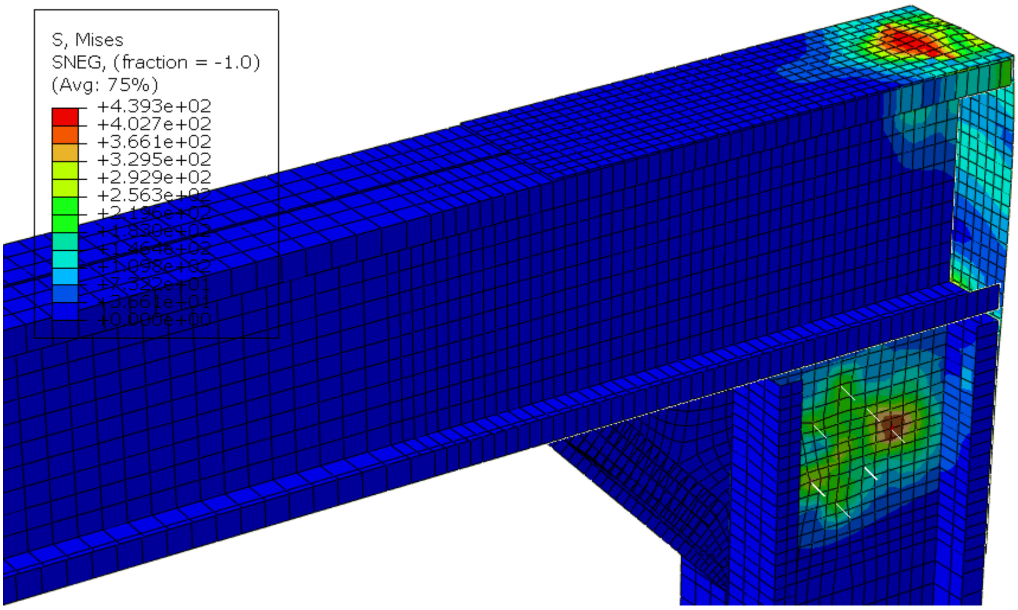

Figure 5- 22: Deformed shape for ST-G3-D

From the moment-rotation relationship illustrated in Figure (5-23)., it can be noticed that model ST-G3-C provided the highest moment capacity equals to 12.6 kN.m at rotation equals 0.08 rad. Model ST-G3-R provided the second highest moment capacity equals to 12.5 kN.m at rotation equals 0.06 rad. The third highest was model ST-G2-R (gusset = 2mm) with moment capacity equals 12.4 kN.m at rotation equals to 0.074 rad. Model ST-G3-D provided the worst performance in terms of strength when subjected to monotonic gravity load with moment capacity equals 11.3 kN.m at rotation equals 0.05 rad. The circular screws arrangement provided better results over the diamond arrangement. In order to provide better insight for the connection strength and behavior, the connections' moment output data were divided by the cold-formed section's nominal flexural strength and provided in Figure (5-24).

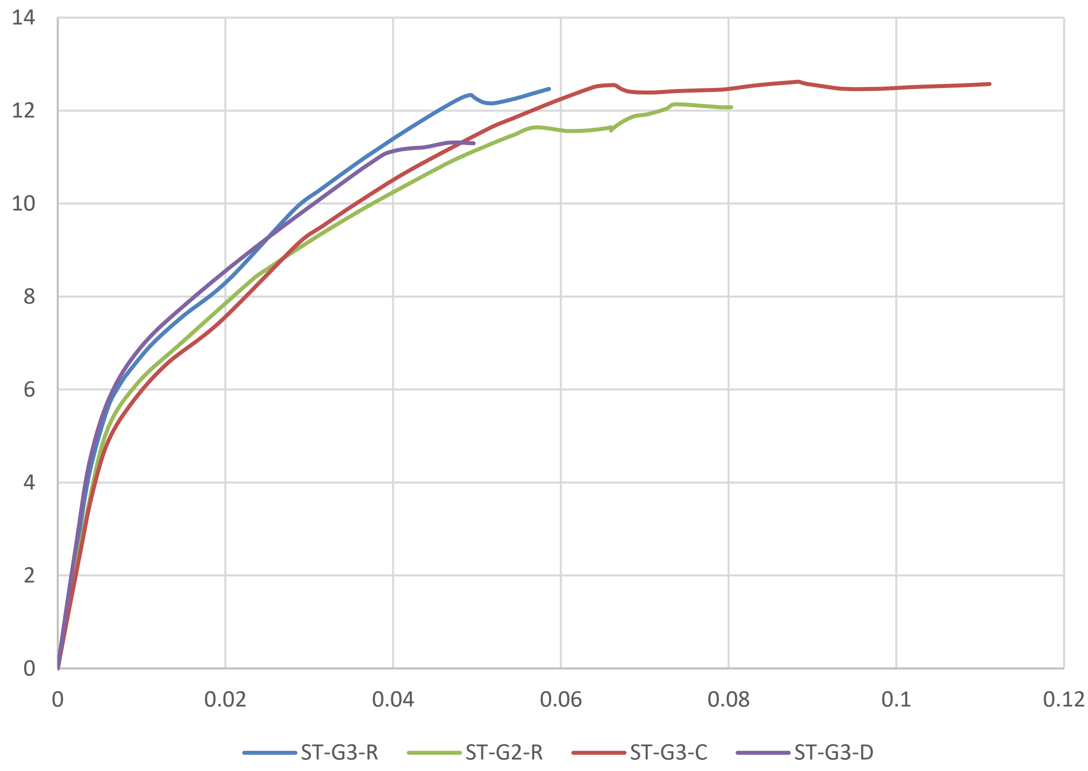

Figure 5- 23: Moment-rotation curves for monotonically loaded models

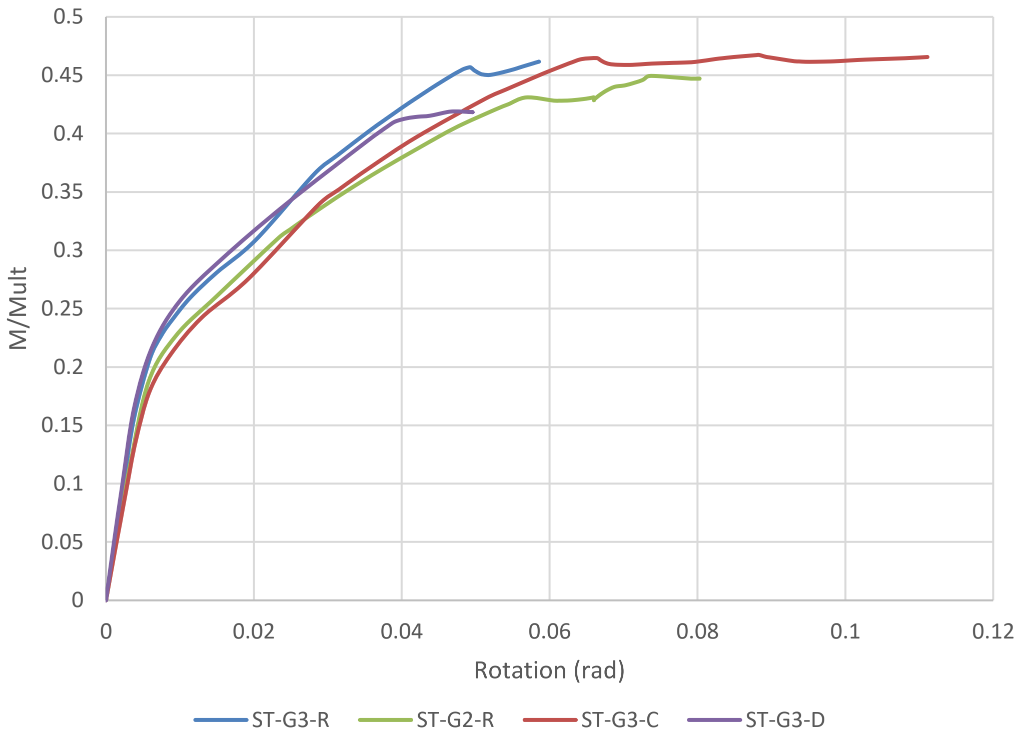

Figure 5- 24: Moment/Section Capacity-rotation curves for monotonically loaded models

The cyclic envelope of the load-displacement (or Moment-rotation) relationship is essential for the assessment of ductility. A number of 40 cycles were applied to each specimen in the models similar to the experimental program even though the models have shown that the specimens can still carry more loads Figure (5-25). It can also be noticed from Figure (5-25) that the hysteresis loops of the connections where similar in behavior and in agreement with the general behavior of screw-fastened connections mentioned earlier in the literature review chapter. The curves for the hysteresis loops for the models are presented separately in appendix A.

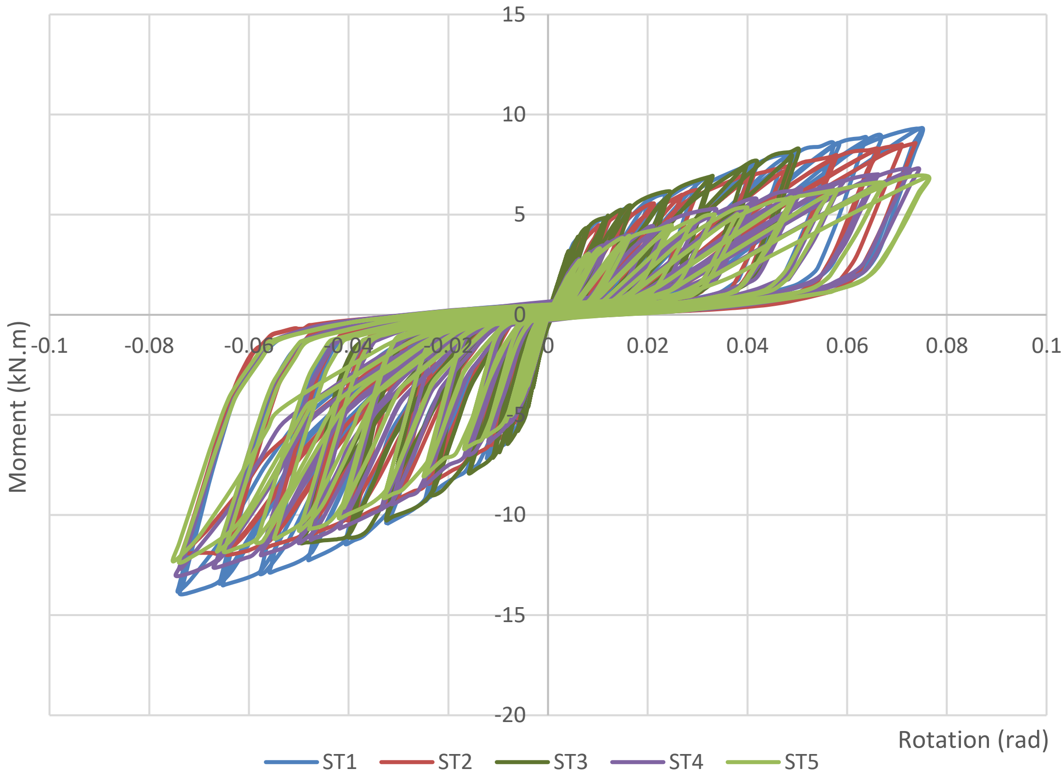

Figure 5- 25: Moment-rotation curves for cyclic loaded models

The envelope of the curves is obtained and presented in Figure (5-26) for further analysis of the results. Moreover, the envelope of the half-cycles in the downward displacement side is separated and compared with the monotonic moment-rotation relationships for all the specimens. The monotonic moment-rotation relationships represent the backbone curve which the cyclic envelope of the same specimens are expected not to exceed. It can be noticed from Figure (5-27) that the cyclic envelopes of the curves are almost coincident, however, due to the fact that 40 cycles were applied to the specimens with maximum applied displacement equals 67.5 mm, the ultimate capacity of these connections were not reached.

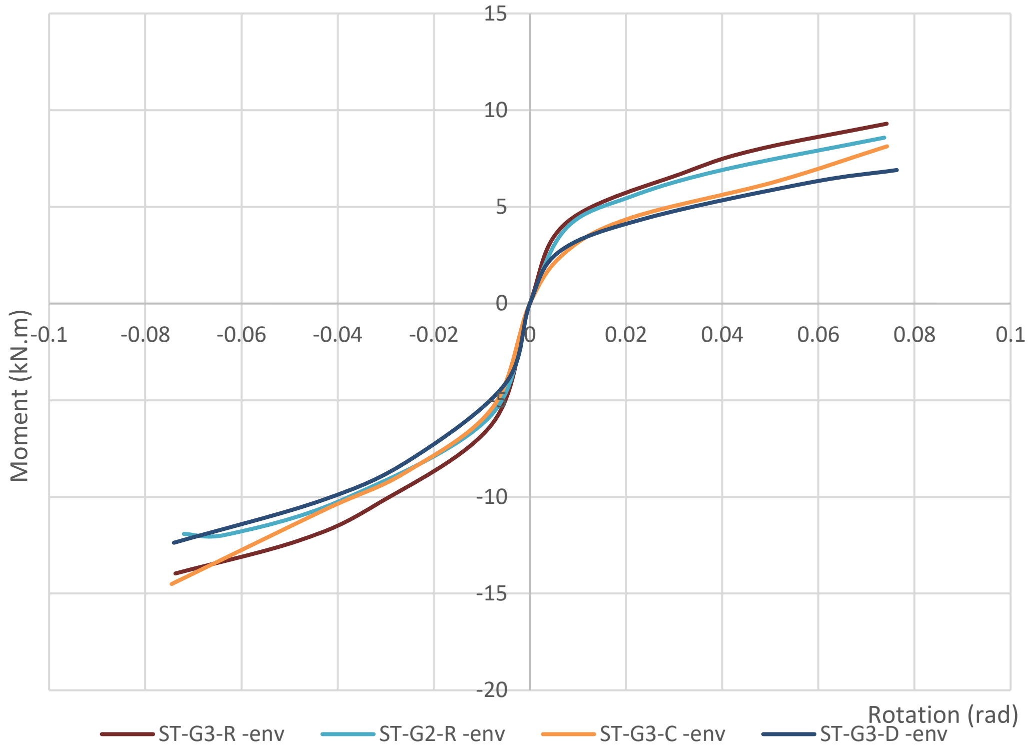

Figure 5- 26: Cyclic envelopes of models

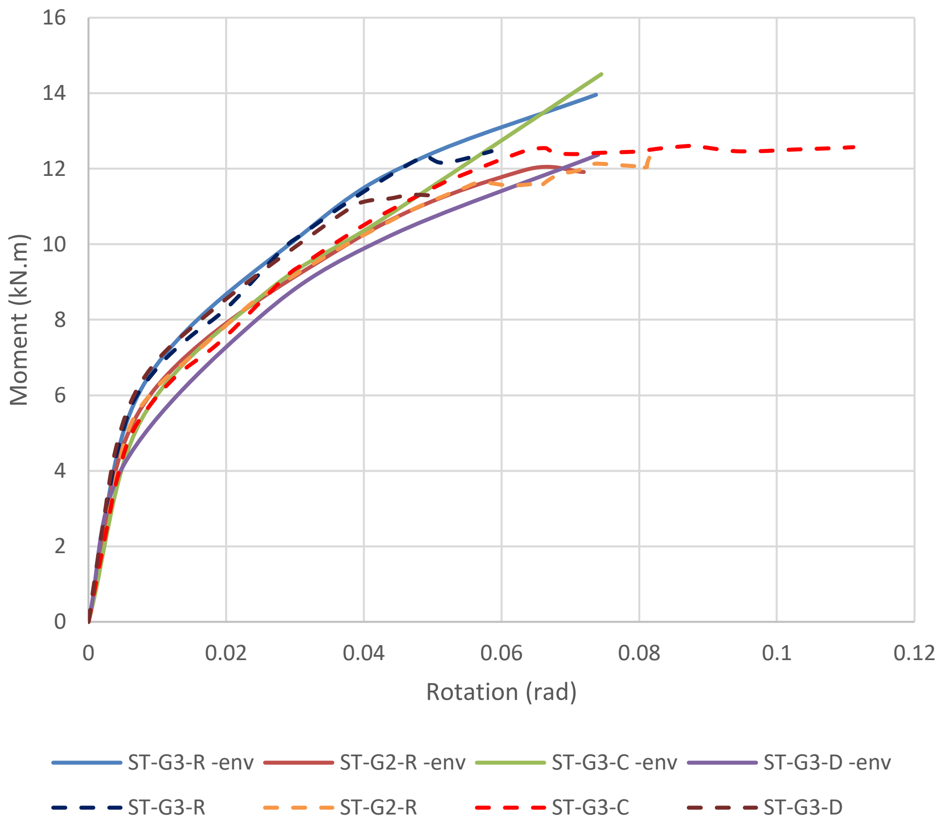

Figure 5- 27: Moment-rotation curves for monotonically and cyclic loaded models

The classification of moment resisting whether they are OMF, IMF or SMF was also considered. It was found that all the specimens mentioned above satisfy the conditions to classify as SMF. These frames were capable of accommodating a rotation of 0.04 rad with degradation in strength less than 20%.

The energy dissipated by the connections is calculated as the area under the cyclic envelope using numerical integration (trapezoidal rule). As illustrated in Figure (5-28), the curve is divided into partitions and the trapezoidal rule was used to get the area under each curve of the five models.

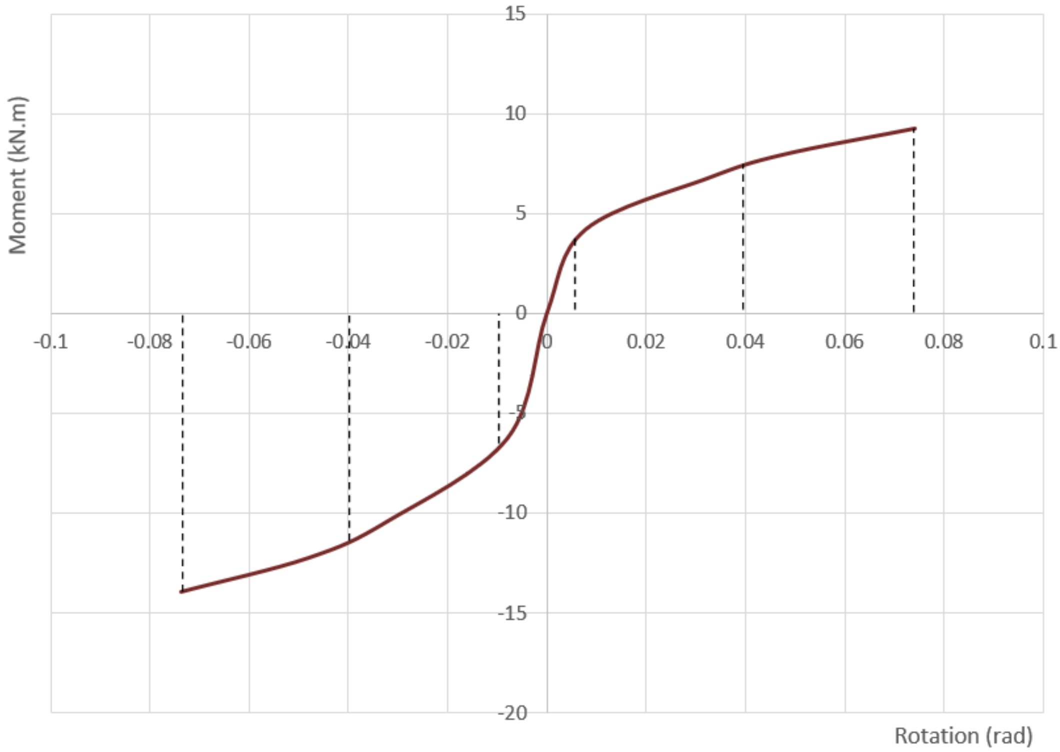

Figure 5- 28: Calculations of energy dissipation using trapezoidal rule

Another measure of the energy dissipative capacity of the connections is the viscous damping coefficient. The damping coefficient considers the peak moment loops where the energy dissipated by the peak moment cycle (area shaded in blue in Figure 5-29) is divided by the total strain energy (area shaded in red in Figure 5-30) and calculated using the following equation:

$$\boldsymbol{C_e = \frac{1}{2\pi}\frac{S_{ABC}+S_{CDA}}{S_{OBE}+S_{ODF}}} \qquad \textbf{\textit{Eq. 2-3}}$$

$$C_e = \frac{1}{2\pi} \times \frac{449}{861} = 0.083$$

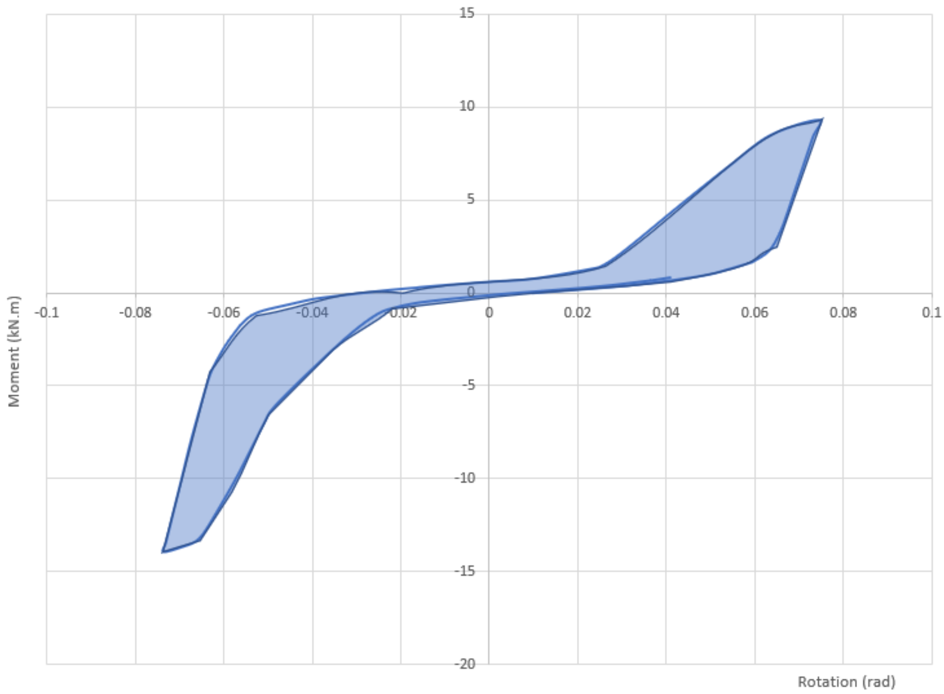

Figure 5- 29: Calculations of energy dissipated during the peak cycle ST-G3-R

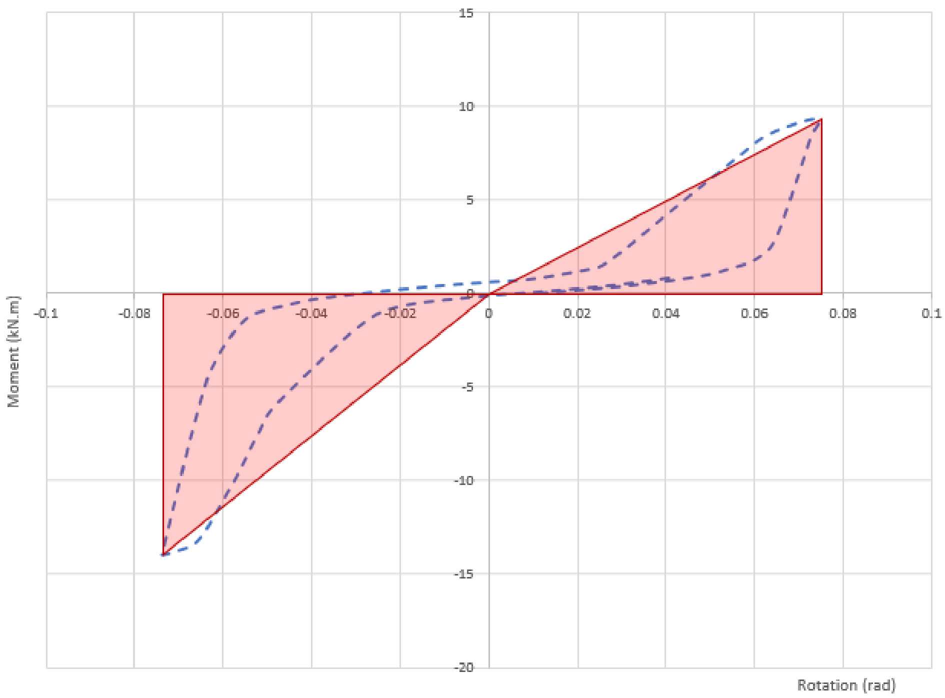

Figure 5- 30: Calculations of the strain energy from the peak cycle ST-G3-R

A summary of the results of the area under the cyclic envelopes for calculating the energy dissipation capacity and the values for the damping coefficient are presented in Table (5-6). It is worth noting that it was intended to test the gusset plate of thickness 4 mm in model ST-G4-R, however, convergence error was a serious issue in model ST-G4-R that could not be overcome, therefore, ST-G4-R was excluded from the results.

Table 5- 6: Comparison of results

	ST-G3-R	ST-G2-R	ST-G3-C	ST-G3-D
Max Load Upwards (kN)	10.3	9.5	8.1	6.9
Max Load Downwards (kN)	-15.5	13.3	-14.5	-12.4
Max +ve Moment (kN.m)	9.3	8.6	7.3	6.5
Max -ve Moment (kN.m)	-14	-12	-13.1	-11.1
Dissipated Energy (J)	1238	1099	1067	917
Damping Coefficient	0.083	0.094	0.076	0.077

5.2.6. Parametric Study 3: Bolted Connections

The third and last parametric investigation conducted is the bolted connection. Similar to the two previous parametric studies, different gusset plate thicknesses and different screw arrangements are investigated. Model B-G2-R is the experimentally verified model, and different parameters varied afterwards. The following table summarizes the models' information for this study:

Model ID	Type of Fasteners used	Fasteners' arrangement	Gusset Plate Thickness
B-G2-R	Bolts	Rectangular	2 mm
B-G3-R	Bolts	Rectangular	3 mm
B-G4-R	Bolts	Rectangular	4 mm
B-G2-C	Bolts	Circular	2 mm
B-G2-D	Bolts	Diamond	2 mm

A monotonic gravity displacement is applied to the specimens and the moment-rotation relationship is recorded as shown in Figure (5-36). The deformed shapes of the models are illustrated in Figures (5-31)-(5-35). Failure modes are not very different from one another as all of the specimens' failure mode involved buckling in the columns' inner flanges and no failure occurred in the bolts as illustrated Figure (5-31) through (5-35). When the gusset plate thickness was 2 mm in models B-G2-R, B-G2-C and B-G2-D, both the gusset plate and the column flanges buckled. When the gusset plate was increased to 3 mm in model B-G3-R, the gusset plate slightly buckled while the column flange deformed as indicated in Figure (5-32). Finally, when the gusset plate of 4 mm thickness was used, only buckling of column flanges took place.

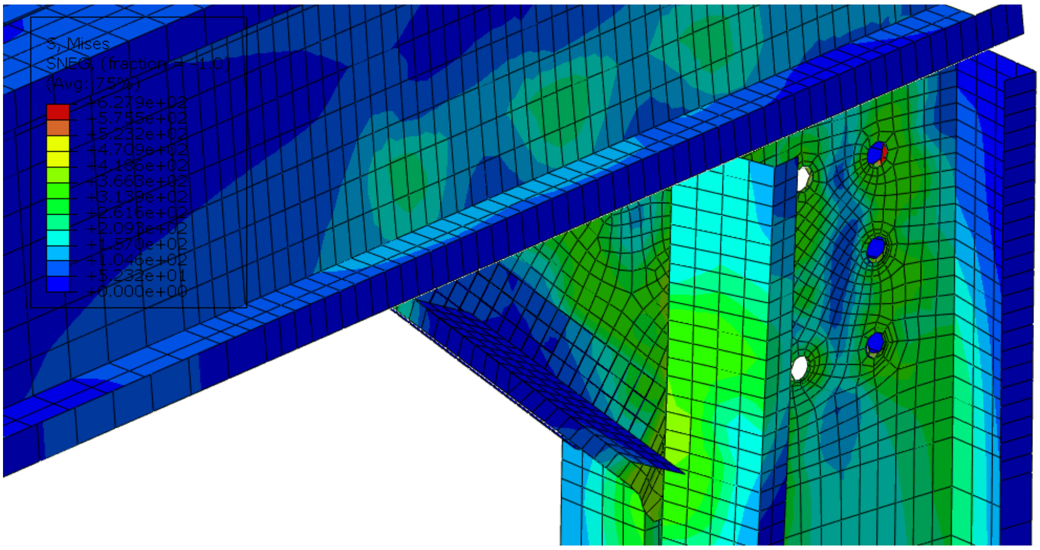

Figure 5- 31: Deformed shape for B-G2-R

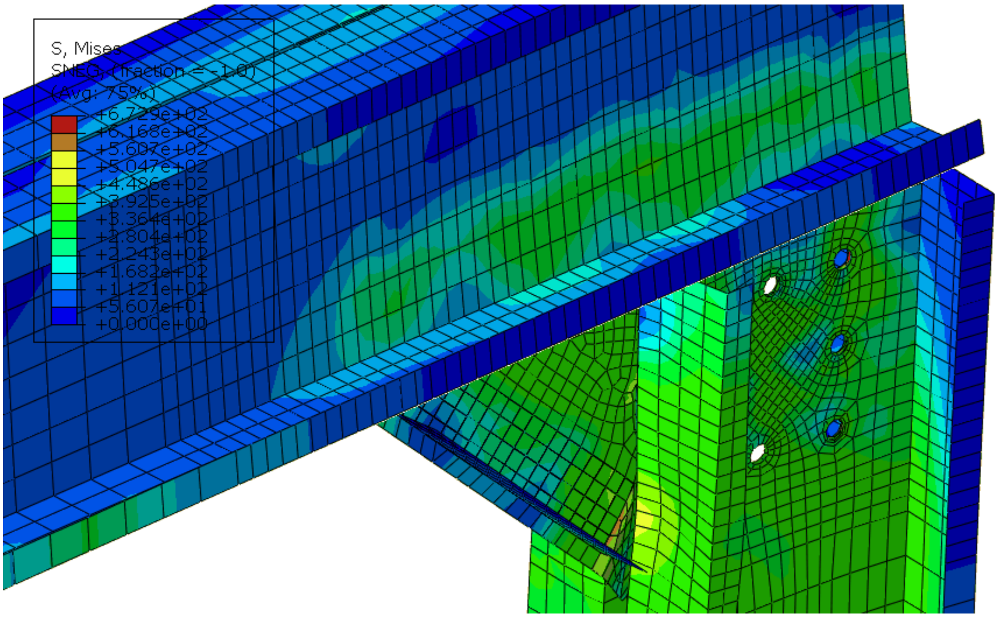

Figure 5- 32: Deformed shape for B-G3-R

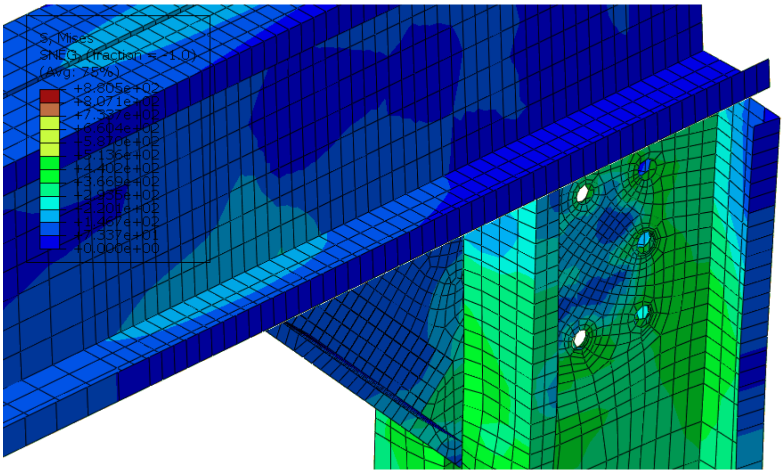

Figure 5- 33: Deformed shape for B-G4-R

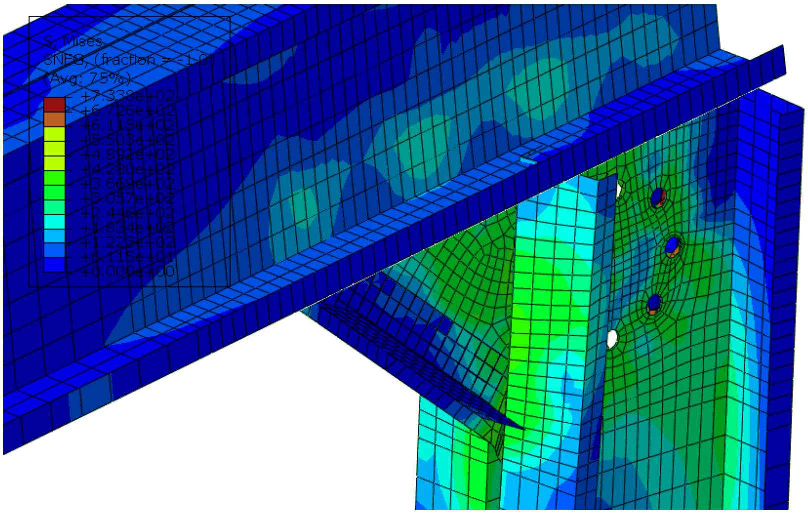

Figure 5- 34: Deformed shape for B-G2-C

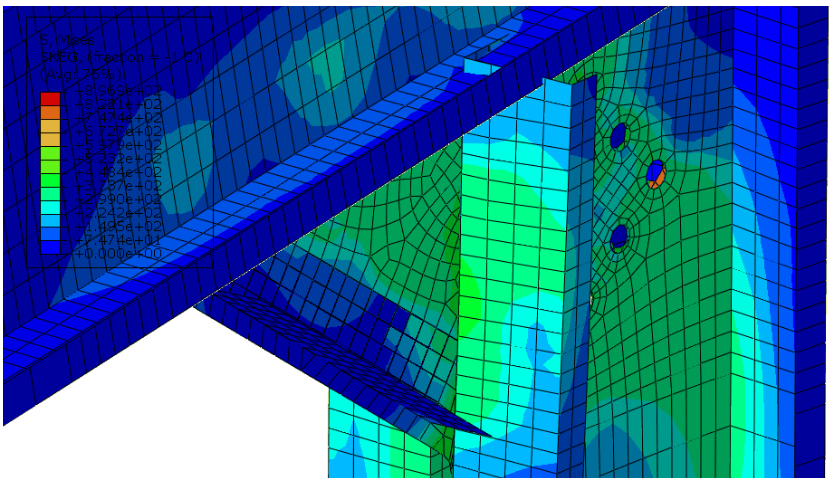

Figure 5- 35: Deformed shape for B-G2-D

From the moment-rotation relationship illustrated in Figure (5-36), it can be noticed that model B-G4-R provided the highest moment capacity equals to 21.4 kN.m at rotation equals 0.092 rad. Model B-G3-R provided the second highest moment capacity equals to 17.52 kN.m at rotation equals 0.07 rad. The third highest was model B-G2-R (gusset = 2 mm, rectangular bolt arrangement) with moment capacity equals 13.4 kN.m at rotation equals to 0.078 rad. Model B-G2-D provided the least performance in terms of strength when subjected to monotonic gravity load with moment capacity equals 11.4 kN.m, however, the rotation significantly increased (0.17 rad). The circular screws arrangement provided better results over the diamond arrangement with moment capacity equals 12.15 kN.m at rotation equals 0.134 rad. In order to provide better insight for the connection strength and behavior, the connections' moment output data were divided by the cold-formed section's nominal flexural strength and provided in Figure (5-37).

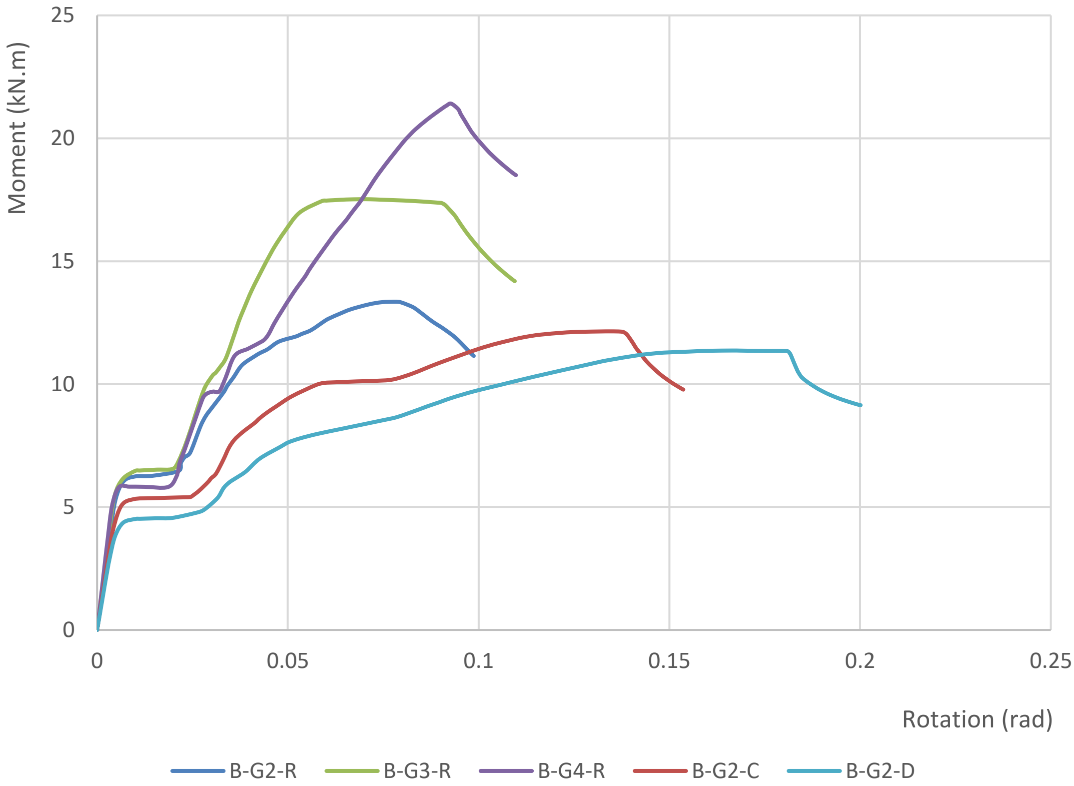

Figure 5- 36: Moment-rotation curves for monotonically loaded models

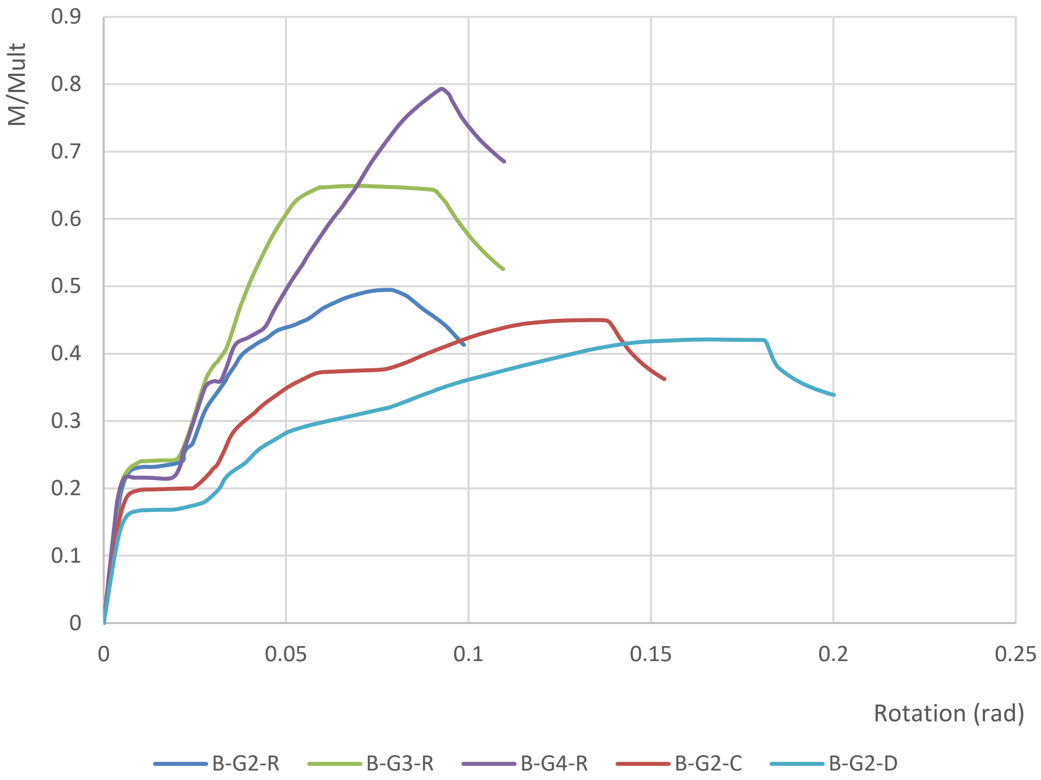

Figure 5- 37: Moment/Section Capacity-rotation curves for monotonically loaded models

As mentioned earlier, the cyclic envelope of the load-displacement (or Moment-rotation) relationship is provided for the assessment of ductility. A number of 40 cycles were applied to each specimen in the models similar to the experimental program even though models B-G3-R and B-G4-R have shown that they can still carry more loads Figure (5-38). It can also be noticed from Figure (5-38) that the hysteresis loops of the connections where similar in behavior and in agreement with the general behavior of bolted connections mentioned earlier in the literature review chapter. The curves for the hysteresis loops for the models are presented separately in appendix A.

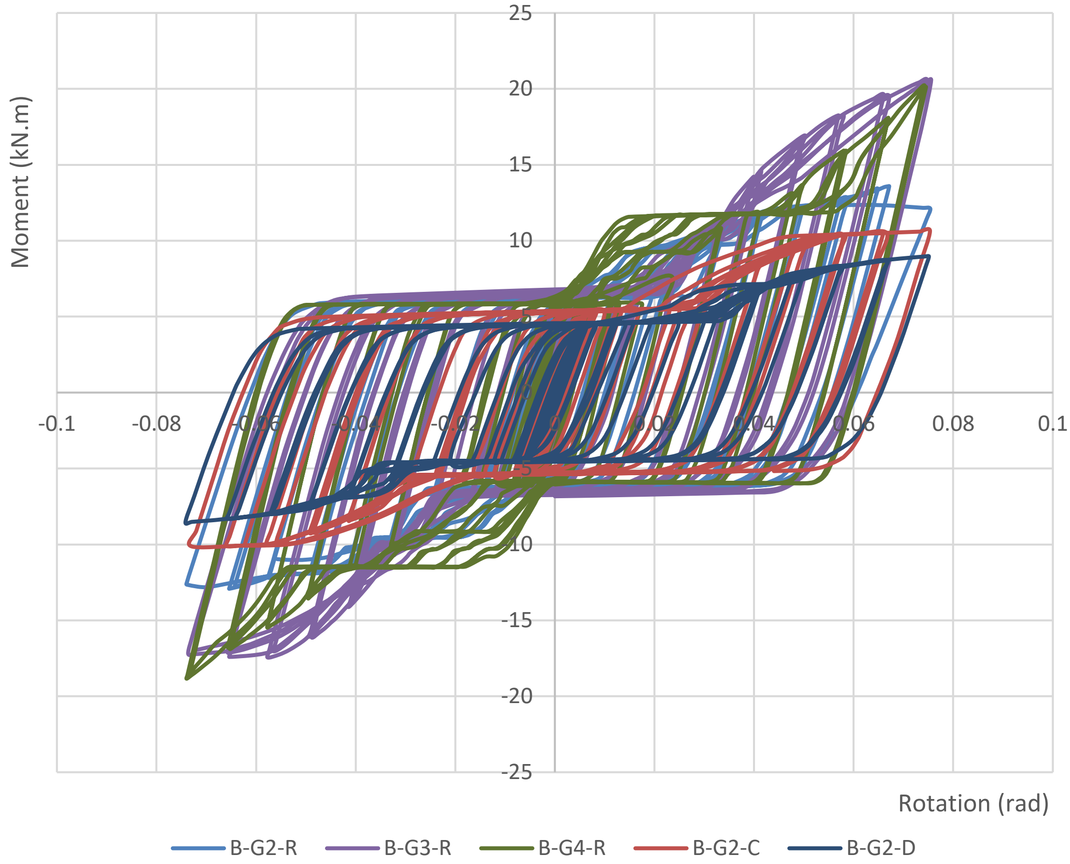

Figure 5- 38: Moment-rotation curves for cyclic loaded models

The envelope of the curves is obtained and presented in Figure (5-39) for further analysis of the results. Moreover, the envelope of the half-cycles in the downward displacement side is separated and compared with the monotonic moment-rotation relationships for all the specimens. It can be noticed from Figure (5-40) that the cyclic envelope of the curve of B-G2-R has about 10% less peak moment than the monotonic loading, however, all other models show that more than 40 cycles were required to reach the peak cyclic moment with applied displacement more than 67.5 mm. Consequently, the monotonic backbone curve was used to calculate the ductility ratio for each specimen. As illustrated in Figure (5-41) for model B-G2-R, the yield capacity (M_y) is taken at the end of the plateau and consequently, its corresponding rotation is obtained. Table (5-7) illustrates the values for the rotations at yielding and ultimate stages.

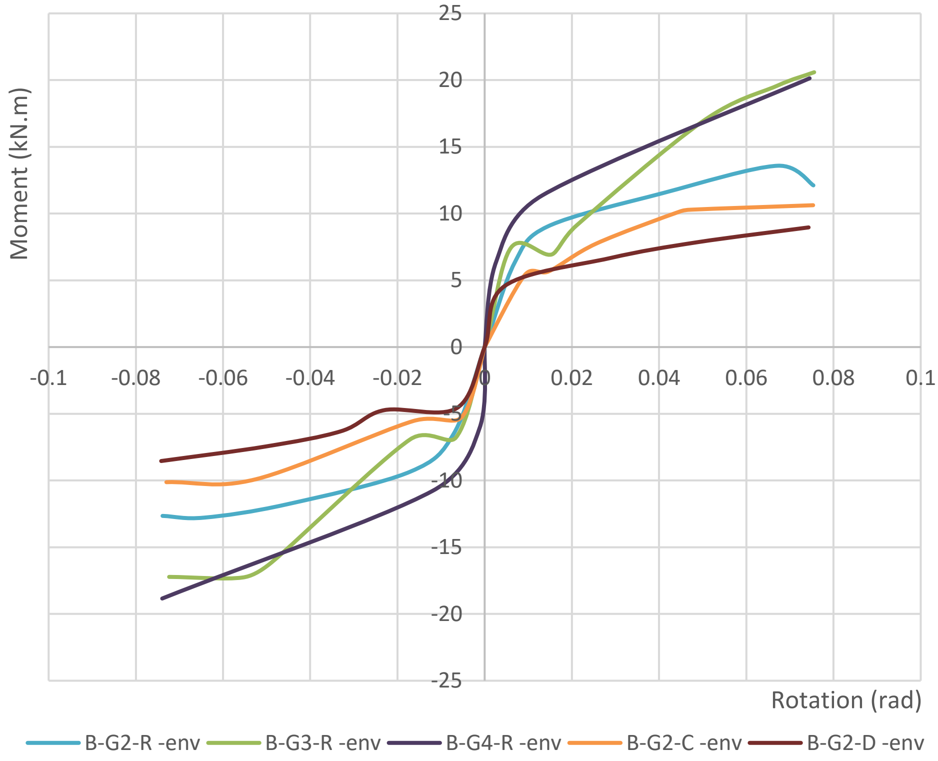

Figure 5- 39: Cyclic envelopes of models

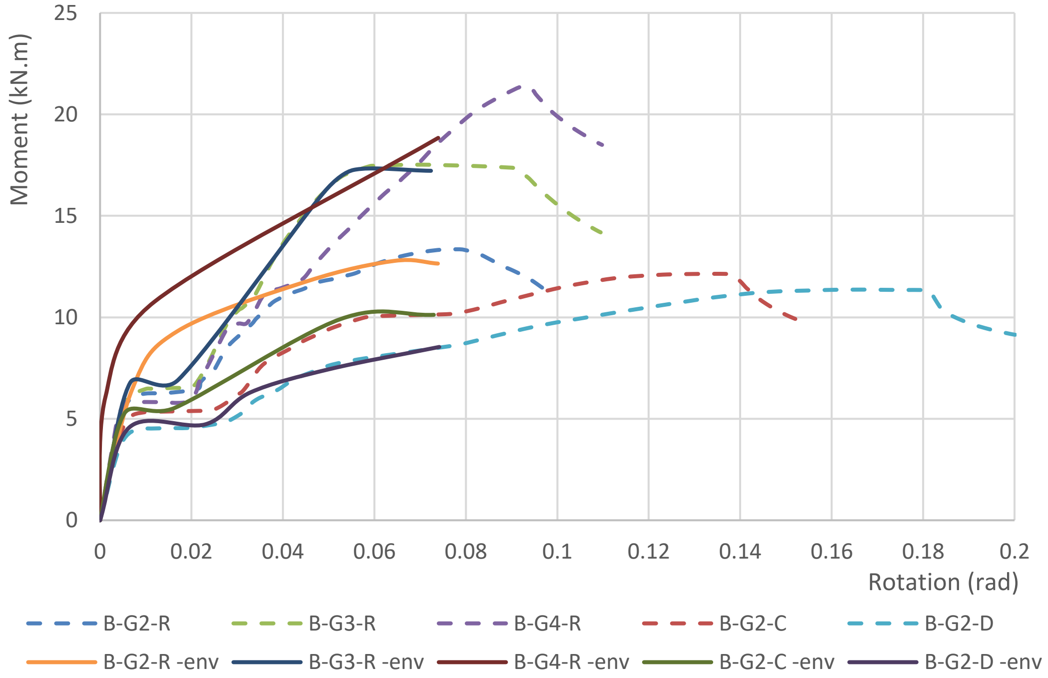

Figure 5- 40: Moment-rotation curves for monotonically and cyclic loaded models

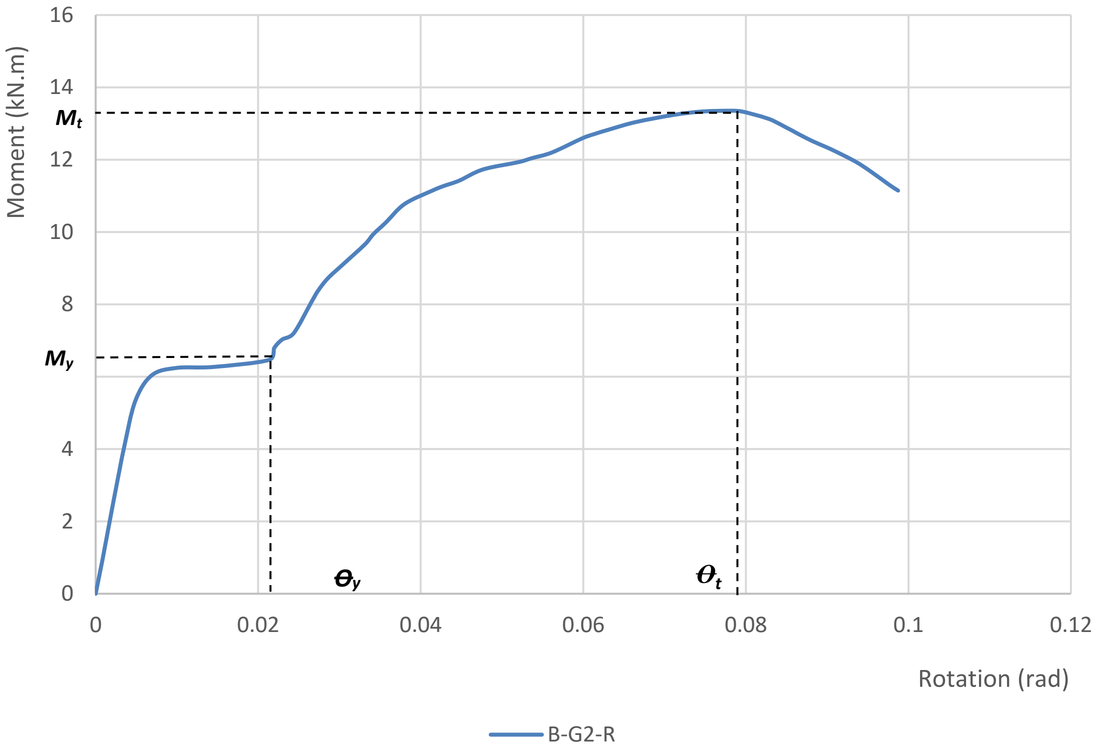

Figure 5- 41: Calculations of energy dissipation using trapezoidal rule

Table 5- 7: Ductility ratio calculation

Model ID	$\boldsymbol{\theta_y}$	$\boldsymbol{\theta_t}$	$\boldsymbol{Ductility\ ratio}$ $\boldsymbol{\mu = \theta_t/\theta_y}$
S-G3-R	0.021	0.078	3.71
S-G2-R	0.02	0.07	3.5
S-G4-R	0.019	0.093	4.9
S-G3-C	0.024	0.134	5.58
S-G3-D	0.028	0.166	6

It can be noticed from table (5-7) that the values for ductility ratios ranges from 3.5 to 6 where model B-G3-R gave the lowest ductility ratio and model B-G2-D gave the highest. Unlike the self-drilling screws models, the diamond bolts arrangement provided higher ductility ratio which indicates that the connection can tolerate larger deformations while maintaining the load carrying capacity. The circular bolts arrangement was the second highest and provided larger moment capacity which also proves that circular arrangement can provide better ductility over the conventional rectangular bolts arrangement

As mentioned earlier, the classification of moment resisting whether they are OMF, IMF or SMF is also investigated for these frames. It was found that all the specimens mentioned above satisfy the conditions to classify as SMF. These frames were capable of accommodating a rotation of 0.04 rad with degradation in strength less than 20%.

The energy dissipation capacity of structural elements is one of the most important aspects of seismic resistant design. The energy dissipated by the connections is calculated as the area under the cyclic envelope using numerical integration (trapezoidal rule). As illustrated in Figure (5-42), the curve is divided into partitions and the trapezoidal rule was used to get the area under each curve of the five models.

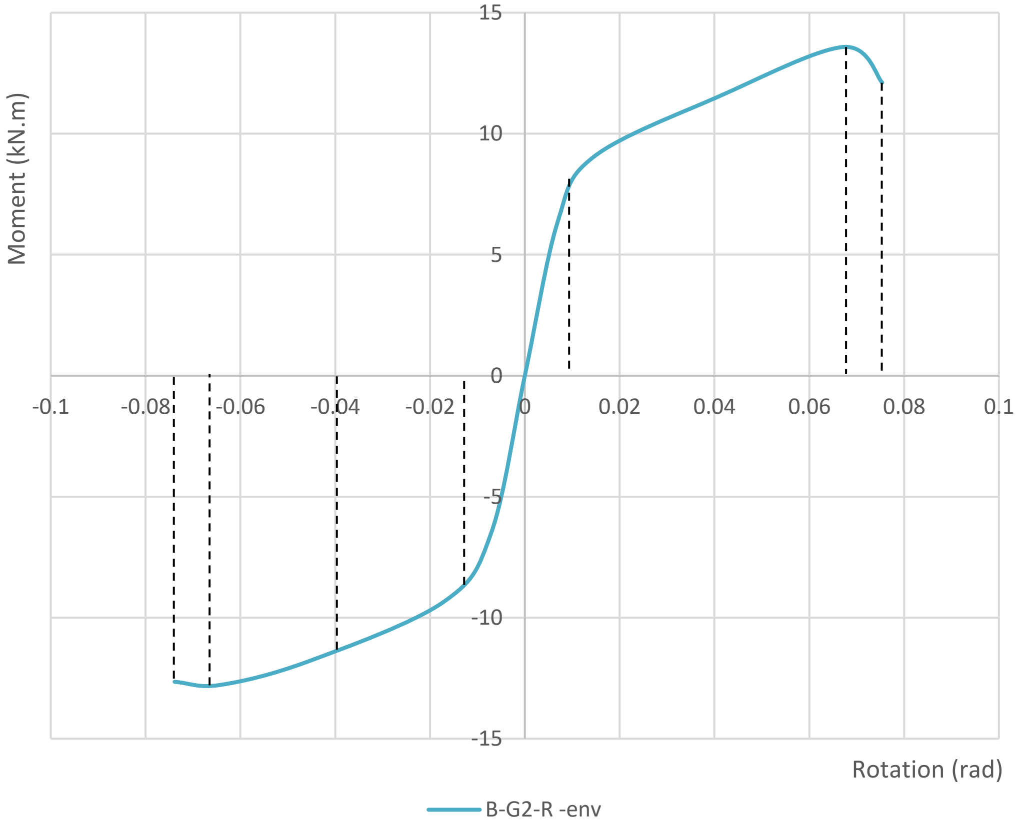

Figure 5- 42: Calculations of energy dissipation using trapezoidal rule

Another measure of the energy dissipative capacity of the connections is the viscous damping coefficient. The damping coefficient considers the peak moment loops where the energy dissipated by the peak moment cycle (area shaded in blue in Figure 5-43) is divided by the total strain energy (area shaded in red in Figure 5-44) and calculated using the following equation:

$$C_e = \frac{1}{2\pi} \frac{S_{ABC} + S_{CDA}}{S_{OBE} + S_{ODF}}$$

$$C_e = \frac{1}{2\pi} \times \frac{1791}{865} = 0.33$$

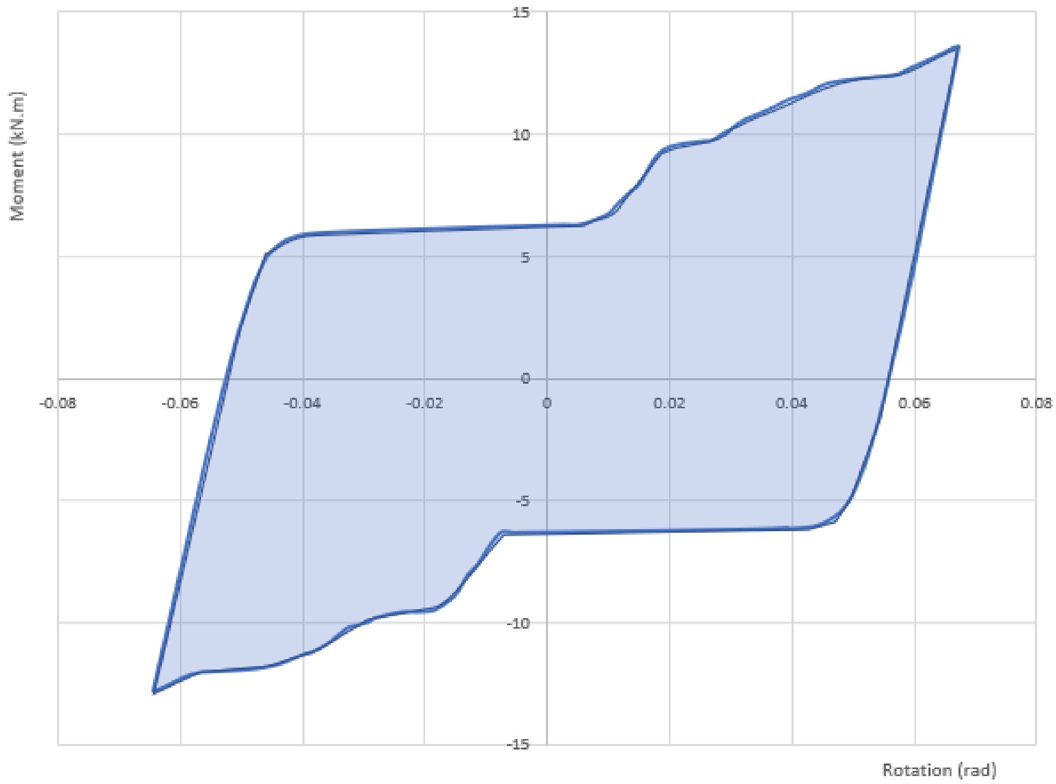

Figure 5- 43: Calculations of energy dissipated during the peak cycle for B-G2-R

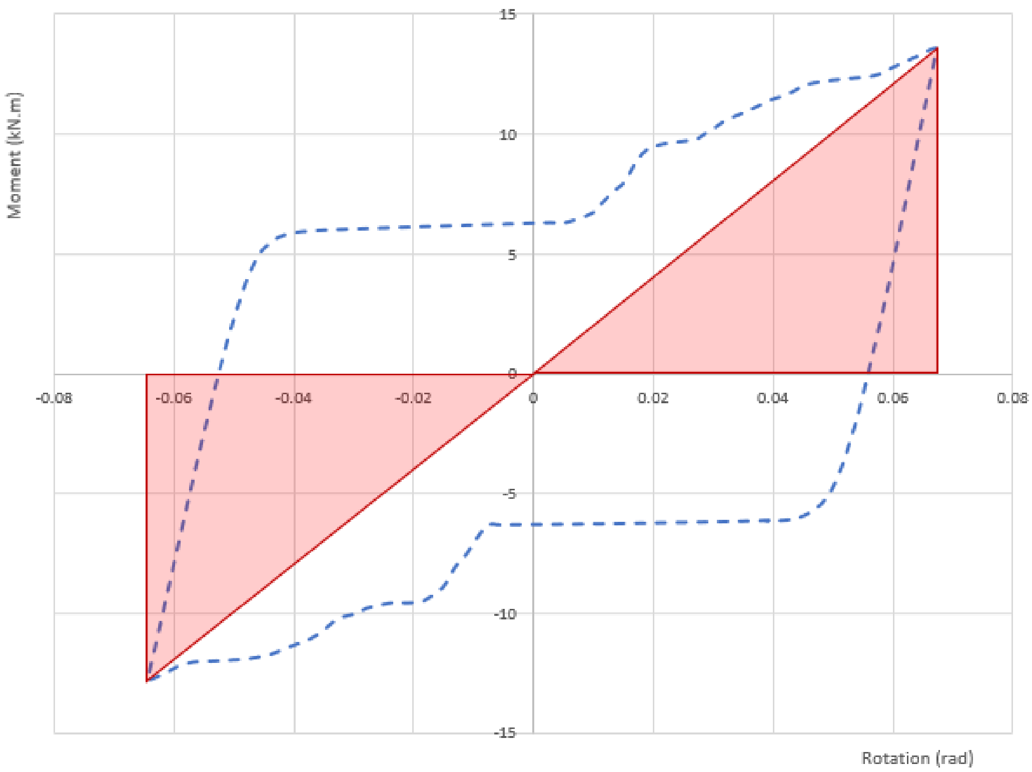

Figure 5- 44: Calculations of the strain energy from the peak cycle for B-G2-R

A summary of the results of the area under the cyclic envelopes for calculating the energy dissipation capacity and the values for the damping coefficient are presented in table (5-8).

Table 5- 8: Comparison of results

	B-G2-R	B-G3-R	B-G4-R	B-G2-C	B-G2-D
Max Load Upwards (kN)	15.1	22.9	22.5	11.8	10
Max Load Downwards (kN)	-14.2	-19.2	-20.9	-11.2	-9.5
Max +ve Moment (kN.m)	13.6	20.6	20.2	10.6	9.0
Max -ve Moment (kN.m)	-12.8	-17.3	-18.8	-10.1	-8.5
Dissipated Energy (J)	1543	1850	2080	1177	963
Damping Coefficient	0.33	0.25	0.25	0.35	0.35

5.3. Summary

As mentioned earlier in this chapter, five main aspects were investigated in each parametric study conducted: (a) moment capacity (b) ductility (c) code requirements (d) energy dissipation (e) damping coefficient. The code requirements considered were those of the AISC and since all models exhibited large ductility, all models satisfied the conditions for SMF. Energy dissipation capacity of the connections were expressed using two approaches, the area under the cyclic envelope curve and the damping coefficient.

The thickness of the gusset plates was found to be the most effective parameter that affects the capacity of the connection, nevertheless, the screw-fastened connections were less affected by the gusset plate thickness. This is attributed to the strength of the bolts compared to the self-drilling screws as tilting occurred in screws when gusset plate increased. Bolted connections exhibited the best performance in terms of moment capacity and energy dissipation compared to the screw-fastened connections. Both the area under the cyclic envelope and the damping ratio were used to measure the energy dissipation capacity of the connections. The difference between the damping ratio in the bolted and screw-fastened connections was significantly high. Damping ratios from bolted connections can reach up to 4.5 times that of the screw fastened connections. This indicates the advantage that bolted connections have in terms of energy dissipation.

Finally, different patterns for bolts and screws were tested where circular and diamond arrangements were investigated. The parametric studies showed that both arrangements showed no advantage over the ordinary square or rectangular arrangements. Nonetheless, circular arrangement of bolts/screws showed better performance over the diamond arrangement in terms of moment capacity and energy dissipation.

Chapter 6 : Discussion and Conclusions

6.1. General

In this chapter, the summary of the research work is first introduced, then, conclusions from the research are discussed. Finally, recommendations for future work are presented.

6.2. Research Summary

Experimental tests and numerical finite element analysis were employed to investigate the behavior of cold-formed steel beam-to-column moment connections subjected to cyclic loading. The aim of this research is to study the performance of these connections when subjected to seismic actions. Three lab tests were conducted as the specimens were subjected to cyclic loading with a total of 40 cycles applied to each specimen. Self-drilling screws were used to fasten the cold-formed sections with the gusset plates in two of the three specimens, while the third specimen used ordinary bolts. The experimental program emphasized the previous work performed on self-drilling screws subjected to cyclic load and the revelations of the experimental work was then used for the verification of the numerical models.

The finite element modelling techniques adopted in this study showed good agreement with the experimental program as the User-Element subroutine (UEL) approach was adopted for modelling the self-drilling screws while the bolts were modelled using high fidelity solid elements.

In the parametric study, three gusset plate thicknesses were investigated in addition to the bolts/screws arrangement in the columns where circular and diamond arrangements were used in addition to the usual rectangular arrangement of bolts/screws. The results were analyzed and the behavior of the connections were compared in terms of deformed shapes, moment capacity and energy dissipation

6.3. Conclusions

From the experimental program, screw-fastened connections were capable of resisting cyclic loads while dissipating energy, however, bolted connections provided better results in terms of ultimate strength and energy dissipation. Moreover, additional top plate added to the screw-fastened connection increase its moment capacity especially when the displacement is applied downwards on the specimen, due to the fact that the top plate can resist tension forces better.

In all three parametric studies conducted, gusset plate thickness was the main contributor to the connection strength, ductility and energy dissipation, while bolts/screws circular and diamond arrangement proved inefficient as discussed in the following concluding remarks:

- In the first parametric study, it was found that the gusset plate of 4 mm thickness provided the highest ultimate strength, however, the difference between using 3 mm and 4 mm thickness plate was only 2.2%, while the difference between 4- and 2-mm plates was 8%. Deformation was mainly in the screws as tilting of the screws was observed. Model “S-G4-R” provided the highest strength and energy dissipation while the circular and diamond arrangement provided no advantage in terms of strength, ductility, or energy dissipation. The diamond screws arrangement “S-G3-C” recorded 33% less ultimate strength compared to “S-G4-R” square screws arrangement, while the circular screws arrangement recorded 60% less ultimate strength compared to “S-G4-R”

- The second parametric study was similar to the first as the gusset plate thickness of 3 mm “ST-G3-R” recorded an ultimate capacity 16% higher than the 2-mm “ST-G2-R” gusset plate thickness. Moreover, the dissipated energy recorded by “ST-G3-R” was 13% higher than “ST-G2-R”.

- The third and last parametric study conducted was the bolted connections. Gusset plate of 4-mm thickness provided a slight increase in strength over the 3-mm thickness that ranged from 2% to 9% since failure occurred in the columns instead of the gusset plates. Nevertheless, 4-mm thickness gusset plate “B-G4-R” gave 50% increase in strength over the 2-mm thickness gusset plate.

- Bolts proved to be superior to screws in every aspect whether it is strength, ductility, and energy dissipation of the connection. Moreover, the pinching behavior of screws when subjected to cyclic load does not allow the connection to dissipate energy as much as the bolted connection. Another measure of the energy dissipation capacity is the damping ratio. Bolted connections had higher damping ratios that reached 3.5 times the screw-fastened connections which also proves that bolted connections have higher energy dissipation capacity.

6.4. Future Recommendations

The following points can be considered for future work:

- Cyclic loading on lap joints using bolts/screws with varying plate thickness can prove to be very beneficial for modelling them on FE packages
- More specimens can be tested under cyclic loading using different screws diameter
- Using different thickness for columns and beams sections and/or using sections of stiffened and curved flanges and testing their effect on energy dissipation capacities on the connection
- Connection can be tested at mid-height of the column instead of an eave connection as tested in this research
- Other types of connections can be tested under cyclic loading.
- Full-scale frame analysis and cyclic testing can also be investigated.

References

[1] W. Yu, R. A. LaBoube, and H. Chen, *Cold-Formed Steel Design*. John Wiley & Sons, 2020.

[2] AISI S400-20, “North American Standard for Seismic Design of Cold-Formed Steel Structural Systems,” 2020.

[3] A. S. of Civil. Engineers, American Society of Civil Engineers, and Structural Engineering Institute., *Seismic Evaluation and Retrofit of Existing Buildings : ASCE/SEI, 41-17.* American Society of Civil Engineers, 2017.

[4] FEMA, “Prestandard And Commentary For The Seismic Rehabilitation Of Buildings FEMA356,” 2000.

[5] J. Ye, S. M. Mojtabaei, and I. Hajirasouliha, “Seismic performance of cold-formed steel bolted moment connections with bolting friction-slip mechanism,” *Journal of Constructional Steel Research*, vol. 156, pp. 122–136, May 2019, doi: 10.1016/j.jcsr.2019.01.013.

[6] “Seismic Provisions for Structural Steel Buildings Supersedes the Seismic Provisions for Structural Steel Buildings,” 2016. [Online]. Available: www.aisc.org

[7] D. A. Padilla-Llano, M. R. Eatherton, and C. D. Moen, “Cyclic flexural response and energy dissipation of cold-formed steel framing members,” *Thin-Walled Structures*, vol. 98, pp. 518–532, Jan. 2016, doi: 10.1016/j.tws.2015.10.021.

[8] M. R. Haidarali and D. A. Nethercot, “Finite element modelling of cold-formed steel beams under local buckling or combined local/distortional buckling,” *Thin-Walled Structures*, vol. 49, no. 12, pp. 1554–1562, Dec. 2011, doi: 10.1016/j.tws.2011.08.003.

[9] B. W. Schafer and T. Peköz, “Computational modeling of cold-formed steel: characterizing geometric imperfections and residual stresses,” 1998.

[10] S. M. Mojtabaei, M. Z. Kabir, I. Hajirasouliha, and M. Kargar, “Analytical and experimental study on the seismic performance of cold-formed steel frames,” *Journal of Constructional Steel Research*, vol. 143, pp. 18–31, Apr. 2018, doi: 10.1016/j.jcsr.2017.12.013.

[11] A. Bagheri Sabbagh, M. Petkovski, K. Pilakoutas, and R. Mirghaderi, “Ductile moment-resisting frames using cold-formed steel sections: An

analytical investigation," *Journal of Constructional Steel Research*, vol. 67, no. 4, pp. 634–646, Apr. 2011, doi: 10.1016/j.jcsr.2010.11.016.

[12] Rinchen and K. J. R. Rasmussen, "Behaviour and modelling of connections in cold-formed steel single C-section portal frames," *Thin-Walled Structures*, vol. 143, Oct. 2019, doi: 10.1016/j.tws.2019.106233.

[13] M. Shahini, A. B. Sabbagh, P. Davidson, and R. Mirghaderi, "Development of cold-formed steel moment-resisting connections with bolting friction-slip mechanism for seismic applications," *Thin-Walled Structures*, vol. 141, pp. 217–231, Aug. 2019, doi: 10.1016/j.tws.2019.04.011.

[14] J. Ye, S. M. Mojtabaei, I. Hajirasouliha, and K. Pilakoutas, "Efficient design of cold-formed steel bolted-moment connections for earthquake resistant frames," *Thin-Walled Structures*, vol. 150, p. 105926, May 2020, doi: 10.1016/j.tws.2018.12.015.

[15] Rinchen and K. J. R. Rasmussen, "Numerical modelling of cold-formed steel single C-section portal frames," *Journal of Constructional Steel Research*, vol. 158, pp. 143–155, Jul. 2019, doi: 10.1016/j.jcsr.2019.03.024.

[16] P. Pouladi, J. Ronaldson, G. C. Clifton, J. M. Ingham, A. M. Wrzesien, and J. B. P. Lim, "Finite-element assisted design of eaves joint of cold-formed steel portal frames having single channel-sections," *Structures*, vol. 20, pp. 452–464, Aug. 2019, doi: 10.1016/j.istruc.2019.05.009.

[17] M. T. Huynh, C. H. Pham, and G. J. Hancock, "On the finite element modeling of the screwed connections of cold-formed steel," in *Lecture Notes in Civil Engineering*, vol. 8, Springer, 2018, pp. 224–232. doi: 10.1007/978-981-10-6713-6_21.

[18] K. Roy, H. H. Lau, T. C. Huon Ting, R. Masood, A. Kumar, and J. B. P. Lim, "Experiments and finite element modelling of screw pattern of self-drilling screw connections for high strength cold-formed steel," *Thin-Walled Structures*, vol. 145, Dec. 2019, doi: 10.1016/j.tws.2019.106393.

[19] M. T. Huynh, C. H. Pham, and G. J. Hancock, "Experimental behaviour and modelling of screwed connections of high strength sheet steels in shear," *Thin-Walled Structures*, vol. 146, Jan. 2020, doi: 10.1016/j.tws.2019.106357.

[20] M. T. Huynh, C. H. Pham, and G. J. Hancock, "Design of screwed connections in cold-formed steels in shear," *Thin-Walled Structures*, vol. 154, Sep. 2020, doi: 10.1016/j.tws.2020.106817.

[21] C. Ding, C. D. Moen, and M. R. Eatherton, “Monotonic and Cyclic Simulation of Screw-Fastened Connections for Cold-Formed Steel Framing.”

[22] S. Kechidi, D. C. Fratamico, B. W. Schafer, J. Miguel Castro, and N. Bourahla, “Simulation of screw connected built-up cold-formed steel back-to-back lipped channels under axial compression,” *Engineering Structures*, vol. 206, Mar. 2020, doi: 10.1016/j.engstruct.2019.110109.

[23] Rinchen and K. J. R. Rasmussen, “Numerical modelling of cold-formed steel single C-section portal frames,” *Journal of Constructional Steel Research*, vol. 158, pp. 143–155, Jul. 2019, doi: 10.1016/j.jcsr.2019.03.024.

[24] A. R. Badr, H. H. Elanwar, and S. A. Mourad, “Numerical and experimental investigation on cold-formed walls sheathed by fiber cement board,” *Journal of Constructional Steel Research*, vol. 158, pp. 366–380, Jul. 2019, doi: 10.1016/j.jcsr.2019.04.004.

[25] S. M. Mojtabaei, M. Z. Kabir, I. Hajirasouliha, and M. Kargar, “Analytical and experimental study on the seismic performance of cold-formed steel frames,” *Journal of Constructional Steel Research*, vol. 143, pp. 18–31, Apr. 2018, doi: 10.1016/j.jcsr.2017.12.013.

[26] J. Mills and R. LaBoube, “Self-drilling screw joints for cold-formed channel portal frames,” in *International Specialty Conference on Cold-Formed Steel Structures: Recent Research and Developments in Cold-Formed Steel Design and Construction*, 2002, pp. 825–838. doi: 10.1061/(asce)0733-9445(2004)130:11(1799).

Appendix A: Hysteresis Loops of the Parametric Study

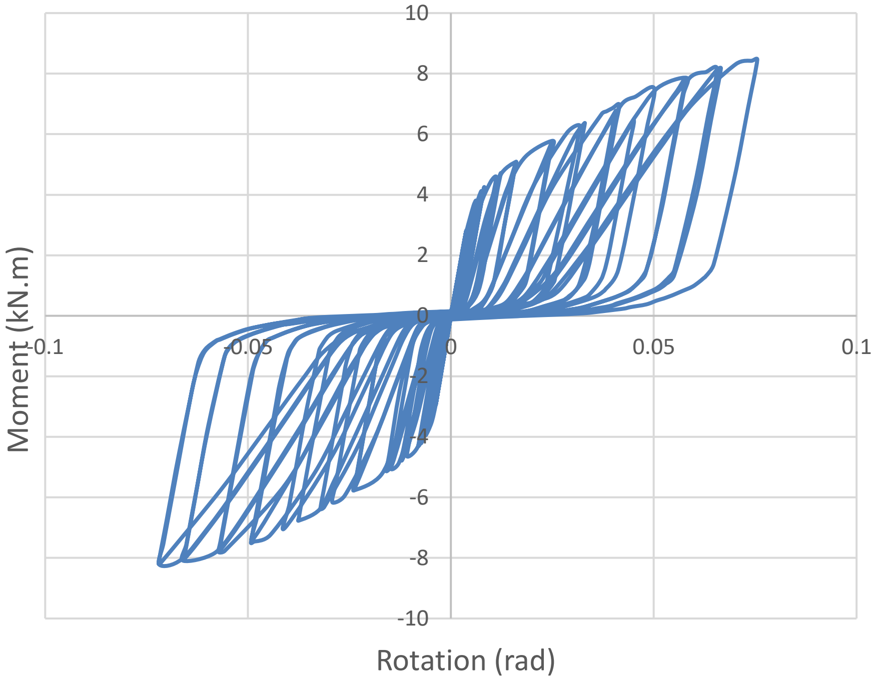

Figure A- 1: Moment-rotation hysteresis response of Model "S-G3-R"

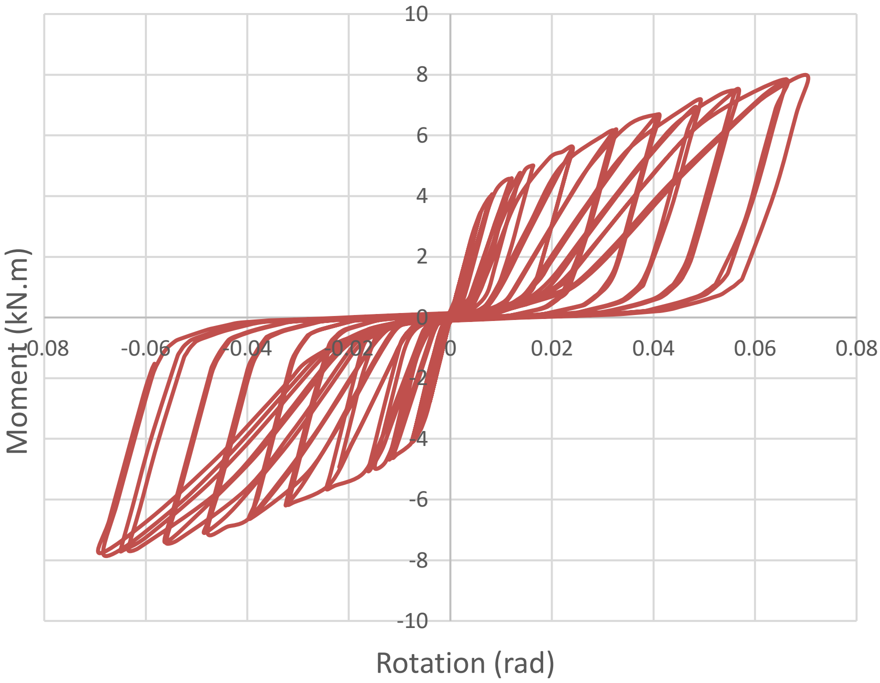

Figure A- 2: Moment-rotation hysteresis response of Model "S-G2-R"

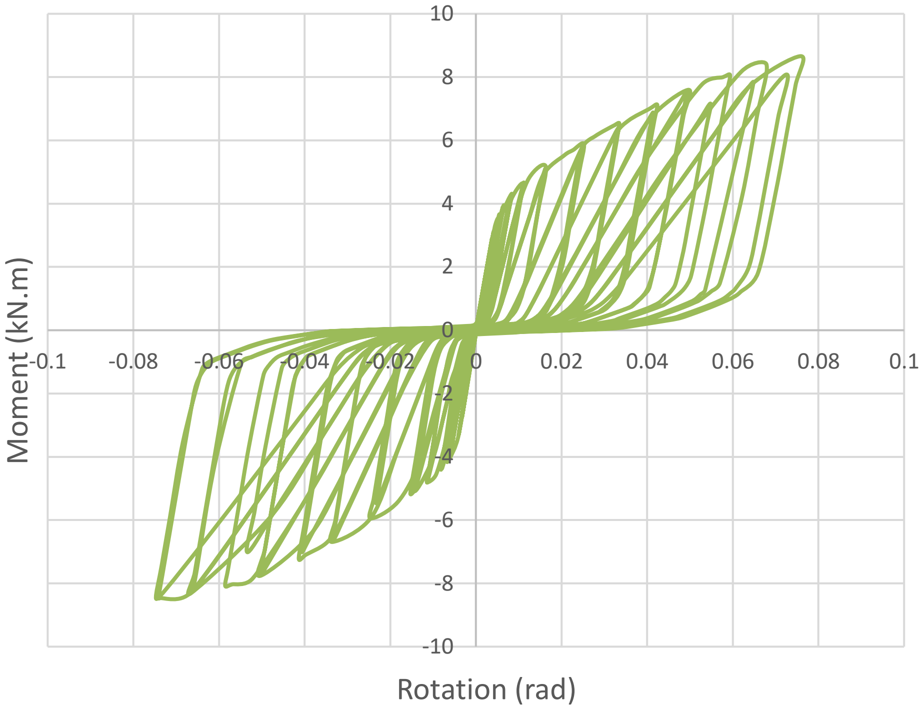

Figure A- 3: Moment-rotation hysteresis response of Model "S-G4-R"

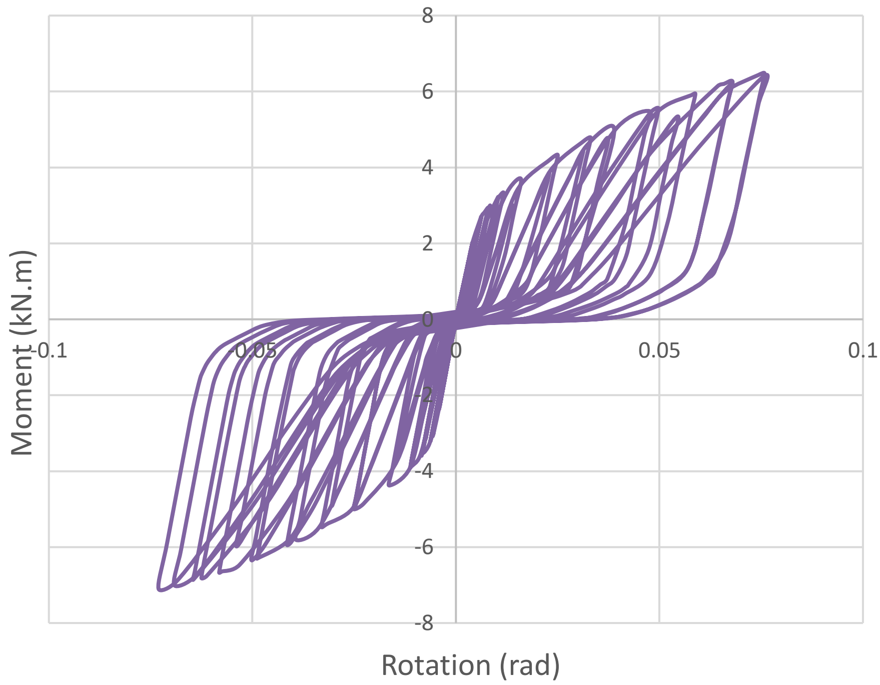

Figure A- 4: Moment-rotation hysteresis response of Model "S-G3-C"

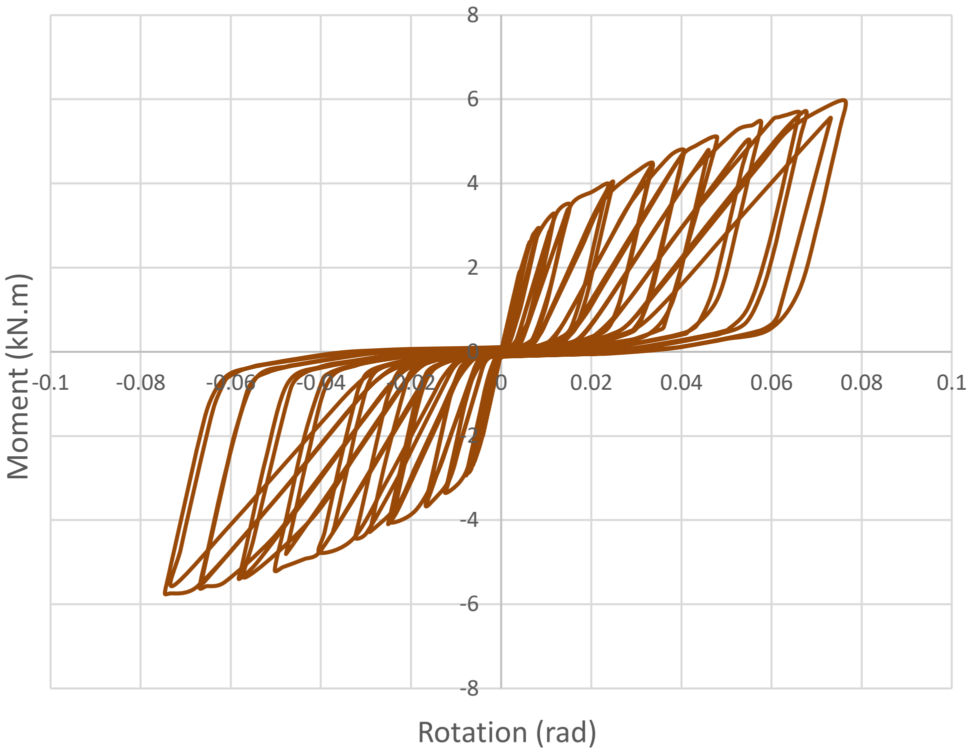

Figure A- 5: Moment-rotation hysteresis response of Model "S-G3-D"

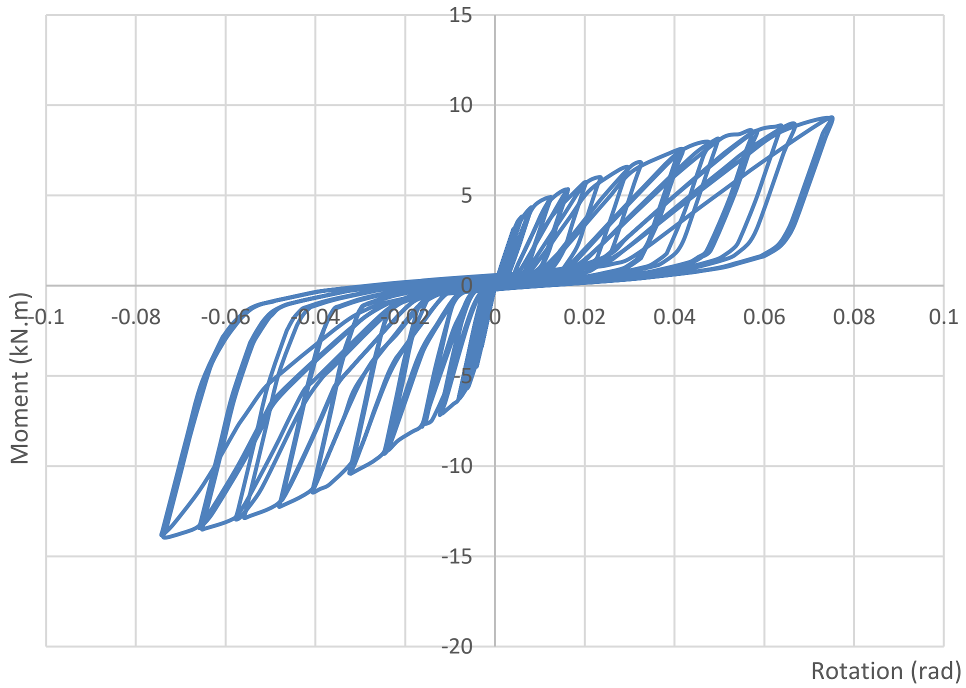

Figure A- 6: Moment-rotation hysteresis response of Model "ST-G3-R"

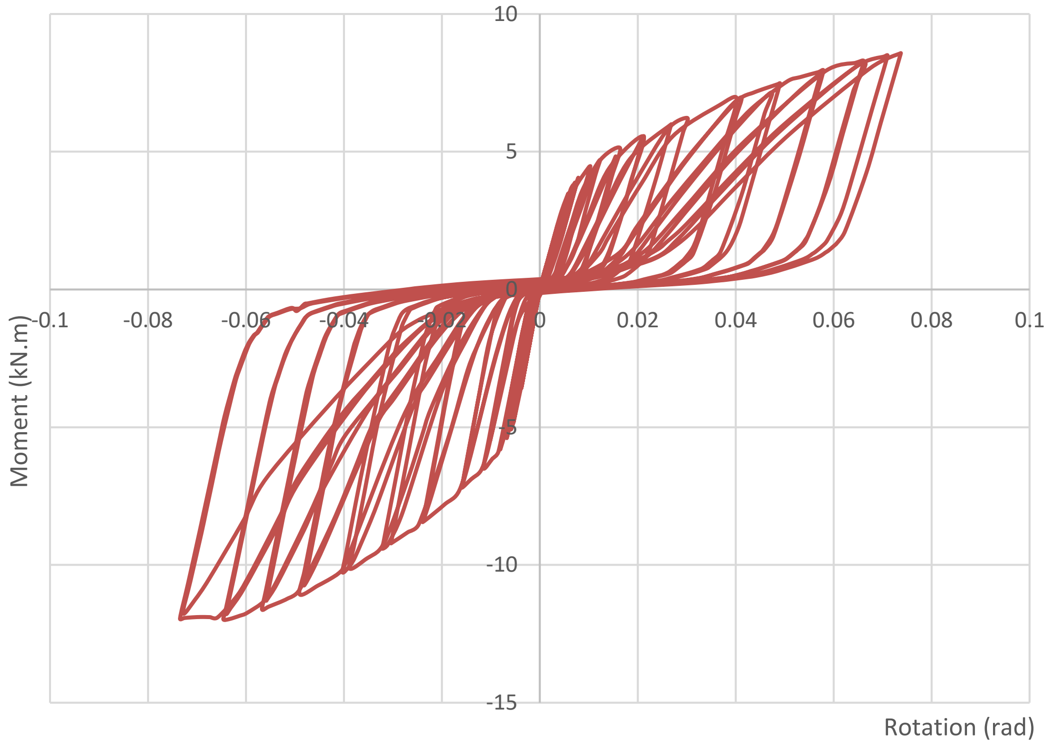

Figure A- 7: Moment-rotation hysteresis response of Model "ST-G2-R"

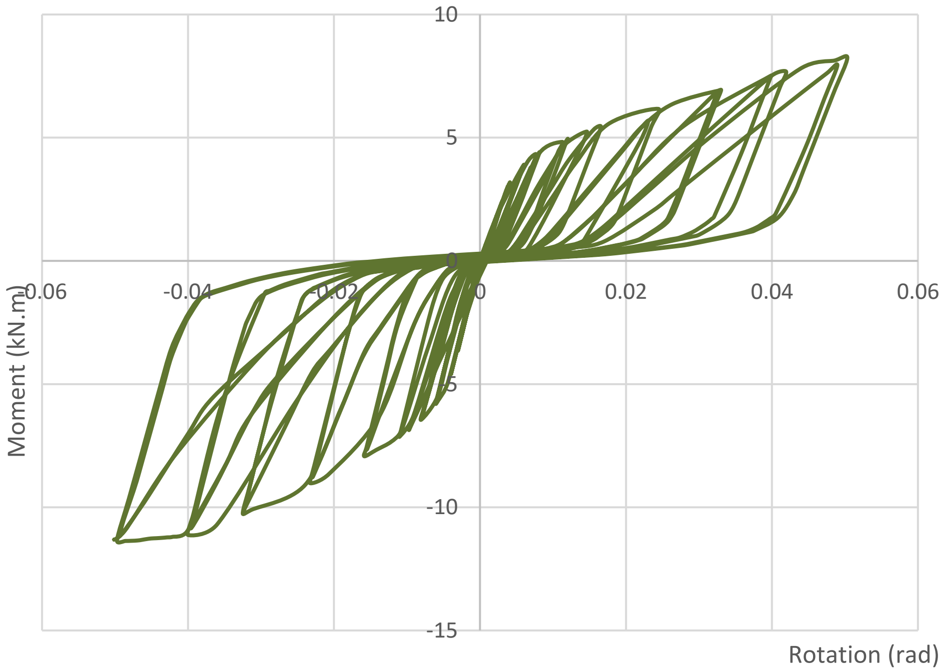

Figure A- 8: Moment-rotation hysteresis response of Model "ST-G4-R"

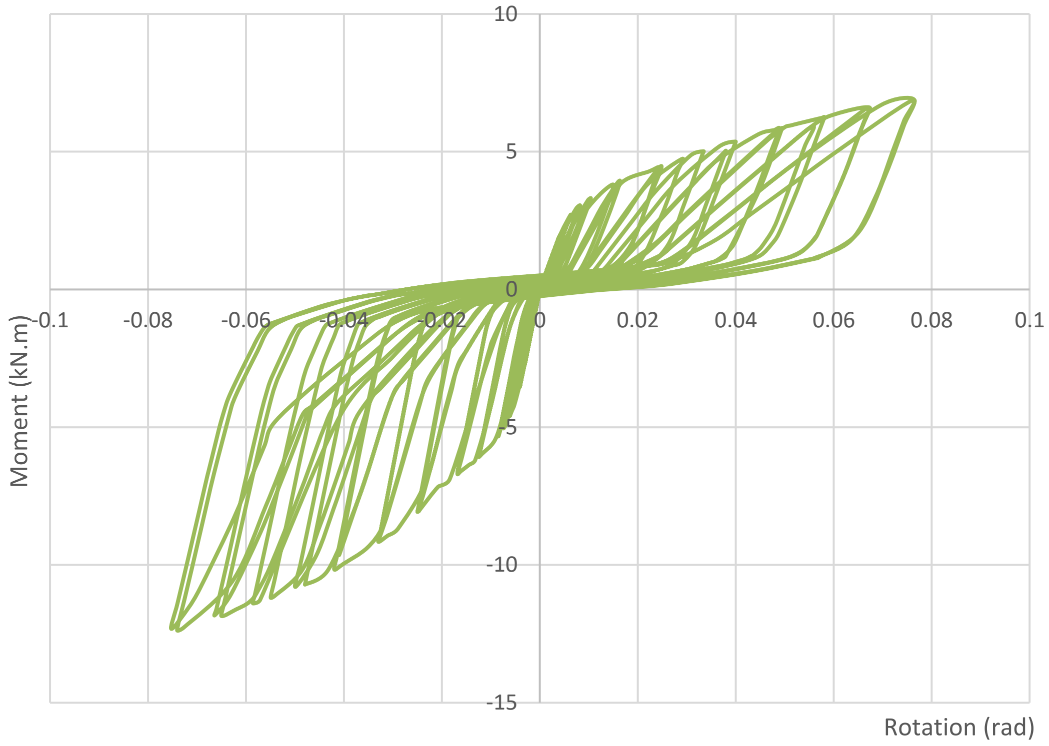

Figure A- 9: Moment-rotation hysteresis response of Model "ST-G3-D"

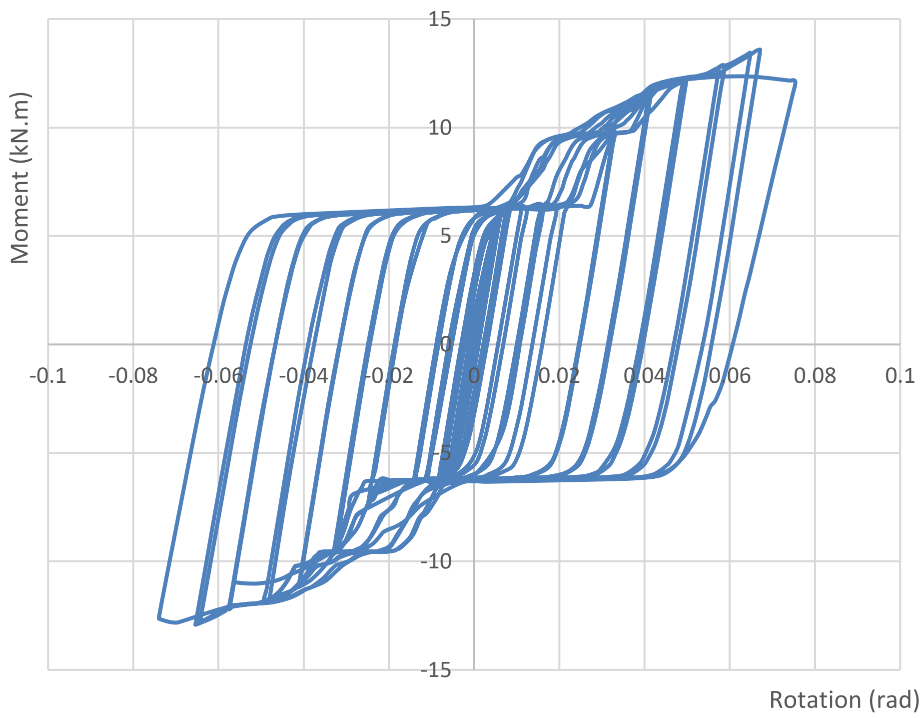

Figure A- 10: Moment-rotation hysteresis response of Model "B-G2-R"

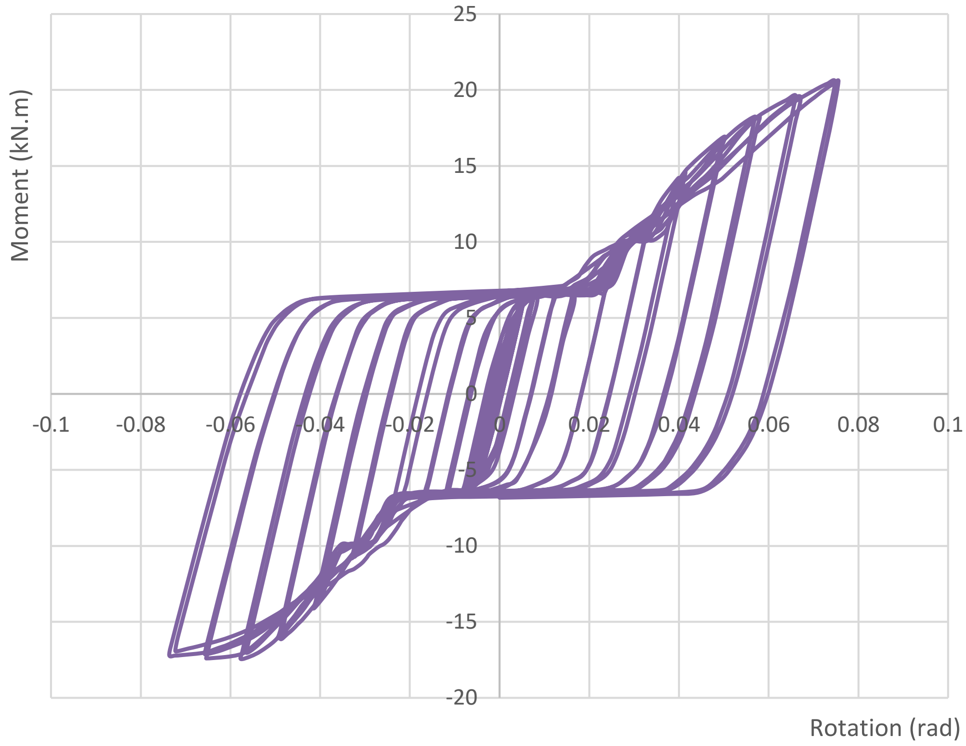

Figure A- 11: Moment-rotation hysteresis response of Model "B-G3-R"

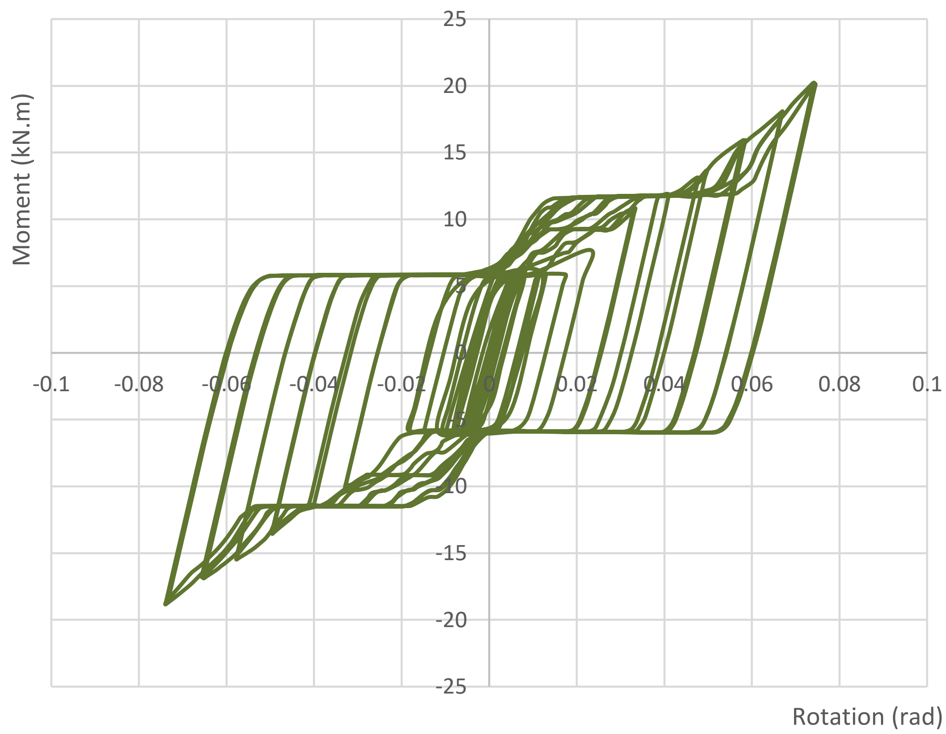

Figure A- 12: Moment-rotation hysteresis response of Model "B-G4-R"

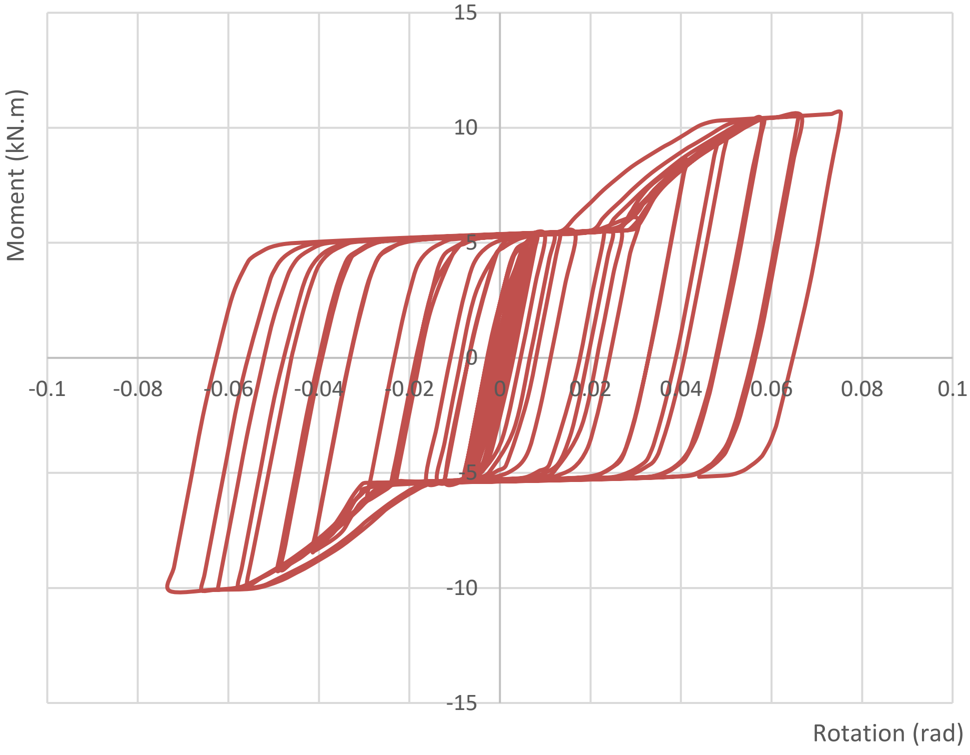

Figure A- 13: Moment-rotation hysteresis response of Model "B-G2-C"

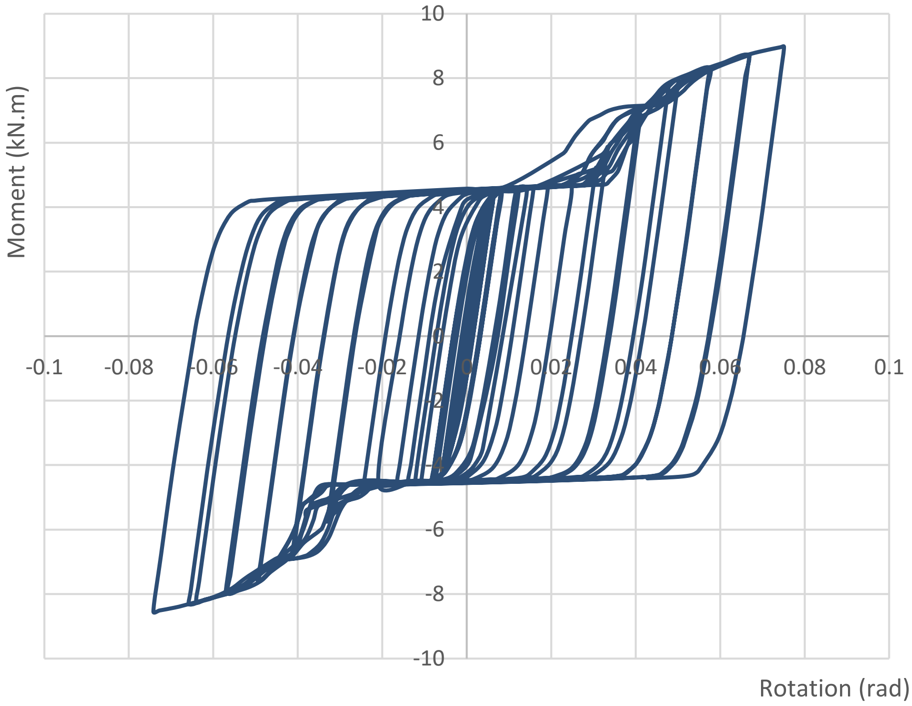

Figure A- 14: Moment-rotation hysteresis response of Model "B-G2-D"

Appendix B: Screw-fastened Model Input File

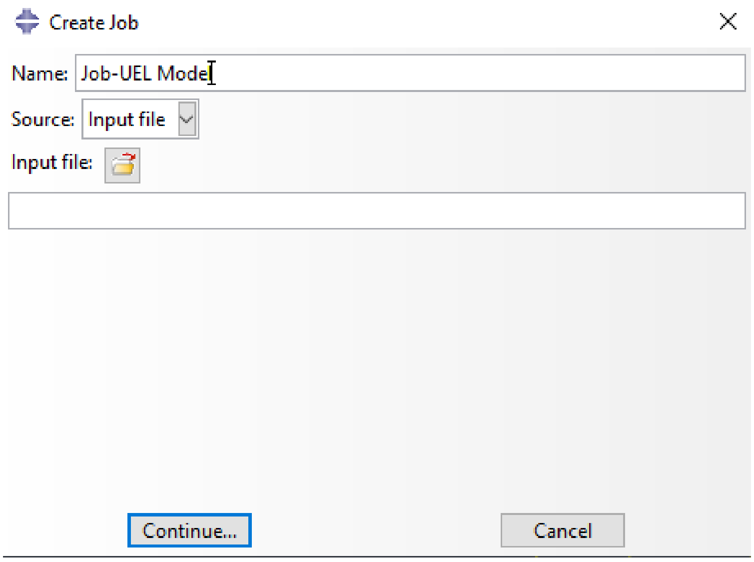

Figure B- 1: Creating a new “Job” on ABAQUS from a .inp file

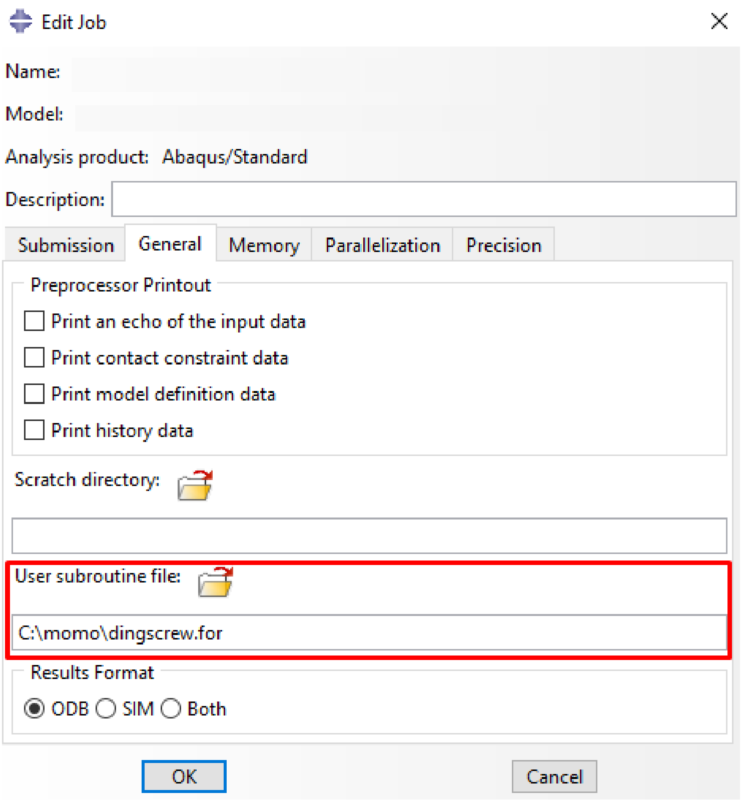

Figure B- 2: Integrating the User Element Subroutine (UEL) in the model

**********************Screws Model S-G3-R .inp file**********************
****

```
Heading
** Job name: Job-S1 Model name: S1-Cyclic
** Generated by: ABAQUS/CAE 2019
*Preprint, echo=NO, model=NO, history=NO, contact=NO
**
** PARTS
**
*Part, name=Beam
*node, input=\nodes\beam
*Element, type=S4R
Input=\elements\beam
** Section: Twomm
*Shell Section, elset=_PickedSet52, material=Test-Material, offset=SNEG
2., 5
** Section: Fourmm
*Shell Section, elset=_PickedSet50, material=Bilinear-ST52
4., 5
** Section: Twomm
*Shell Section, elset=_PickedSet51, material=Test-Material, offset=SPOS
2., 5
*End Part
**
*Part, name=Column
*node, input=\nodes\column
*Element, type=S4R
Input=\elements\column
** Section: Twomm
*Shell Section, elset=_PickedSet54, material=Test-Material, offset=SNEG
2., 5
** Section: Twomm
*Shell Section, elset=_PickedSet53, material=Test-Material, offset=SPOS
2., 5
*End Part
**
*Part, name=Gusset
*Node, input=\nodes\gusset
*Element, type=S4R
Input=\elements\gusset
** Section: threemm
*Shell Section, elset=_PickedSet14, material=Bilinear-ST52
3., 5
*End Part
**
*Part, name=L40x40x4
*Node, input=\nodes\angle
*Element, type=S4R
Input=\elements\angle
```

```
** Section: Fourmm-HR
*Shell Section, elset=_PickedSet2, material=Bilinear-ST52, offset=SPOS
4., 5
*End Part
**
*Part, name = fastn_pro_1
**
*Node
1, 0.0, 0, 0.0
2, 1.5, 0, 0.0
**
*User element, nodes=2, type=U101, properties=41, coordinates=3, variables=200
1, 2, 3
**
*Element, type=U101, elset=steel_to_osb_spr
**
1, 1, 2
**
*UEL property, elset=steel_to_osb_spr
0.07, 1.86, 6.93, 12.23, 9540, 18080, 23240, 2280,
-0.07, -1.86, -6.93, -12.23, -9540, -18080, -23240, -2280,
0.42, 0.01, 0.001, 0.42, 0.01, 0.001, 0.0, 0.0,
0.0, 0.0, 0.0, 0.0, 0., 0.0, 0.0, 0.0,
0.0, 0.0, 0.0, 0.0, 0.0, 1.0, 0.0, 2,
3
**
*End Part
**
**
** ASSEMBLY
**
*Assembly, name=Assembly
**
*Instance, name=BeaB-G2-R, part=Beam
          0.,           50.,          -40.
*End Instance
**
*Instance, name=Gusset-1, part=Gusset
-1.5,         150.,         280.
-1.5,         150.,         280., -1.5, 149,         280., 90
*End Instance
**
*Instance, name=L40x40x4-1, part=L40x40x4
       -11.5, -14.3965517222867, 302.241379312108
       -11.5, -14.3965517222867, 302.241379312108,       -11.5, -13.4774066746221,
301.847460022996,         180.
*End Instance
**
*Instance, name=Column-1, part=Column
          0.,           0.,           0.
```

```
     0.,          0.,          0., 1.,          0.,          0., 90
*End Instance
**
*Instance, name=L40x40x4-2, part=L40x40x4
8.5, -141.12, 181.551724139695
8.5, -141.12, 181.551724139695, 7.5, -141.12, 181.551724139695, 46.4
*End Instance
**
** First line of screws
** screw 1
*Instance, name = fastn_line_1, part = fastn_pro_1
-1.5, -50, 10.
*End instance
**
*Instance, name = fastn_line_2, part = fastn_pro_1
-3, -50, 10.
*End instance
** screw 2
*Instance, name = fastn_line_3, part = fastn_pro_1
-1.5, -100, 10.
*End instance
*Instance, name = fastn_line_4, part = fastn_pro_1
-3, -100, 10.
*End instance
**screw 3
*Instance, name = fastn_line_5, part = fastn_pro_1
-1.5, -150, 10.
*End instance
**
*Instance, name = fastn_line_6, part = fastn_pro_1
-3, -150, 10.
*End instance
**
**
** second line of screws
** screw 1
*Instance, name = fastn_line_7, part = fastn_pro_1
-1.5, -50, 60.
*End instance
**
*Instance, name = fastn_line_8, part = fastn_pro_1
-3, -50, 60.
*End instance
** screw 2
**Instance, name = fastn_line_9, part = fastn_pro_1
**-1.5, -100, 60.
**End instance
**Instance, name = fastn_line_10, part = fastn_pro_1
**-3, -100, 60.
**End instance
```

```
**screw 3
*Instance, name = fastn_line_11, part = fastn_pro_1
-1.5, -150, 60.
*End instance
**
*Instance, name = fastn_line_12, part = fastn_pro_1
-3, -150, 60.
*End instance
**
**
** third line of screws
** screw 1
*Instance, name = fastn_line_13, part = fastn_pro_1
-1.5, -50, 110.
*End instance
**
*Instance, name = fastn_line_14, part = fastn_pro_1
-3, -50, 110.
*End instance
** screw 2
*Instance, name = fastn_line_15, part = fastn_pro_1
-1.5, -100, 110.
*End instance
*Instance, name = fastn_line_16, part = fastn_pro_1
-3, -100, 110.
*End instance
**screw 3
*Instance, name = fastn_line_17, part = fastn_pro_1
-1.5, -150, 110.
*End instance
**
*Instance, name = fastn_line_18, part = fastn_pro_1
-3, -150, 110.
*End instance
**
**
**
*Node
      1,        -1.5,         210.,        1060.
*Node
      2,        -1.5,         110.,        1160.
*Node
      3,          0.,          10.,        1060.
*Node
      4,         3.5,         210.,        1060.
*Node
      5,         60.,          10.,         460.
*Node
      6,         60.,          30.,         460.
*Node
```

```
      7,          60.,         190.,         460.
*Node
      8,          60.,         210.,         460.
*Node
      9,         -63.,          10.,         460.
*Node
     10,         -63.,          30.,         460.
*Node
     11,         -63.,         190.,         460.
*Node
     12,         -63.,         210.,         460.
*Node
     13,         -1.5,         210.,         960.
*Node
     14,           0.,        -150.,         110.
     15,           0.,        -100.,         110.
     16,           0.,         -50.,         110.
     17,           0.,        -150.,          60.
     18,           0.,        -100.,          60.
     19,           0.,         -50.,          60.
     20,           0.,        -150.,          10.
     21,           0.,        -100.,          10.
     22,           0.,         -50.,          10.
     23,           0.,          60.,         310.
     24,           0.,         110.,         310.
     25,           0.,         160.,         310.
     26,           0.,          60.,         210.
     27,           0.,         110.,         210.
     28,           0.,         160.,         210.
     29,           0.,          60.,         110.
     30,           0.,         110.,         110.
     31,           0.,         160.,         110.
     32,           0.,          60.,          10.
     33,           0.,         110.,          10.
     34,           0.,         160.,          10.
*Nset, nset="Attachment PointS-G3-R-Set-2", generate
 23,  34,   1
*Nset, nset="Attachment PointS-G2-R-Set-1", generate
 14,  22,   1
*Nset, nset=Set-84, generate
 23,  34,   1
*Nset, nset=Set-85, generate
 14,  34,   1
*Nset, nset=Set-86
 18, 23, 24, 25, 26, 27, 28, 29, 30, 31, 32, 33, 34
*Nset, nset=Set-LS1
 8,
*Nset, nset=Set-LS2
 7,
*Nset, nset=Set-LS3
```

```
6,
*Nset, nset=Set-LS4
5,
*Nset, nset=Set-LS5
12,
*Nset, nset=Set-LS6
11,
*Nset, nset=Set-LS7
10,
*Nset, nset=Set-LS8
9,
*Nset, nset=Set-LVDT, instance=BeaB-G2-R
1510,
*Nset, nset=Set-RP-3, instance=BeaB-G2-R
1264,
*Nset, nset=Set-RP-4
13,
*Nset, nset=Set-RP-5
4,
*Nset, nset="m_Set-RP 1"
1,
*Nset, nset=_PickedSet223, internal
2,
*Nset, nset=_PickedSet229, internal, instance=L40x40x4-1
4,
*Nset, nset=_PickedSet230, internal, instance=Gusset-1
4,
*Nset, nset=_PickedSet231, internal, instance=Gusset-1
5,
*Nset, nset=_PickedSet232, internal, instance=Gusset-1
5,
*Nset, nset=_PickedSet233, internal, instance=Gusset-1
15,
*Nset, nset=_PickedSet234, internal, instance=Gusset-1
15,
*Nset, nset=_PickedSet235, internal, instance=L40x40x4-1
11,
*Nset, nset=_PickedSet236, internal, instance=Gusset-1
13,
*Nset, nset=_PickedSet256, internal, instance=Column-1
  3,   4,   6,   8,  10,  12,  23,  24,  26,  28,  30,  32,  74, 144, 145, 146
147, 148, 200, 201, 202, 203, 204, 205, 206, 207, 208, 209, 210, 211, 212, 213
214, 215, 216, 217, 218, 256, 257, 258, 259, 260, 294, 712, 782, 783, 784, 785
786, 838, 839, 840, 841, 842, 843, 844, 845, 846, 847, 848, 849, 850, 851, 852
853, 854, 855, 856, 894, 895, 896, 897, 898, 932
*Elset, elset=_PickedSet256, internal, instance=Column-1
  65,   66,  259,  260,  261,  262,  263,  264,  905,  906,  907,  908,  909,  910,  911, 912
 913,  914,  915,  916,  917,  918,  919,  920,  921,  922,  923,  924, 1117, 1118, 1119, 1120
```

1121, 1122, 1187, 1188, 3305, 3306, 3499, 3500, 3501, 3502, 3503, 3504, 4145, 4146, 4147, 4148
4149, 4150, 4151, 4152, 4153, 4154, 4155, 4156, 4157, 4158, 4159, 4160, 4161, 4162, 4163, 4164
4357, 4358, 4359, 4360, 4361, 4362, 4427, 4428
*Nset, nset=_PickedSet268, internal, instance=L40x40x4-1
3,
*Nset, nset=_PickedSet269, internal, instance=Gusset-1
1,
*Nset, nset=_PickedSet270, internal, instance=L40x40x4-1
7,
*Nset, nset=_PickedSet271, internal, instance=Gusset-1
6,
*Nset, nset=_PickedSet272, internal, instance=L40x40x4-1
13,
*Nset, nset=_PickedSet273, internal, instance=Gusset-1
9,
*Nset, nset=_PickedSet274, internal, instance=L40x40x4-1
14,
*Nset, nset=_PickedSet275, internal, instance=Gusset-1
14,
*Nset, nset=_PickedSet276, internal, instance=Gusset-1
12,
*Nset, nset=_PickedSet277, internal, instance=Gusset-1
12,
*Nset, nset=_PickedSet278, internal, instance=Gusset-1
11,
*Nset, nset=_PickedSet279, internal, instance=Gusset-1
11,
*Nset, nset=_PickedSet280, internal, instance=Gusset-1
8,
*Nset, nset=_PickedSet281, internal, instance=Gusset-1
8,
*Nset, nset=_PickedSet282, internal, instance=Gusset-1
3,
*Nset, nset=_PickedSet283, internal, instance=Gusset-1
3,
*Nset, nset=_PickedSet284, internal, instance=Gusset-1
2,
*Nset, nset=_PickedSet285, internal, instance=Gusset-1
2,
*Nset, nset=_PickedSet286, internal, instance=Gusset-1
10,
*Nset, nset=_PickedSet287, internal, instance=Gusset-1
10,
*Nset, nset=_PickedSet288, internal, instance=Gusset-1
7,
*Nset, nset=_PickedSet289, internal, instance=Gusset-1
7,
*Nset, nset=_PickedSet299, internal, instance=L40x40x4-2

11,
*Nset, nset=_PickedSet300, internal, instance=Gusset-1
4,
*Nset, nset=_PickedSet301, internal, instance=L40x40x4-2
12,
*Nset, nset=_PickedSet302, internal, instance=Gusset-1
1,
*Nset, nset=_PickedSet303, internal, instance=L40x40x4-2
15,
*Nset, nset=_PickedSet304, internal, instance=Gusset-1
5,
*Nset, nset=_PickedSet305, internal, instance=L40x40x4-2
14,
*Nset, nset=_PickedSet306, internal, instance=Gusset-1
6,
*Nset, nset=_PickedSet307, internal, instance=L40x40x4-2
13,
*Nset, nset=_PickedSet308, internal, instance=Gusset-1
9,
*Nset, nset=_PickedSet309, internal, instance=L40x40x4-2
7,
*Nset, nset=_PickedSet310, internal, instance=Gusset-1
14,
*Nset, nset=_PickedSet311, internal, instance=L40x40x4-2
8,
*Nset, nset=_PickedSet312, internal, instance=Gusset-1
15,
*Nset, nset=_PickedSet313, internal, instance=L40x40x4-2
3,
*Nset, nset=_PickedSet314, internal, instance=Gusset-1
12,
*Nset, nset=_PickedSet315, internal, instance=L40x40x4-2
4,
*Nset, nset=_PickedSet316, internal, instance=Gusset-1
13,
*Nset, nset=_PickedSet317, internal, instance=L40x40x4-2
1,
*Nset, nset=_PickedSet318, internal, instance=Gusset-1
11,
*Nset, nset=_PickedSet319, internal, instance=L40x40x4-2
5,
*Nset, nset=_PickedSet320, internal, instance=Gusset-1
8,
*Nset, nset=_PickedSet321, internal, instance=L40x40x4-2
10,
*Nset, nset=_PickedSet322, internal, instance=Gusset-1
3,
*Nset, nset=_PickedSet355, internal, instance=BeaB-G2-R
25, 28, 31, 34, 61, 64, 67, 70
*Nset, nset=_PickedSet358, internal, instance=BeaB-G2-R

2, 3, 38, 39, 78, 79, 80, 81, 82, 83, 84, 85, 86, 946, 947, 948
949, 950, 951, 952, 953, 954
*Elset, elset=_PickedSet358, internal, instance=BeaB-G2-R
6, 12, 18, 24, 30, 36, 42, 48, 54, 60, 3581, 3601, 3621, 3641, 3661, 3681
3701, 3721, 3741, 3761, 4566, 4572, 4578, 4584, 4590, 4596, 4602, 4608, 4614, 4620, 8141, 8161
8181, 8201, 8221, 8241, 8261, 8281, 8301, 8321
*Nset, nset=_PickedSet359, internal
13,
*Nset, nset=_PickedSet362, internal, instance=Column-1
2, 3, 5, 6, 7, 8, 9, 10, 22, 23, 25, 26, 27, 28, 29, 30
42, 43, 44, 45, 46, 47, 48, 49, 50, 51, 52, 53, 54, 55, 56, 57
58, 59, 60, 61, 62, 63, 64, 65, 66, 67, 68, 69, 70, 71, 72, 73
107, 108, 109, 110, 111, 112, 113, 114, 115, 116, 117, 118, 119, 120, 121, 122
123, 124, 125, 126, 127, 128, 129, 130, 131, 132, 133, 134, 135, 136, 137, 138
139, 140, 141, 142, 143, 144, 145, 146, 147, 148, 168, 169, 170, 171, 172, 173
174, 175, 176, 177, 178, 179, 180, 181, 182, 183, 184, 185, 186, 187, 188, 189
190, 191, 192, 193, 194, 195, 196, 197, 198, 199, 219, 220, 221, 222, 223, 224
225, 226, 227, 228, 229, 230, 231, 232, 233, 234, 235, 236, 237, 238, 239, 240
241, 242, 243, 244, 245, 246, 247, 248, 249, 250, 251, 252, 253, 254, 255, 256
257, 258, 259, 260, 680, 681, 682, 683, 684, 685, 686, 687, 688, 689, 690, 691
692, 693, 694, 695, 696, 697, 698, 699, 700, 701, 702, 703, 704, 705, 706, 707
708, 709, 710, 711, 745, 746, 747, 748, 749, 750, 751, 752, 753, 754, 755, 756
757, 758, 759, 760, 761, 762, 763, 764, 765, 766, 767, 768, 769, 770, 771, 772
773, 774, 775, 776, 777, 778, 779, 780, 781, 782, 783, 784, 785, 786, 806, 807
808, 809, 810, 811, 812, 813, 814, 815, 816, 817, 818, 819, 820, 821, 822, 823
824, 825, 826, 827, 828, 829, 830, 831, 832, 833, 834, 835, 836, 837, 857, 858
859, 860, 861, 862, 863, 864, 865, 866, 867, 868, 869, 870, 871, 872, 873, 874
875, 876, 877, 878, 879, 880, 881, 882, 883, 884, 885, 886, 887, 888, 889, 890
891, 892, 893, 894, 895, 896, 897, 898, 1349, 1350, 1351, 1352, 1353, 1354, 1355, 1356
1357, 1358, 1359, 1360, 1361, 1362, 1363, 1364, 1365, 1366, 1367, 1368, 1369, 1370, 1371, 1372

1373, 1374, 1375, 1376, 1377, 1378, 1379, 1380, 1381, 1382, 1383, 1384, 1385, 1386, 1387, 1388

1389, 1390, 1391, 1392, 1393, 1394, 1395, 1396, 1397, 1398, 1399, 1400, 1401, 1402, 1403, 1404

1405, 1406, 1407, 1408, 1409, 1410, 1411, 1412, 1413, 1414, 1415, 1416, 1417, 1418, 1419, 1420

1421, 1422, 1423, 1424, 1425, 1426, 1427, 1428, 1429, 1430, 1431, 1432, 1433, 1434, 1435, 1436

1437, 1438, 1439, 1440, 1441, 1442, 1443, 1444, 1445, 1446, 1447, 1448, 1449, 1450, 1451, 1452

1453, 1454, 1455, 1456, 1457, 1458, 1459, 1460, 1461, 1462, 1463, 1464, 1465, 1466, 1467, 1468

1469, 1470, 1471, 1472, 1473, 1474, 1475, 1476, 1477, 1478, 1479, 1480, 1481, 1482, 1483, 1484

1485, 1486, 1487, 1488, 1489, 1490, 1491, 1492, 1493, 1494, 1495, 1496, 1497, 1498, 1499, 1500

1501, 1502, 1503, 1504, 1505, 1506, 1507, 1508, 2117, 2118, 2119, 2120, 2121, 2122, 2123, 2124

2125, 2126, 2127, 2128, 2129, 2130, 2131, 2132, 2133, 2134, 2135, 2136, 2137, 2138, 2139, 2140

2141, 2142, 2143, 2144, 2145, 2146, 2147, 2148, 2149, 2150, 2151, 2152, 2153, 2154, 2155, 2156

2157, 2158, 2159, 2160, 2161, 2162, 2163, 2164, 2165, 2166, 2167, 2168, 2169, 2170, 2171, 2172

2173, 2174, 2175, 2176, 2177, 2178, 2179, 2180, 2181, 2182, 2183, 2184, 2185, 2186, 2187, 2188

2189, 2190, 2191, 2192, 2193, 2194, 2195, 2196, 2197, 2198, 2199, 2200, 2201, 2202, 2203, 2204

2205, 2206, 2207, 2208, 2209, 2210, 2211, 2212, 2213, 2214, 2215, 2216, 2217, 2218, 2219, 2220

2221, 2222, 2223, 2224, 2225, 2226, 2227, 2228, 2229, 2230, 2231, 2232, 2233, 2234, 2235, 2236

2237, 2238, 2239, 2240, 2241, 2242, 2243, 2244, 2245, 2246, 2247, 2248, 2249, 2250, 2251, 2252

2253, 2254, 2255, 2256, 2257, 2258, 2259, 2260, 2261, 2262, 2263, 2264, 2265, 2266, 2267, 2268

2269, 2270, 2271, 2272, 2273, 2274, 2275, 2276, 4058, 4059, 4060, 4061, 4062, 4063, 4064, 4065

4066, 4067, 4068, 4069, 4070, 4071, 4072, 4073, 4074, 4075, 4076, 4077, 4078, 4079, 4080, 4081

4082, 4083, 4084, 4085, 4086, 4087, 4088, 4089, 4090, 4091, 4092, 4093, 4094, 4095, 4096, 4097

4098, 4099, 4100, 4101, 4102, 4103, 4104, 4105, 4106, 4107, 4108, 4109, 4110, 4111, 4112, 4113

4114, 4115, 4116, 4117, 4118, 4119, 4120, 4121, 4122, 4123, 4124, 4125, 4126, 4127, 4128, 4129

4130, 4131, 4132, 4133, 4134, 4135, 4136, 4137, 4138, 4139, 4140, 4141, 4142, 4143, 4144, 4145

4146, 4147, 4148, 4149, 4150, 4151, 4152, 4153, 4154, 4155, 4156, 4157, 4158, 4159, 4160, 4161

4162, 4163, 4164, 4165, 4166, 4167, 4168, 4169, 4170, 4171, 4172, 4173, 4174, 4175, 4176, 4177
4178, 4179, 4180, 4181, 4182, 4183, 4184, 4185, 4186, 4187, 4188, 4189, 4190, 4191, 4192, 4193
4194, 4195, 4196, 4197, 4198, 4199, 4200, 4201, 4202, 4203, 4204, 4205, 4206, 4207, 4208, 4209
4210, 4211, 4212, 4213, 4214, 4215, 4216, 4217, 4826, 4827, 4828, 4829, 4830, 4831, 4832, 4833
4834, 4835, 4836, 4837, 4838, 4839, 4840, 4841, 4842, 4843, 4844, 4845, 4846, 4847, 4848, 4849
4850, 4851, 4852, 4853, 4854, 4855, 4856, 4857, 4858, 4859, 4860, 4861, 4862, 4863, 4864, 4865
4866, 4867, 4868, 4869, 4870, 4871, 4872, 4873, 4874, 4875, 4876, 4877, 4878, 4879, 4880, 4881
4882, 4883, 4884, 4885, 4886, 4887, 4888, 4889, 4890, 4891, 4892, 4893, 4894, 4895, 4896, 4897
4898, 4899, 4900, 4901, 4902, 4903, 4904, 4905, 4906, 4907, 4908, 4909, 4910, 4911, 4912, 4913
4914, 4915, 4916, 4917, 4918, 4919, 4920, 4921, 4922, 4923, 4924, 4925, 4926, 4927, 4928, 4929
4930, 4931, 4932, 4933, 4934, 4935, 4936, 4937, 4938, 4939, 4940, 4941, 4942, 4943, 4944, 4945
4946, 4947, 4948, 4949, 4950, 4951, 4952, 4953, 4954, 4955, 4956, 4957, 4958, 4959, 4960, 4961
4962, 4963, 4964, 4965, 4966, 4967, 4968, 4969, 4970, 4971, 4972, 4973, 4974, 4975, 4976, 4977
4978, 4979, 4980, 4981, 4982, 4983, 4984, 4985
*Elset, elset=_PickedSet362, internal, instance=Column-1
67, 68, 69, 70, 71, 72, 73, 74, 75, 76, 77, 78, 79, 80, 81, 82
83, 84, 85, 86, 87, 88, 89, 90, 91, 92, 93, 94, 95, 96, 97, 98
99, 100, 101, 102, 103, 104, 105, 106, 107, 108, 109, 110, 111, 112, 113, 114
115, 116, 117, 118, 119, 120, 121, 122, 123, 124, 125, 126, 127, 128, 129, 130
131, 132, 133, 134, 135, 136, 137, 138, 139, 140, 141, 142, 143, 144, 145, 146
147, 148, 149, 150, 151, 152, 153, 154, 155, 156, 157, 158, 159, 160, 161, 162
163, 164, 165, 166, 167, 168, 169, 170, 171, 172, 173, 174, 175, 176, 177, 178
179, 180, 181, 182, 183, 184, 185, 186, 187, 188, 189, 190, 191, 192, 193, 194
195, 196, 197, 198, 199, 200, 201, 202, 203, 204, 205, 206, 207, 208, 209, 210
211, 212, 213, 214, 215, 216, 217, 218, 219, 220, 221, 222, 223, 224, 225, 226
227, 228, 229, 230, 231, 232, 233, 234, 235, 236, 237, 238, 239, 240, 241, 242
243, 244, 245, 246, 247, 248, 249, 250, 251, 252, 253, 254, 255, 256, 257, 258

259, 260, 261, 262, 263, 264, 925, 926, 927, 928, 929, 930, 931, 932, 933, 934
935, 936, 937, 938, 939, 940, 941, 942, 943, 944, 945, 946, 947, 948, 949, 950
951, 952, 953, 954, 955, 956, 957, 958, 959, 960, 961, 962, 963, 964, 965, 966
967, 968, 969, 970, 971, 972, 973, 974, 975, 976, 977, 978, 979, 980, 981, 982
983, 984, 985, 986, 987, 988, 989, 990, 991, 992, 993, 994, 995, 996, 997, 998
999, 1000, 1001, 1002, 1003, 1004, 1005, 1006, 1007, 1008, 1009, 1010, 1011, 1012, 1013, 1014
1015, 1016, 1017, 1018, 1019, 1020, 1021, 1022, 1023, 1024, 1025, 1026, 1027, 1028, 1029, 1030
1031, 1032, 1033, 1034, 1035, 1036, 1037, 1038, 1039, 1040, 1041, 1042, 1043, 1044, 1045, 1046
1047, 1048, 1049, 1050, 1051, 1052, 1053, 1054, 1055, 1056, 1057, 1058, 1059, 1060, 1061, 1062
1063, 1064, 1065, 1066, 1067, 1068, 1069, 1070, 1071, 1072, 1073, 1074, 1075, 1076, 1077, 1078
1079, 1080, 1081, 1082, 1083, 1084, 1085, 1086, 1087, 1088, 1089, 1090, 1091, 1092, 1093, 1094
1095, 1096, 1097, 1098, 1099, 1100, 1101, 1102, 1103, 1104, 1105, 1106, 1107, 1108, 1109, 1110
1111, 1112, 1113, 1114, 1115, 1116, 1117, 1118, 1119, 1120, 1121, 1122, 3307, 3308, 3309, 3310
3311, 3312, 3313, 3314, 3315, 3316, 3317, 3318, 3319, 3320, 3321, 3322, 3323, 3324, 3325, 3326
3327, 3328, 3329, 3330, 3331, 3332, 3333, 3334, 3335, 3336, 3337, 3338, 3339, 3340, 3341, 3342
3343, 3344, 3345, 3346, 3347, 3348, 3349, 3350, 3351, 3352, 3353, 3354, 3355, 3356, 3357, 3358
3359, 3360, 3361, 3362, 3363, 3364, 3365, 3366, 3367, 3368, 3369, 3370, 3371, 3372, 3373, 3374
3375, 3376, 3377, 3378, 3379, 3380, 3381, 3382, 3383, 3384, 3385, 3386, 3387, 3388, 3389, 3390
3391, 3392, 3393, 3394, 3395, 3396, 3397, 3398, 3399, 3400, 3401, 3402, 3403, 3404, 3405, 3406
3407, 3408, 3409, 3410, 3411, 3412, 3413, 3414, 3415, 3416, 3417, 3418, 3419, 3420, 3421, 3422
3423, 3424, 3425, 3426, 3427, 3428, 3429, 3430, 3431, 3432, 3433, 3434, 3435, 3436, 3437, 3438
3439, 3440, 3441, 3442, 3443, 3444, 3445, 3446, 3447, 3448, 3449, 3450, 3451, 3452, 3453, 3454
3455, 3456, 3457, 3458, 3459, 3460, 3461, 3462, 3463, 3464, 3465, 3466, 3467, 3468, 3469, 3470
3471, 3472, 3473, 3474, 3475, 3476, 3477, 3478, 3479, 3480, 3481, 3482, 3483, 3484, 3485, 3486
3487, 3488, 3489, 3490, 3491, 3492, 3493, 3494, 3495, 3496, 3497, 3498, 3499, 3500, 3501, 3502

3503, 3504, 4165, 4166, 4167, 4168, 4169, 4170, 4171, 4172, 4173, 4174, 4175, 4176, 4177, 4178
4179, 4180, 4181, 4182, 4183, 4184, 4185, 4186, 4187, 4188, 4189, 4190, 4191, 4192, 4193, 4194
4195, 4196, 4197, 4198, 4199, 4200, 4201, 4202, 4203, 4204, 4205, 4206, 4207, 4208, 4209, 4210
4211, 4212, 4213, 4214, 4215, 4216, 4217, 4218, 4219, 4220, 4221, 4222, 4223, 4224, 4225, 4226
4227, 4228, 4229, 4230, 4231, 4232, 4233, 4234, 4235, 4236, 4237, 4238, 4239, 4240, 4241, 4242
4243, 4244, 4245, 4246, 4247, 4248, 4249, 4250, 4251, 4252, 4253, 4254, 4255, 4256, 4257, 4258
4259, 4260, 4261, 4262, 4263, 4264, 4265, 4266, 4267, 4268, 4269, 4270, 4271, 4272, 4273, 4274
4275, 4276, 4277, 4278, 4279, 4280, 4281, 4282, 4283, 4284, 4285, 4286, 4287, 4288, 4289, 4290
4291, 4292, 4293, 4294, 4295, 4296, 4297, 4298, 4299, 4300, 4301, 4302, 4303, 4304, 4305, 4306
4307, 4308, 4309, 4310, 4311, 4312, 4313, 4314, 4315, 4316, 4317, 4318, 4319, 4320, 4321, 4322
4323, 4324, 4325, 4326, 4327, 4328, 4329, 4330, 4331, 4332, 4333, 4334, 4335, 4336, 4337, 4338
4339, 4340, 4341, 4342, 4343, 4344, 4345, 4346, 4347, 4348, 4349, 4350, 4351, 4352, 4353, 4354
4355, 4356, 4357, 4358, 4359, 4360, 4361, 4362
*Nset, nset=_PickedSet364, internal
13,
*Elset, elset=_s_Surf-11_E2, internal, instance=BeaB-G2-R
1366, 1372, 1378, 1384, 1390, 1396, 1402, 1408, 1414, 1420, 5926, 5932, 5938, 5944, 5950, 5956
5962, 5968, 5974, 5980
*Surface, type=ELEMENT, name=s_Surf-11
_s_Surf-11_E2, E2
*Elset, elset=_s_Surf-12_SPOS, internal, instance=BeaB-G2-R, generate
5921, 5980, 1
*Elset, elset=_s_Surf-12_SNEG, internal, instance=BeaB-G2-R, generate
1361, 1420, 1
*Surface, type=ELEMENT, name=s_Surf-12
_s_Surf-12_SPOS, SPOS
_s_Surf-12_SNEG, SNEG
*Elset, elset=__PickedSurf222_E3, internal, instance=BeaB-G2-R
1309, 1310, 1355, 1356, 1357, 1358, 1359, 1360, 1501, 1502, 1503, 1504, 1505, 1506, 1507, 1508
1509, 1510, 1511, 1512, 1513, 1514, 1515, 1516, 1517, 1518, 1519, 1520, 1745, 1746, 1747, 1748
1749, 1750, 1819, 1820, 5869, 5870, 5915, 5916, 5917, 5918, 5919, 5920, 6061, 6062, 6063, 6064
6065, 6066, 6067, 6068, 6069, 6070, 6071, 6072, 6073, 6074, 6075, 6076, 6077, 6078, 6079, 6080
6305, 6306, 6307, 6308, 6309, 6310, 6379, 6380

```
*Surface, type=ELEMENT, name=_PickedSurf222, internal
__PickedSurf222_E3, E3
*Elset, elset=__PickedSurf238_SPOS, internal, instance=Gusset-1, generate
   65,  1232,     1
*Surface, type=ELEMENT, name=_PickedSurf238, internal
__PickedSurf238_SPOS, SPOS
*Elset, elset=__PickedSurf241_SNEG, internal, instance=Gusset-1, generate
   65,  1232,     1
*Surface, type=ELEMENT, name=_PickedSurf241, internal
__PickedSurf241_SNEG, SNEG
*Elset, elset=__PickedSurf250_SNEG, internal, instance=BeaB-G2-R, generate
   61,  1060,     1
*Elset, elset=__PickedSurf250_SNEG, internal, instance=Column-1, generate
 1189,  1608,     1
*Surface, type=ELEMENT, name=_PickedSurf250, internal
__PickedSurf250_SNEG, SNEG
*Elset, elset=__PickedSurf251_SPOS, internal, instance=BeaB-G2-R, generate
 4621,  5620,     1
*Elset, elset=__PickedSurf251_SPOS, internal, instance=Column-1, generate
 4429,  4848,     1
*Surface, type=ELEMENT, name=_PickedSurf251, internal
__PickedSurf251_SPOS, SPOS
*Surface, type=NODE, name=_PickedSet358_CNS_, internal
_PickedSet358, 1.
*Surface, type=NODE, name=_PickedSet229_CNS_, internal
_PickedSet229, 1.
*Surface, type=NODE, name=_PickedSet231_CNS_, internal
_PickedSet231, 1.
*Surface, type=NODE, name=_PickedSet233_CNS_, internal
_PickedSet233, 1.
*Surface, type=NODE, name=_PickedSet235_CNS_, internal
_PickedSet235, 1.
*Surface, type=NODE, name=_PickedSet268_CNS_, internal
_PickedSet268, 1.
*Surface, type=NODE, name=_PickedSet270_CNS_, internal
_PickedSet270, 1.
*Surface, type=NODE, name=_PickedSet272_CNS_, internal
_PickedSet272, 1.
*Surface, type=NODE, name=_PickedSet274_CNS_, internal
_PickedSet274, 1.
*Surface, type=NODE, name=_PickedSet276_CNS_, internal
_PickedSet276, 1.
*Surface, type=NODE, name=_PickedSet278_CNS_, internal
_PickedSet278, 1.
*Surface, type=NODE, name=_PickedSet280_CNS_, internal
_PickedSet280, 1.
*Surface, type=NODE, name=_PickedSet282_CNS_, internal
_PickedSet282, 1.
*Surface, type=NODE, name=_PickedSet284_CNS_, internal
_PickedSet284, 1.
```

*Surface, type=NODE, name=_PickedSet286_CNS_, internal
_PickedSet286, 1.
*Surface, type=NODE, name=_PickedSet288_CNS_, internal
_PickedSet288, 1.
*Surface, type=NODE, name=_PickedSet299_CNS_, internal
_PickedSet299, 1.
*Surface, type=NODE, name=_PickedSet301_CNS_, internal
_PickedSet301, 1.
*Surface, type=NODE, name=_PickedSet303_CNS_, internal
_PickedSet303, 1.
*Surface, type=NODE, name=_PickedSet305_CNS_, internal
_PickedSet305, 1.
*Surface, type=NODE, name=_PickedSet307_CNS_, internal
_PickedSet307, 1.
*Surface, type=NODE, name=_PickedSet309_CNS_, internal
_PickedSet309, 1.
*Surface, type=NODE, name=_PickedSet311_CNS_, internal
_PickedSet311, 1.
*Surface, type=NODE, name=_PickedSet313_CNS_, internal
_PickedSet313, 1.
*Surface, type=NODE, name=_PickedSet315_CNS_, internal
_PickedSet315, 1.
*Surface, type=NODE, name=_PickedSet317_CNS_, internal
_PickedSet317, 1.
*Surface, type=NODE, name=_PickedSet319_CNS_, internal
_PickedSet319, 1.
*Surface, type=NODE, name=_PickedSet321_CNS_, internal
_PickedSet321, 1.
** Constraint: Constraint-2
*Coupling, constraint name=Constraint-2, ref node=_PickedSet223, surface=_PickedSurf222
*Kinematic
** Constraint: Cpl at load
*Coupling, constraint name="Cpl at load", ref node=_PickedSet359, surface=_PickedSet358_CNS_
*Kinematic
** Constraint: MPC 1
*MPC
BEAM, _PickedSet229, _PickedSet230
** Constraint: MPC 2
*MPC
BEAM, _PickedSet231, _PickedSet232
** Constraint: MPC 3
*MPC
BEAM, _PickedSet233, _PickedSet234
** Constraint: MPC 4
*MPC
BEAM, _PickedSet235, _PickedSet236
** Constraint: MPC5
*MPC

```
BEAM, _PickedSet268, _PickedSet269
** Constraint: MPC6
*MPC
BEAM, _PickedSet270, _PickedSet271
** Constraint: MPC7
*MPC
BEAM, _PickedSet272, _PickedSet273
** Constraint: MPC8
*MPC
BEAM, _PickedSet274, _PickedSet275
** Constraint: MPC9
*MPC
BEAM, _PickedSet276, _PickedSet277
** Constraint: MPC10
*MPC
BEAM, _PickedSet278, _PickedSet279
** Constraint: MPC11
*MPC
BEAM, _PickedSet280, _PickedSet281
** Constraint: MPC12
*MPC
BEAM, _PickedSet282, _PickedSet283
** Constraint: MPC13
*MPC
BEAM, _PickedSet284, _PickedSet285
** Constraint: MPC14
*MPC
BEAM, _PickedSet286, _PickedSet287
** Constraint: MPC15
*MPC
BEAM, _PickedSet288, _PickedSet289
** Constraint: MPC16
*MPC
BEAM, _PickedSet299, _PickedSet300
** Constraint: MPC17
*MPC
BEAM, _PickedSet301, _PickedSet302
** Constraint: MPC18
*MPC
BEAM, _PickedSet303, _PickedSet304
** Constraint: MPC19
*MPC
BEAM, _PickedSet305, _PickedSet306
** Constraint: MPC20
*MPC
BEAM, _PickedSet307, _PickedSet308
** Constraint: MPC21
*MPC
BEAM, _PickedSet309, _PickedSet310
** Constraint: MPC22
```

```
*MPC
BEAM, _PickedSet311, _PickedSet312
** Constraint: MPC23
*MPC
BEAM, _PickedSet313, _PickedSet314
** Constraint: MPC24
*MPC
BEAM, _PickedSet315, _PickedSet316
** Constraint: MPC25
*MPC
BEAM, _PickedSet317, _PickedSet318
** Constraint: MPC26
*MPC
BEAM, _PickedSet319, _PickedSet320
** Constraint: MPC27
*MPC
BEAM, _PickedSet321, _PickedSet322
**
** POINT-BASED FASTENER: FastenerS-G3-R
*Fastener Property, name=FastenerS-G3-R
3.
*Connector Section, elset=_FastenerS-G3-R_pf_, behavior=Cartesian
Cartesian,
*Fastener, interaction name=FastenerS-G3-R, property=FastenerS-G3-R, reference node set=Set-86, elset=_FastenerS-G3-R_pf_,
coupling=CONTINUUM, attachment method=FACETOFACE, weighting method=UNIFORM, adjust orientation=YES
**
**
**
**
**
**
**
**
*Equation
2
fastn_line_1.1, 1, 1, Gusset-1.27, 1, -1
*Equation
2
fastn_line_1.1, 2, 1, Gusset-1.27, 2, -1
*Equation
2
fastn_line_1.1, 3, 1, Gusset-1.27, 3, -1
**
*Equation
2
fastn_line_1.2, 1, 1, Column-1.5307, 1, -1
*Equation
2
```

```
fastn_line_1.2, 2, 1, Column-1.5307, 2, -1
*Equation
2
fastn_line_1.2, 3, 1, Column-1.5307, 3, -1
**
**
**
*Equation
2
fastn_line_2.1, 2, 1, Column-1.2598, 2, -1
*Equation
2
fastn_line_2.1, 3, 1, Column-1.2598, 3, -1
*Equation
2
fastn_line_2.1, 1, 1, Column-1.2598, 1, -1
**
*Equation
2
fastn_line_2.2, 2, 1, Gusset-1.27, 2, -1
*Equation
2
fastn_line_2.2, 3, 1, Gusset-1.27, 3, -1
*Equation
2
fastn_line_2.2, 1, 1, Gusset-1.27, 1, -1
**
**
**
*Equation
2
fastn_line_3.1, 2, 1, Gusset-1.29, 2, -1
*Equation
2
fastn_line_3.1, 3, 1, Gusset-1.29, 3, -1
*Equation
2
fastn_line_3.1, 1, 1, Gusset-1.29, 1, -1
**
*Equation
2
fastn_line_3.2, 2, 1, Column-1.5212, 2, -1
*Equation
2
fastn_line_3.2, 3, 1, Column-1.5212, 3, -1
*Equation
2
fastn_line_3.2, 1, 1, Column-1.5212, 1, -1
**
**
```

```
**
*Equation
2
fastn_line_4.1, 2, 1, Column-1.2503, 2, -1
*Equation
2
fastn_line_4.1, 3, 1, Column-1.2503, 3, -1
*Equation
2
fastn_line_4.1, 1, 1, Column-1.2503, 1, -1
**
*Equation
2
fastn_line_4.2, 2, 1, Gusset-1.29, 2, -1
*Equation
2
fastn_line_4.2, 3, 1, Gusset-1.29, 3, -1
*Equation
2
fastn_line_4.2, 1, 1, Gusset-1.29, 1, -1
**
**
**
**
*Equation
2
fastn_line_5.1, 2, 1, Gusset-1.25, 2, -1
*Equation
2
fastn_line_5.1, 3, 1, Gusset-1.25, 3, -1
*Equation
2
fastn_line_5.1, 1, 1, Gusset-1.25, 1, -1
**
*Equation
2
fastn_line_5.2, 2, 1, Column-1.5117, 2, -1
*Equation
2
fastn_line_5.2, 3, 1, Column-1.5117, 3, -1
*Equation
2
fastn_line_5.2, 1, 1, Column-1.5117, 1, -1
**
**
**
*Equation
2
fastn_line_6.1, 2, 1, Column-1.2408, 2, -1
*Equation
```

```
2
fastn_line_6.1, 3, 1, Column-1.2408, 3, -1
*Equation
2
fastn_line_6.1, 1, 1, Column-1.2408, 1, -1
**
*Equation
2
fastn_line_6.2, 2, 1, Gusset-1.25, 2, -1
*Equation
2
fastn_line_6.2, 3, 1, Gusset-1.25, 3, -1
*Equation
2
fastn_line_6.2, 1, 1, Gusset-1.25, 1, -1
**
**
*Equation
2
fastn_line_7.1, 1, 1, Gusset-1.21, 1, -1
*Equation
2
fastn_line_7.1, 2, 1, Gusset-1.21, 2, -1
*Equation
2
fastn_line_7.1, 3, 1, Gusset-1.21, 3, -1
**
*Equation
2
fastn_line_7.2, 1, 1, Column-1.5312, 1, -1
*Equation
2
fastn_line_7.2, 2, 1, Column-1.5312, 2, -1
*Equation
2
fastn_line_7.2, 3, 1, Column-1.5312, 3, -1
**
**
**
*Equation
2
fastn_line_8.1, 2, 1, Column-1.2603, 2, -1
*Equation
2
fastn_line_8.1, 3, 1, Column-1.2603, 3, -1
*Equation
2
fastn_line_8.1, 1, 1, Column-1.2603, 1, -1
**
*Equation
```

```
2
fastn_line_8.2, 2, 1, Gusset-1.21, 2, -1
*Equation
2
fastn_line_8.2, 3, 1, Gusset-1.21, 3, -1
*Equation
2
fastn_line_8.2, 1, 1, Gusset-1.21, 1, -1
**
**
**
**
**
**
**
**
*Equation
2
fastn_line_11.1, 2, 1, Gusset-1.23, 2, -1
*Equation
2
fastn_line_11.1, 3, 1, Gusset-1.23, 3, -1
*Equation
2
fastn_line_11.1, 1, 1, Gusset-1.23, 1, -1
**
*Equation
2
fastn_line_11.2, 2, 1, Column-1.5122, 2, -1
*Equation
2
fastn_line_11.2, 3, 1, Column-1.5122, 3, -1
*Equation
2
fastn_line_11.2, 1, 1, Column-1.5122, 1, -1
**
**
**
*Equation
2
fastn_line_12.1, 2, 1, Column-1.2413, 2, -1
*Equation
2
fastn_line_12.1, 3, 1, Column-1.2413, 3, -1
*Equation
2
fastn_line_12.1, 1, 1, Column-1.2413, 1, -1
**
*Equation
2
```

fastn_line_12.2, 2, 1, Gusset-1.23, 2, -1
*Equation
2
fastn_line_12.2, 3, 1, Gusset-1.23, 3, -1
*Equation
2
fastn_line_12.2, 1, 1, Gusset-1.23, 1, -1
**
**
**
*Equation
2
fastn_line_13.1, 2, 1, Gusset-1.19, 2, -1
*Equation
2
fastn_line_13.1, 3, 1, Gusset-1.19, 3, -1
*Equation
2
fastn_line_13.1, 1, 1, Gusset-1.19, 1, -1
**
*Equation
2
fastn_line_13.2, 2, 1, Column-1.5317, 2, -1
*Equation
2
fastn_line_13.2, 3, 1, Column-1.5317, 3, -1
*Equation
2
fastn_line_13.2, 1, 1, Column-1.5317, 1, -1
**
**
**
*Equation
2
fastn_line_14.1, 2, 1, Column-1.2608, 2, -1
*Equation
2
fastn_line_14.1, 3, 1, Column-1.2608, 3, -1
*Equation
2
fastn_line_14.1, 1, 1, Column-1.2608, 1, -1
**
*Equation
2
fastn_line_14.2, 2, 1, Gusset-1.19, 2, -1
*Equation
2
fastn_line_14.2, 3, 1, Gusset-1.19, 3, -1
*Equation
2

```
fastn_line_14.2, 1, 1, Gusset-1.19, 1, -1
**
**
**
**
*Equation
2
fastn_line_15.1, 2, 1, Gusset-1.20, 2, -1
*Equation
2
fastn_line_15.1, 3, 1, Gusset-1.20, 3, -1
*Equation
2
fastn_line_15.1, 1, 1, Gusset-1.20, 1, -1
**
*Equation
2
fastn_line_15.2, 2, 1, Column-1.5222, 2, -1
*Equation
2
fastn_line_15.2, 3, 1, Column-1.5222, 3, -1
*Equation
2
fastn_line_15.2, 1, 1, Column-1.5222, 1, -1
**
**
**
*Equation
2
fastn_line_16.1, 2, 1, Column-1.2513, 2, -1
*Equation
2
fastn_line_16.1, 3, 1, Column-1.2513, 3, -1
*Equation
2
fastn_line_16.1, 1, 1, Column-1.2513, 1, -1
**
*Equation
2
fastn_line_16.2, 2, 1, Gusset-1.20, 2, -1
*Equation
2
fastn_line_16.2, 3, 1, Gusset-1.20, 3, -1
*Equation
2
fastn_line_16.2, 1, 1, Gusset-1.20, 1, -1
**
**
**
**
```

```
*Equation
2
fastn_line_17.1, 2, 1, Gusset-1.16, 2, -1
*Equation
2
fastn_line_17.1, 3, 1, Gusset-1.16, 3, -1
*Equation
2
fastn_line_17.1, 1, 1, Gusset-1.16, 1, -1
**
*Equation
2
fastn_line_17.2, 2, 1, Column-1.5127, 2, -1
*Equation
2
fastn_line_17.2, 3, 1, Column-1.5127, 3, -1
*Equation
2
fastn_line_17.2, 1, 1, Column-1.5127, 1, -1
**
**
**
*Equation
2
fastn_line_18.1, 2, 1, Column-1.2418, 2, -1
*Equation
2
fastn_line_18.1, 3, 1, Column-1.2418, 3, -1
*Equation
2
fastn_line_18.1, 1, 1, Column-1.2418, 1, -1
**
*Equation
2
fastn_line_18.2, 2, 1, Gusset-1.16, 2, -1
*Equation
2
fastn_line_18.2, 3, 1, Gusset-1.16, 3, -1
*Equation
2
fastn_line_18.2, 1, 1, Gusset-1.16, 1, -1
**
**
**
**
*End Assembly
*Amplitude, name=Cycles
             0.,              0.,            0.25,             2.8,             0.5,              0.,            0.75,
-2.8
```

1.,	0.,	1.25,	2.8,	1.5,	0.,	1.75,	-2.8
2.,	0.,	2.25,	2.8,	2.5,	0.,	2.75,	-2.8
3.,	0.,	3.25,	2.8,	3.5,	0.,	3.75,	-2.8
4.,	0.,	4.25,	2.8,	4.5,	0.,	4.75,	-2.8
5.,	0.,	5.25,	2.8,	5.5,	0.,	5.75,	-2.8
6.,	0.,	6.25,	3.75,	6.5,	0.,	6.75,	-3.75
7.,	0.,	7.25,	3.75,	7.5,	0.,	7.75,	-3.75
8.,	0.,	8.25,	3.75,	8.5,	0.,	8.75,	-3.75
9.,	0.,	9.25,	3.75,	9.5,	0.,	9.75,	-3.75
10.,	0.,	10.25,	3.75,	10.5,	0.,	10.75,	-3.75
11.,	0.,	11.25,	3.75,	11.5,	0.,	11.75,	-3.75
12.,	0.,	12.25,	5.63,	12.5,	0.,	12.75,	-5.63
13.,	0.,	13.25,	5.63,	13.5,	0.,	13.75,	-5.63
14.,	0.,	14.25,	5.63,	14.5,	0.,	14.75,	-5.63
15.,	0.,	15.25,	5.63,	15.5,	0.,	15.75,	-5.63
16.,	0.,	16.25,	5.63,	16.5,	0.,	16.75,	-5.63
17.,	0.,	17.25,	5.63,	17.5,	0.,	17.75,	-5.63
18.,	0.,	18.25,	7.5,	18.5,	0.,	18.75,	-7.5
19.,	0.,	19.25,	7.5,	19.5,	0.,	19.75,	-7.5
20.,	0.,	20.25,	7.5,	20.5,	0.,	20.75,	-7.5
21.,	0.,	21.25,	7.5,	21.5,	0.,	21.75,	-7.5
22.,	0.,	22.25,	11.25,	22.5,	0.,	22.75,	-11.25
23.,	0.,	23.25,	11.25,	23.5,	0.,	23.75,	-11.25
24.,	0.,	24.25,	15.,	24.5,	0.,	24.75,	-15.
25.,	0.,	25.25,	15.,	25.5,	0.,	25.75,	-15.

```
              26.,            0.,          26.25,           22.5,           26.5,            0.,          26.75,
-22.5
              27.,            0.,          27.25,           22.5,           27.5,            0.,          27.75,
-22.5
              28.,            0.,          28.25,            30.,           28.5,            0.,          28.75,
-30.
              29.,            0.,          29.25,            30.,           29.5,            0.,          29.75,
-30.
              30.,            0.,          30.25,           37.5,           30.5,            0.,          30.75,
-37.5
              31.,            0.,          31.25,           37.5,           31.5,            0.,          31.75,
-37.5
              32.,            0.,          32.25,            45.,           32.5,            0.,          32.75,
-45.
              33.,            0.,          33.25,            45.,           33.5,            0.,          33.75,
-45.
              34.,            0.,          34.25,           52.5,           34.5,            0.,          34.75,
-52.5
              35.,            0.,          35.25,           52.5,           35.5,            0.,          35.75,
-52.5
              36.,            0.,          36.25,            60.,           36.5,            0.,          36.75,
-60.
              37.,            0.,          37.25,            60.,           37.5,            0.,          37.75,
-60.
              38.,            0.,          38.25,           67.5,           38.5,            0.,          38.75,
-67.5
              39.,            0.,          39.25,           67.5,           39.5,            0.,          39.75,
-67.5
              40.,            0.
  **
  *Amplitude, name=TB
              0.,             0.,            0.5,             1.,             1.,            -1.
  ** MATERIALS
  **
  *Material, name=Bilinear-ST37
  *Density
   7.85e-09,
  *Elastic
  210000., 0.3
  *Plastic, hardening=KINEMATIC
  240.,   0.
  360., 0.06
  *Material, name=Bilinear-ST52
  *Density
   7.85e-09,
  *Elastic
  210000., 0.3
  *Plastic, hardening=KINEMATIC
  360.,   0.
  520., 0.08
```

```
*Material, name=Test-Material
*Density
 7.85e-09,
*Elastic
210000., 0.3
*Plastic
336.,    0.
355., 0.013
440., 0.118
402., 0.208
**
** INTERACTION PROPERTIES
**
*Surface Interaction, name="Contact G to B"
1.,
*Friction
0.,
*Surface Behavior, pressure-overclosure=HARD
*Connector Behavior, name=Cartesian
*Connector Elasticity, rigid
1, 2, 3
**Connector Plasticity, component=1
**Connector Hardening, definition=TABULAR
**3500.,  0.3,   0.
**6300., 1.94,   0.
**6500., 5.11,   0.
**9700., 9.56,   0.
**Connector Plasticity, component=2
**Connector Hardening, definition=TABULAR
**3500.,  0.3,   0.
**6300., 1.94,   0.
**6500., 5.11,   0.
**9700., 9.56,   0.
**Connector Plasticity, component=3
**Connector Hardening, definition=TABULAR
**3500.,  0.3,   0.
**6300., 1.94,   0.
**6500., 5.11,   0.
**9700., 9.56,   0.
**
** BOUNDARY CONDITIONS
**
** Name: BC-Fix 2 Type: Displacement/Rotation
*Boundary
_PickedSet256, 1, 1
_PickedSet256, 2, 2
_PickedSet256, 3, 3
**
** INTERACTIONS
**
```

```
** Interaction: Int-1
*Contact Pair, interaction="Contact G to B", type=SURFACE TO SURFACE
_PickedSurf238, _PickedSurf250
** Interaction: Int-2
*Contact Pair, interaction="Contact G to B", type=SURFACE TO SURFACE
_PickedSurf241, _PickedSurf251
** ----------------------------------------------------------------
**
** STEP: Cyclic
**
*Step, name=Cyclic, nlgeom=YES, inc=1000000
*Static
0.01, 40., 1e-09, 0.1
**
** BOUNDARY CONDITIONS
**
** Name: BC-Fix 1 Type: Displacement/Rotation
*Boundary
_PickedSet362, 1, 1
_PickedSet362, 2, 2
_PickedSet362, 3, 3
** Name: BC-Lateral Type: Displacement/Rotation
*Boundary
_PickedSet355, 1, 1
** Name: BC-Load Type: Displacement/Rotation
*Boundary, amplitude=Cycles
_PickedSet364, 2, 2, -1.
**
** CONTROLS
**
*Controls, reset
*Controls, parameters=time incrementation
, , , , , , , 20, , ,
**
** OUTPUT REQUESTS
**
*Restart, write, frequency=0
**
** FIELD OUTPUT: F-Output-1
**
*Output, field
*Node Output
CF, PHILSM, PSILSM, RF, RM, RT, TF, U
UR, UT, V, VF, VR, VT
*Element Output, directions=YES
ALPHA, ALPHAN, BF, CENTMAG, CENTRIFMAG, CFAILURE, CORIOMAG, CS11, CTSHR, DAMAGEC, DAMAGEFC, DAMAGEFT, DAMAGEMC, DAMAGEMT, DAMAGESHR, DAMAGET
DMICRT, E, EE, ER, ERPRATIO, ESF1, GRAV, HP, HSNFCCRT, HSNFTCRT, HSNMCCRT, HSNMTCRT, IE, JK, LE, MISES
```

MISESMAX, MISESONLY, NE, NFORC, NFORCSO, P, PE, PEEQ, PEEQMAX, PEEQT, PEMAG, PEQC, PRESSONLY, PS, ROTAMAG, S

SALPHA, SDEG, SE, SEE, SEP, SEPE, SF, SHRRATIO, SPE, SSAVG, THE, TRIAX, TRNOR, TRSHR, TSHR, VE

VEEQ, VS

*Contact Output

BDSTAT, CRSTS, CSDMG, CSMAXSCRT, CSMAXUCRT, CSQUADSCRT, CSQUADUCRT, DBS, DBSF, DBT, EFENRRTR, ENRRT, OPENBC

**

** HISTORY OUTPUT: H-Output-2

**

*Output, history

*Node Output, nset=Set-LVDT

UT,

**

** HISTORY OUTPUT: H-Output-1

**

*Node Output, nset=Set-RP-4

RT,

*End Step

Appendix C: Cold-formed Section Capacity

Section Properties:

H	200 mm	7.9 inch
b	60 mm	2.4 inch
D	20 mm	0.8 inch
d	15 mm	0.6 inch
t	2 mm	0.1 inch
R	3 mm	0.1 inch
R'	4 mm	0.2 inch

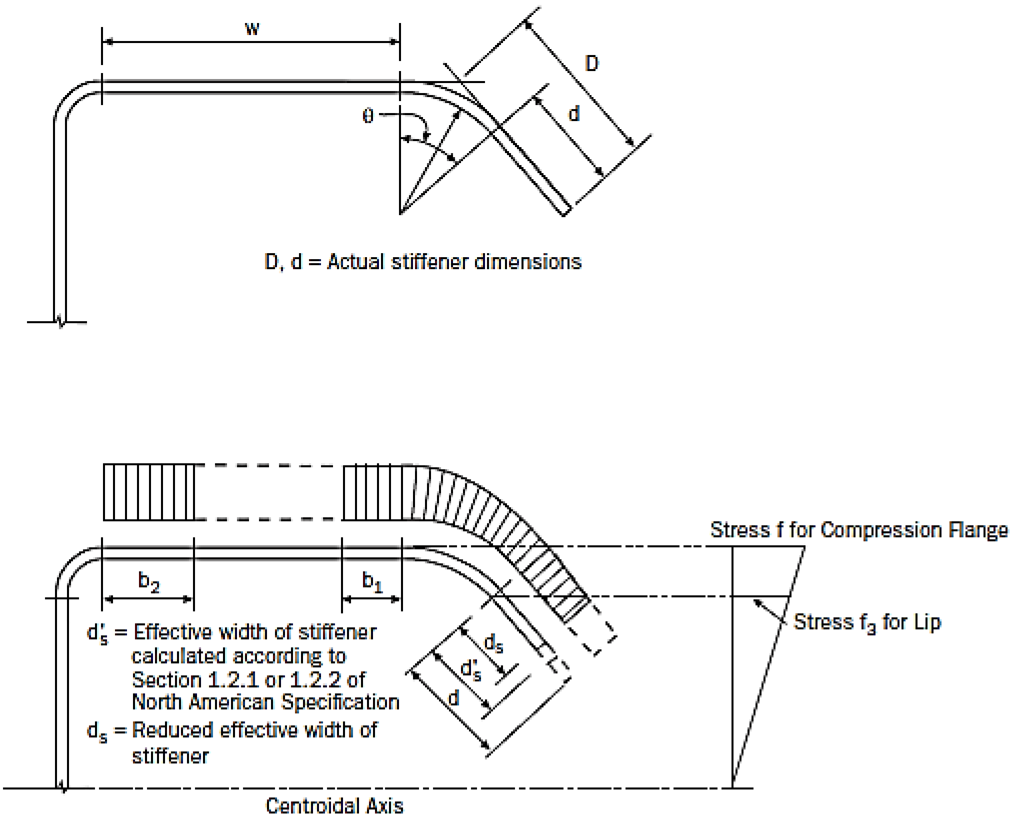

Figure C- 1: Effective flange width in CFS

Effective Width of Compression Flange:

$$w = 1.97\ inch$$

$$\frac{w}{t} = 25$$

$$S = 1.28\sqrt{\frac{E}{f}} = 30.9\ inch$$

$$0.328 * S = 10.14\ inch$$

$$\frac{w}{t} > 0.328 * S$$

$$I_a = 399t^4\left(\frac{w}{t * S} - 0.328\right)^3 = 0.0017 \leq t^4\left(115\frac{w}{t * S} + 5\right) = 0.0037$$

$$I_s = \frac{1}{12}(d^3 t \sin^2\theta) = 0.0014$$

$$R_I = \frac{I_s}{I_a} = 0.8$$

$$b = \rho w = 1 \times 1.97 = 1.97\ inch$$

$$b_1 = \frac{1}{2}(b)(R_I) = 0.5 * 1.97 * 0.8 = 19.8\ mm$$

$$b_2 = b - b_1 = 60 - 19.8 = 40.2\ mm$$

$$\therefore The\ effective\ length\ of\ the\ flange\ is\ equal\ to\ the\ total\ length$$

$$\therefore M_{n_{beam}} = F_y \times S_x = 350 \times \frac{8\times10^6}{200/2} = 28\ kN.m$$

الملخص

هذا البحث يدرس السلوك الإنشائي لوصلات القطاعات المعدنية المشكلة على البارد ومعرضة لعزوم انحناء ناتجة عن حمل ترددي. اضافة الى هذا يهدف البحث الى وضع إطار لنمذجة و تحليل هذه الوصلات. في هذا البحث تم تقسيم الوصلات الى فئتين: الاولى للوصلات باستخدام المسامير ذاتية الثقب والثانية للوصلات باستخدام مسامير بصامولة. في هذه الدراسة تم اختبار ثلاث وصلات تحت تأثير حمل ترددي، الاولى والثانية مثبتة باستخدام مسامير ذاتية الثقب بقطر 6 مم بينما الثالثة باستخدام مسامير بصامولة بقطر 12 مم. كما تم استخدام نماذج رقمية باستخدام برنامج تحليل بطريقة العناصر المحددة. تم التأكد من دقة النماذج العددية من خلال مقارنة نتائجها بنتائج الاختبارات المعملية. تمت نمذجة قطاعة الصلب المشكلة على البارد باستخدام عناصر قشرية، والمسامير ذاتية الثقب بواسطة عناصر يتم برمجتها من خلال المستخدم وربطها مع برنامج التحليل الإنشائي، في حين تم نمذجة المسامير بصامولة باستخدام عناصر صلبة.

هذا البحث يوضح الفرق بين استخدام الطرق المتعارف عليها في نمذجة المسامير تحت تأثير احمال إستاتيكية واحمال ترددية. أخيرا، تمت دراسة تأثير التغير في سمك القطاعات، وترتيب المسامير، واماكن التقويات على اداء الوصلات.

مهندس: ياسر نصر ابراهيم مصطفى

تاريخ الميلاد: 1994\10\29

الجنسية: مصري

تاريخ التسجيل: 2019\03\01

تاريخ المنح: 2022\....\....

القسم: الهندسة الانشائية

الدرجة: ماجستير العلوم

المشرفون:

أ.د. شريف احمد مراد

د. حازم حسام الدين الأنور

أ.د. ماجد توفيق حنا

الممتحنون:

أ.د. شريف احمد مراد (المشرف الرئيسي)

أ.د. ماجد توفيق حنا (المشرف الخارجي)

– أستاذ المنشآت المعدنية بالمركز القومي لبحوث الاسكان والبناء

أ.د. محمد حسانين محمد سرور (الممتحن الداخلي)

أ.د. مصطفى حسنين (الممتحن الخارجي)

– أستاذ المنشآت المعدنية – كلية الهندسة – جامعة طنطا

عنوان الرسالة:

تقييم سلوك وصلات الإطارات المصنعة من قطاعات الصلب المشكل على البارد تحت تأثير حمل ترددي

الكلمات الدالة:

الحديد المشكل على البارد، الاحمال الترددية، وصلات ركنية، مسامير ذاتية الثقب

ملخص الرسالة:

هذا البحث يدرس السلوك الإنشائي لوصلات القطاعات المعدنية المشكلة على البارد ومعرضة لعزوم انحناء ناتجة عن حمل ترددي. اضافة الى هذا يهدف البحث الى وضع إطار لنمذجة وتحليل هذه الوصلات. في هذا البحث تم تقسيم الوصلات الى فئتين: الاولى للوصلات باستخدام المسامير ذاتية الثقب والثانية للوصلات باستخدام مسامير بصامولة. في هذه الدراسة تم اختبار ثلاث وصلات تحت تأثير حمل ترددي، الاولى والثانية مثبتة باستخدام مسامير ذاتية الثقب بقطر 6 مم بينما الثالثة باستخدام مسامير بصامولة بقطر 12 مم. كما تم استخدام نماذج رقمية باستخدام برنامج تحليل بطريقة العناصر المحددة. تم التأكد من دقة النماذج العددية من خلال مقارنة نتائجها بالنتائج الاختبارات المعملية. تمت نمذجة قطاعة الصلب المشكلة على البارد باستخدام عناصر قشرية، والمسامير ذاتية الثقب بواسطة عناصر يتم برمجتها من خلال المستخدم وربطها مع برنامج التحليل الإنشائي، في حين تم نمذجة المسامير بصامولة باستخدام عناصر صلبة.

تقييم سلوك وصلات الإطارات المصنعة من قطاعات الصلب المشكل على البارد تحت تأثير حمل ترددي

اعداد

ياسر نصر ابراهيم مصطفى

رسالة مقدمة إلى كلية الهندسة – جامعة القاهرة
كجزء من متطلبات الحصول على درجة
ماجستير العلوم
في
الهندسة الانشائية

يعتمد من لجنة الممتحنين:

الاستاذ الدكتور: شريف احمد مراد **المشرف الرئيسي**
أستاذ المنشآت والكباري المعدنية - كلية الهندسة - جامعة القاهرة

الاستاذ الدكتور: ماجد توفيق حنا **مشرف خارجي**
أستاذ المنشآت المعدنية - المركز القومي لبحوث الاسكان والبناء

الاستاذ الدكتور: محمد حسانين محمد سرور **الممتحن الداخلي**
أستاذ المنشآت المعدنية - كلية الهندسة - جامعة القاهرة

الاستاذ الدكتور: مصطفى فهمي حسنين **الممتحن الخارجي**
أستاذ المنشآت المعدنية - كلية الهندسة - جامعة طنطا

كليــة الهندســة - جامعــة القاهــرة
الجيـزة - جمهوريـة مصر العربية
2022

تقييم سلوك وصلات الإطارات المصنعة من قطاعات الصلب المشكل على البارد
تحت تأثير حمل ترددي

اعداد
ياسر نصر ابراهيم مصطفى

رسالة مقدمة إلى كلية الهندسة – جامعة القاهرة
كجزء من متطلبات الحصول على درجة
ماجستير العلوم
في
الهندسة الانشائية

تحت اشراف

أ.د. شريف احمد مراد
....
أستاذ المنشآت والكباري المعدنية
كلية الهندسة – جامعة القاهرة

أ.د. ماجد توفيق حنا
....
أستاذ المنشآت المعدنية
المركز القومي لبحوث الاسكان والبناء

د. حازم حسام الدين الأنور
....
مدرس بقسم الهندسة الانشائية
كلية الهندسة – جامعة القاهرة

كليــة الهندســة - جامعــة القاهــرة
الجيـزة - جمهوريـة مصر العربية
2022

تقييم سلوك وصلات الإطارات المصنعة من قطاعات الصلب المشكل على البارد

تحت تأثير حمل ترددي

اعداد

ياسر نصر ابراهيم مصطفى

رسالة مقدمة إلى كلية الهندسة – جامعة القاهرة
كجزء من متطلبات الحصول على درجة
ماجستير العلوم
في
الهندسة الانشائية

كليـــة الهندســـة - جامعـــة القاهـــرة
الجيـزة - جمهوريـة مصر العربية
2022